COMPARATIVE ANALYSIS, MODELING, AND EXPERIMENTAL VALIDATION OF CURRENT REGULATION STRATEGIES FOR A GRID-TIED INVERTER

by

Chandra Sekhar Goli

A thesis submitted to the faculty of
The University of North Carolina at Charlotte
in partial fulfillment of the requirements
for the degree of Master of Science in
Electrical Engineering

Charlotte

2022

Approved by:

_____
Dr. Madhav Manjrekar

_____
Dr. Sukumar Kamalasadan

_____
Dr. Tiefu Zhao

ABSTRACT

CHANDRA SEKHAR GOLI. Comparative Analysis, Modeling, and Experimental Validation of Current Regulation Strategies for A Grid-Tied Inverter
(Under the direction of DR. MADHAV MANJREKAR)

Current regulation strategies for a grid-tied inverter with LCL filter in both stationary and synchronous reference frames are presented. Analytical models of the proportional-integral controller in the synchronous reference frame (Sy-PI), a stationary reference frame regulation strategy of synchronous reference frame current controller (St/Sy-PI), and the proportional resonant controller in the stationary reference frame (St-PR) are established. Detailed analysis reveals that these current regulators are inherently different. However, the perceived resemblance that appears in the literature amongst these three controllers is established by underlining the effect of cross-coupling elements which results in an identical forward path transfer function. A generalized current control strategy which encompasses all these three controllers has also been established. Bode plot and root locus analysis are presented to determine the stability limits of control parameters. The results of current regulation strategies are validated using PSIM and verified by employing controller hardware in the loop with Typhoon.

ACKNOWLEDGMENTS

I gratefully acknowledge the valuable guidance received from my advisor Dr. Madhav Manjrekar throughout this academic journey. I am thankful to Dr. Sukumar Kamalasadan and Dr. Tiefu Zhao for their insightful reviews and discussions.

I would like to express my gratitude towards my parents, siblings, and girlfriend for their continuous support in achieving this endeavor.

I am also thankful to friends at the University of North Carolina at Charlotte for their helpful suggestions. My special thanks to Dr. Prasanth Kumar Sahu, Dr. Somasundaram Essakiappan, Dr. Abilash Thakallapelli, Dr. Rubin Bisht, and Dr. Aniket Joshi for their worthy feedback.

I would also like to acknowledge the support received from Energy Production and Infrastructure Center.

TABLE OF CONTENTS

LIST OF FIGURES

LIST OF ABBREVIATIONS

STATCOM	Static Synchronous Compensator
UPFC	Unified Power Flow Controller
DVR	Dynamic Voltage Restorer
SVC	Static VAR Compensator
St-PI	Stationary Reference Frame Proportional Integral Controller
Sy-PI	Synchronous Reference Frame Proportional Integral Controller
St/Sy-PI	Stationary Reference Frame Equivalence of Synchronous Reference Frame Proportional Integral Controller
St-PR	Stationary Reference Frame Proportional Resonant Controller
C-HIL	Controller in Hardware in Loop
ADC	Analog to Digital Converter
SPWM	Sinusoidal Pulse Width Modulation
CCS	Code Composer Studio
DSP	Digital Signal Processor

CHAPTER 1: INTRODUCTION

1.1. Introduction

This chapter presents a brief introduction and organization of the thesis. The importance of a grid-tied inverter system and different stages of power processing from a renewable energy source have been presented in section 1.2. The motivation behind this thesis is presented in section 1.3. The organization of the thesis has been discussed in section 1.4.

1.2. Grid-Tied Inverter

Energy is available in different forms throughout the universe. Natural resources have been processed in different means to harness energy from their crude form. Fossil fuels have been processed all over the world to generate power at a larger scale for more than a century of the timeline. A global database of power plants [1] has reported there are approximately 30,000 power plants from 164 countries generating energy from coal, gas, oil, nuclear, biomass, geothermal, hydro, wind, solar, and other renewables. The thermal power plant utilizes any one or combination of several fossil fuel sources e.g., coal, gas, oil, nuclear, biomass, and geothermal to generate power. An electricity market report in [2] has mentioned approximately 70% of power generation is contributed by thermal power plants. A significant amount of toxic emissions is released by these power plants causing irrevocable damage to the earth. In this regard, a quest to increase the power generation from alternate resources e.g., solar, wind, and hydro has begun.

Synchronous generators have been in use to generate power from coal, gas, nuclear, oil, biomass, geothermal, and hydro. Induction generators have been employed to generate power from wind and tidal. Power generated by these electric machines is transformed and synchronized to a standard specification of the grid. Thus, generators are tied to the grid after synchronization to transfer the power to consumers located in distant places. Solar panels are in use to transform solar

energy from the sun into electrical energy. Energy generated by solar panels is stored in a battery in the form of DC. Thus, energy in this form is required to be transformed into a standard AC to make it compatible with the application of end-users. An inverter has been used to transform power from DC to AC at a voltage and frequency of the grid. Thus, a solar energy source is tied to the grid by means of a power conversion apparatus called a grid-tied inverter. Grid-tied inverter serves as a virtual synchronous machine to match the voltage and frequency output of it to the standard specification of the distribution grid.

1.3.Thesis Motivation

Many countries have identified thermal power plants as a major cause of toxic emissions leading to global warming. Several countries have legislated to disintegrate thermal power plants from operation to address the cause of global warming. In this regard, an increase in power generation contribution from renewable energy resources has been commissioned at larger scales. Solar energy is one of the renewable energy resources, could be utilized to harness power at larger scales in addition to the wind, hydro, and tidal. A grid-tied inverter is used to interface solar energy resources to the grid. A grid must be capable of handling the balance between power generation and consumption. Any change in the loading conditions of a grid will reflect onto the source of it. The power flow between the battery-powered solar panels and loads is required to be balanced. Any change in loading conditions will cause a change in current, swell or sag in the voltage and then power. The grid-tied inverters can also be operated as STATCOM, UPFC, DVR, and SVC to address the voltage and current imbalances due to dynamic changes in the loading conditions of the grid. Most of these control strategies have an outer loop to control power or voltage and an inner loop to control the current.

The objective of this thesis has been limited to current control strategies in the stationary reference frame and synchronous reference frame. Analytical equations of the classical proportional-integral controller in the synchronous reference frame (Sy-PI), stationary reference frame regulation of synchronous reference frame proportional-integral controller (St/Sy-PI), and stationary reference frame proportional resonant controller (St-PR) of the grid-tied inverter have been synthesized to verify the equivalence between them which is lacking in the existing literature. The outcome of this analysis has been used to realize a generalized control strategy consisting of Sy-PI, St/Sy-PI, and St-PR. The motive of this thesis is to present a generalized current regulation strategy that may help as a better resource to understand the similarity and discrepancies between Sy-PI, St/Sy-PI, and St-PR.

1.4.Organization of Thesis

A brief overview of the organization of the thesis has been discussed in this section.

Chapter 1: Introduction

This chapter has been focused on detailing the importance of grid-tied inverters for renewable energy applications in Section 1.2. The motivation behind this thesis is discussed in Section 1.3. The organization of the thesis has been presented in Section 1.4.

Chapter 2: Literature Review of Grid-Tied Inverters

A literature review of the grid-tied inverter has been presented in this chapter. The basic topology of the grid-tied inverter has been discussed in Section 2.1. A review of the switching function model of the inverter is discussed in Section 2.2. A thorough review of the stationary reference frame and synchronous reference frame transformations is presented in Section 2.4. A review of different types of filters has been discussed in Section 2.5. A brief review of current regulation strategies and a discussion have been presented in Section 2.6 and Section 2.7.

Chapter 3: Description & Analysis of Current Controllers

A detailed analysis of various current regulation strategies has been presented in this chapter. State-space analysis of the circuit topology of the grid-tied inverter has been presented in Section 3.1. Analytical derivation of stationary reference frame proportional-integral controller (St-PI), synchronous reference frame proportional-integral controller (Sy-PI), stationary reference frame regulation of synchronous reference frame proportional-integral controller (St/Sy-PI), stationary reference frame proportional resonant controller has been presented in Section 3.2, Section 3.3, Section 3.4, and Section 3.5. A generalized current regulation strategy has been realized in Section 3.5.

Chapter 4: Modeling & Simulation of A Grid-Tied Inverter

Modeling and simulation of various current controller strategies have been discussed in this Chapter. An introduction to the modeling and simulation of the grid-tied inverter is presented in Section 4.1. A schematic block diagram of the circuit topology of the grid-tied inverter in the PSIM simulation platform is presented in section 4.2. Analog to digital conversion and modeling of phase-locked loops are discussed in Section 4.3 and Section 4.4. Reference current generation and current control strategies in the stationary reference frame and synchronous reference frame have been discussed in Section 4.5, Section 4.6, Section 4.7, and Section 4.8. A brief overview of the sinusoidal pulse width modulation technique is presented in Section 4.9. Simulation models of St-PI, Sy-PI, St/Sy-PI, and St-PR have been presented in Section 4.10, Section 4.11, Section 4.12, and Section 4.13. A simulation model of generalized current regulation strategy has been presented in Section 4.14.

Chapter 5: Simulation Results

This chapter is focused on presenting the simulation results of the various current control strategies. An introduction detailing the consideration of reference currents in respective reference frames is presented in Section 5.1. Simulation results of St-PI, Sy-PI, St/Sy-PI, and St-PR have been presented in Section 5.3.1, Section 5.3.2, Section 5.3.3, and Section 5.3.4. These simulation results are discussed in Section 5.4.

Chapter 6: Experimental Validation of Current Regulation Strategies

This chapter has been allotted to detail experimental setup and to report experimental results. An introduction to the experimental setup is presented in Section 6.1. Different stages of controller hardware in the loop (C-HIL) have been discussed in Section 6.2. Details of the power stage, analog to digital conversion and a serial communication interface to process the reference signals have been discussed in Section 6.2.1, Section 6.2.2, and Section 6.2.3. Experimental setup and experimental results have been presented in Section 6.3. and Section 6.4. A discussion on experimental validation is presented in Section 6.5.

Chapter 7: Conclusion

This chapter consists of a conclusive discussion on the outcome of comparative analysis, modeling, and experimental validation of current regulation strategies for a grid-tied inverter with an LCL filter. A summary of research outcomes discussed in this thesis has been reported as an overview in Section 7.1. A future scope detailing a generic current regulation strategy is presented in Section 7.2.

All the references used in this thesis have been listed in bibliography.

CHAPTER 2: LITERATURE REVIEW OF GRID-TIED INVERTERS

2.1. Introduction

A literature review of the grid-tied inverter has been presented in this chapter. The basic topology of the grid-tied inverter has been discussed in Section 2.1. A review of the switching function model of the inverter is discussed in Section 2.2. A thorough review of the stationary reference frame and synchronous reference frame transformations is presented in Section 2.4. A review of different types of filters has been discussed in Section 2.5. A brief review of current regulation strategies and a discussion have been presented in Section 2.6 and Section 2.7.

2.2. Switching Function Model of Inverter

A literature review of the basic circuit topology of a three-phase inverter/rectifier has been presented in many papers. The three-phase inverter/rectifier consists of two switches in each phase-leg as shown in figure.2.1. These switches are operated in a specific logic by employing pulse width modulation to invert DC into AC or to rectify AC into DC. Thus, the input and output of a three-phase inverter/rectifier are related through a switching function. The switching function concept of the three-phase inverter presented in [3], [4], [5], [6], and [7] has been reviewed to detail the basic principle of operation in this section.

A switching function that relates the input and output of a specific phase or phase to the phase of an inverter/rectifier is discontinuous, time-varying, and nonlinear. Thus, switching functions of three phases of an inverter/rectifier are required to be averaged over a cycle to translate them as time-continuous functions in a three-phase stationary reference frame. However, the time-varying and non-linear behavior of the currents and voltages of the average model of the inverter/rectifier are difficult to track. Thus, an improvised average model of inverter/rectifier is realized in a synchronous reference frame or rotating reference frame at grid frequency by applying transformation techniques presented in [8], [9], [10], and [11]. The time-continuous currents and

voltages relating to the input and output of a three-phase inverter in a synchronous reference frame are easy to track because of their time-invariant nature. The small-signal analysis is performed on currents and voltages of the three-phase inverter to linearize the model. Thus, a switching function model of a three-phase inverter/rectifier is required to be analyzed in four steps listed here to ease the process of control [6],

1. Switching model: time-discontinuous, time-varying, and nonlinear
2. Average model in a stationary reference frame: time-continuous, time-varying, and nonlinear
3. Average model in a synchronous reference frame: time-continuous, time-invariant, and nonlinear
4. Small-signal model: time-continuous, time-invariant, and linear

A three-phase inverter/rectifier topology presented in [6] has been considered to establish switching functions relating to input and output.

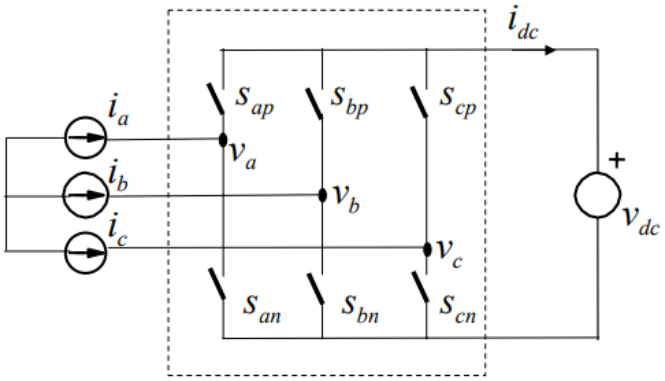

Figure.2.1. A schematic of circuit topology of switching model of three-phase inverter/rectifier [6].

The schematic of circuit topology of a switching function model of a three-phase inverter/rectifier is shown in figure.2.1. consists of six switches, three-current sources, and a battery source.

Rectifier mode of operation of the circuit topology has been considered to establish the analytical switching functions. Thus, a phase-leg switching function may be defined as,

$$S_i = S_{ip} = 1 - S_{in}; \quad i \in \{a, b, c\} \tag{2.1}$$

The phase-leg switching function of each phase of the three-phase inverter/rectifier may be expressed as,

$$S_a = S_{ap} = 1 - S_{an} \tag{2.2}$$

$$S_b = S_{bp} = 1 - S_{bn} \tag{2.3}$$

$$S_c = S_{cp} = 1 - S_{cn} \tag{2.4}$$

Each phase-leg of the three-phase inverter/rectifier consists of two switches e.g., S_{ap} and $S_{an}$of phase a. Two switches under the same phase leg are not operated simultaneously to avoid short circuits. As an example, for a specific sequence of switches $S_a = 0$, $S_b = 1$, and $S_c = 0$ or $S_{ap} = 0$ & $S_{an} = 1$, $S_{bp} = 1$ & $S_{bn} = 0$, and $S_{cp} = 0$ & $S_{cn} = 1$, dc current through the battery may be expressed as

$$i_{dc} = i_b \tag{2.5}$$

Phase to phase voltages of the three-phase rectifier may be expressed as,

$$v_{ab} = -v_{dc} \tag{2.6}$$

$$v_{bc} = v_{dc} \tag{2.7}$$

$$v_{ca} = 0 \tag{2.8}$$

Thus, based on the different combinations of switches, currents and voltages at the input and output of the three-phase rectifier may be expressed as shown in table 2.1.

TABLE 2.1. Relationship between the output current and input voltages of a three-phase inverter/rectifier [6].

S_a	S_b	S_c	$S_a - S_b$	$S_b - S_c$	$S_c - S_a$	i_{dc}	v_{ab}	v_{bc}	v_{ca}
0	0	0	0	0	0	0	0	0	0
0	0	1	0	-1	1	i_c	0	$-v_{dc}$	v_{dc}
0	1	0	-1	1	0	i_b	$-v_{dc}$	v_{dc}	
0	1	1	-1	0	1	$i_b + i_c$	$-v_{dc}$	0	v_{dc}
1	0	0	1	0	-1	i_a	v_{dc}	0	$-v_{dc}$
1	0	1	1	-1	0	$i_a + i_c$	v_{dc}	$-v_{dc}$	0
1	1	0	0	1	-1	$i_a + i_b$	0	v_{dc}	$-v_{dc}$
1	1	1	0	0	0	$i_a + i_b + i_c$	0	0	0

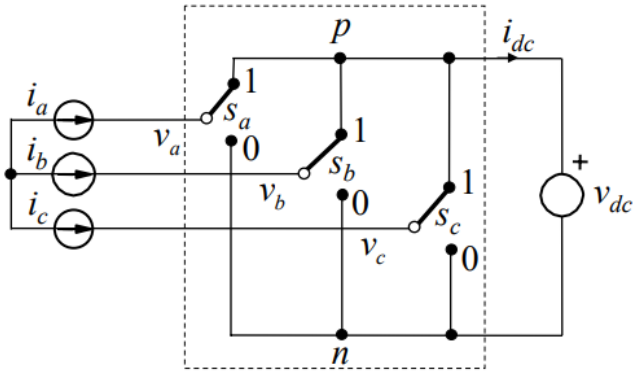

Figure.2.2. Schematic of modified circuit topology of switching model of a three-phase inverter/rectifier [6].

Modified circuit topology of a three-phase inverter/rectifier may be realized from equation (2.1) is shown in figure.2.2. Instantaneous phase to phase voltages in terms of switching functions of the circuit topology shown in figure.1. may be expressed as,

$$\begin{bmatrix} v_{ab} \\ v_{bc} \\ v_{ca} \end{bmatrix} = \begin{bmatrix} S_a - S_b \\ S_b - S_c \\ S_c - S_a \end{bmatrix} v_{dc} = \begin{bmatrix} S_{ab} \\ S_{bc} \\ S_{ca} \end{bmatrix} v_{dc} \tag{2.9}$$

Similarly, instantaneous currents relating the output DC current and input AC phase currents of the three-phase rectifier/inverter may be expressed as,

$$i_{dc} = [S_a \quad S_b \quad S_c] \begin{bmatrix} i_a \\ i_b \\ i_c \end{bmatrix} \tag{2.10}$$

Thus, the DC current may be expressed as,

$$i_{dc} = S_a i_a + S_b i_b + S_c i_c \tag{2.11}$$

$$i_{dc} = S_a(i_{ab} - i_{ca}) + S_b(i_{bc} - i_{ab}) + S_c(i_{ca} - i_{bc}) \tag{2.12}$$

Where,

$$\begin{bmatrix} i_{ab} \\ i_{bc} \\ i_{ca} \end{bmatrix} = \begin{bmatrix} i_{ab} - i_{ca} \\ i_{bc} - i_{ab} \\ i_{ca} - i_{bc} \end{bmatrix} \tag{2.13}$$

Equation (2.12) is equivalent to equation (2.11) under balanced condition of $i_a + i_b + i_c = 0$. Thus, equation (2.12) may be modified as,

$$i_{dc} = i_{ab}(S_a - S_b) + i_{bc}(S_b - S_c) + i_{ca}(S_c - S_a) \tag{2.14}$$

Therefore, DC current may be expressed in terms of line to line switching functions and line to line current as shown in below expression,

$$i_{dc} = [S_{ab} \quad S_{bc} \quad S_{ca}] \begin{bmatrix} i_{ab} \\ i_{bc} \\ i_{ca} \end{bmatrix} \tag{2.15}$$

Phase to phase voltages in (9) and DC current in (2.15) may be represented in a generalized form as expressed below,

$$v_{ll} = S_{ll} v_{dc} \tag{2.16}$$

$$i_{dc} = S_{ll}^T i_{ll} \tag{2.17}$$

Where,

$$v_{ll} = \begin{bmatrix} v_{ab} \\ v_{bc} \\ v_{ca} \end{bmatrix} \tag{2.18}$$

$$S_{ll} = [S_{ab} \quad S_{bc} \quad S_{ca}] \tag{2.19}$$

$$i_{ll} = \begin{bmatrix} i_{ab} \\ i_{bc} \\ i_{ca} \end{bmatrix} \tag{2.20}$$

Input phase to phase voltages and output DC current in (2.16) and (2.17) are discrete switching functions. These functions are averaged over a cycle to realize continuous functions as shown below,

Considering an average function of line voltage between phase a and phase b,

$$v_{ab} = S_{ab} v_{dc} \tag{2.21}$$

Averaging the above function over a cycle of time period 'T' may result in the following expression,

$$\bar{v}_{ab} = \frac{1}{T}\int_{t-T}^{t} S_{ab}(\tau)v_{dc}(\tau)d\tau = \bar{S}_{ab}\bar{v}_{dc} = d_{ab}\bar{v}_{dc} \tag{2.22}$$

Where, d_{ab} is an average value of switching function called as modulation depth. Similarly, expression (2.17) of currents may be averaged to express it as an average time-continuous function. The generalized averaged functions of voltages and currents in time-continuous form may be expressed as,

$$\bar{v}_{ll} = d_{ll}\bar{v}_{dc} \tag{2.23}$$

$$\bar{\imath}_{dc} = d_{ll}^{T}\bar{\imath}_{ll} \tag{2.24}$$

Above functions are time-continuous, time-varying, and nonlinear. Thus, switching functions are transformed into continuous functions by averaging them. However, time-varying signals are difficult to track. Clarke's transformation and Park's transformation techniques are used to transform these time-varying functions into time-invariant or DC functions. These two transformation techniques are detailed in Section 2.3 and Section 2.4.

2.3. Stationary Reference Frame

Three-phase time varying signals of 120 degrees of phase difference are represented by two orthogonal time-varying signals of 90 degree apart and a zero-sequence signal by applying Clarke's transformation [7]. This transformation technique may be used to control the orthogonal currents and voltages corresponding to active and reactive components of power in the grid. Considering a set of three-phase instantaneous signals in equations (1) to (3),

$$x_a = \hat{x}\cos(\omega t) \tag{2.25}$$

$$x_b = \hat{x}\cos\left(\omega t - \frac{2\pi}{3}\right) \tag{2.26}$$

$$x_c = \hat{x}\cos\left(\omega t - \frac{4\pi}{3}\right) \tag{2.27}$$

Resultant vector $\bar{x}$ along a-phase may be represented as spatial vector sum of (2.25), (2.26), and (2.27). Thus,

$$\bar{x} = \frac{2}{3}\left(x_a + x_b e^{j\frac{2}{3}\pi} + x_c e^{j\frac{4}{3}\pi}\right) = \frac{2}{3}(x_a + a x_b + a^2 x_c) \tag{2.28}$$

Where, a=$e^{j\frac{2}{3}\pi}$ and a scaling factor of 2/3 has been included in the above equation to avoid a scaling factor while performing stationary reference frame to three-phase reference frame transformation. Thus, the resultant vector consists of real and imaginary components as given below,

$$\bar{x} = \tfrac{2}{3}\left(x_a - \tfrac{1}{2}x_b - \tfrac{1}{2}x_c\right) + j\left(\tfrac{1}{\sqrt{3}}(x_b - x_c)\right) = x_d^s + j x_q^s \tag{2.29}$$

Under unbalanced condition, a DC or zero sequence component exists in the above equation. Thus,

$$\bar{x} = \frac{2}{3}\left(x_a - \frac{1}{2}x_b - \frac{1}{2}x_c\right) + j\left(\frac{1}{\sqrt{3}}(x_b - x_c)\right) + \frac{1}{3}(x_a + x_b + x_c) \tag{2.30}$$

Above equation may be expressed in a matrix form as given below,

$$\begin{bmatrix} x_d^s \\ x_q^s \\ x_o \end{bmatrix} = \begin{bmatrix} \frac{2}{3} & -\frac{1}{3} & -\frac{1}{3} \\ 0 & \frac{1}{\sqrt{3}} & -\frac{1}{\sqrt{3}} \\ \frac{1}{3} & \frac{1}{3} & \frac{1}{3} \end{bmatrix} \begin{bmatrix} x_a \\ x_b \\ x_c \end{bmatrix} \tag{2.31}$$

A generalized consolidated form of above expression is given below,

$$x_{dqo}^s = T_{abc} x_{abc} \tag{2.32}$$

Where, Clarke's transformation matrix T_{abc} may be expressed as,

$$T_{abc} = \begin{bmatrix} \frac{2}{3} & -\frac{1}{3} & -\frac{1}{3} \\ 0 & \frac{1}{\sqrt{3}} & -\frac{1}{\sqrt{3}} \\ \frac{1}{3} & \frac{1}{3} & \frac{1}{3} \end{bmatrix} \tag{2.33}$$

Thus, three-phase functions may be transformed into stationary reference frame by applying (2.32). These functions in stationary reference frame may be transformed into three-phase reference frame by applying the transformation given below,

$$x_{abc} = T_{abc}^{-1} x_{dqo}^{s} \tag{2.34}$$

2.4. Synchronous Reference Frame

Despite the advantage of decoupling of the functions, stationary reference frame functions are time-varying in behavior. Thus, tracking time-varying sinusoidal signals is difficult and may prone to steady state errors. Orthogonal components in stationary reference frame are time-varying and rotates at speed of fundamental frequency of the system. The magnitude of stationary reference frame functions x_d^s and x_q^s have been marked on respective stationary reference frame axes d^s and q^s as shown in figure.2.3. (a). These stationary reference frame functions look steady or time-invariant when they are observed from a reference frame that is rotating at the same speed or frequency as stationary reference frame. The angle between stationary reference frame of axes d^s & q^s and rotating reference frame axes d^e & q^e is considered as θ.

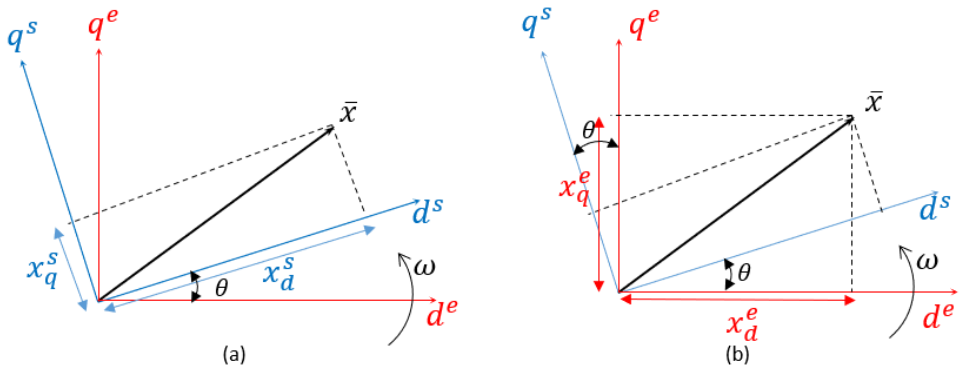

Figure. 2.3. (a). Graphical representation of magnitudes of stationary reference frame functions.

(b). Graphical representation of magnitudes of synchronous reference frame functions.

This angle θ between them remains constant if the rotating reference frame is at a speed of system frequency ω. Thus, resultant vector $\bar{x}$ in stationary reference frame and rotating reference frame may be expressed as,

$$\bar{x} = x_d^s + jx_q^s = x_d^e + jx_q^e \tag{2.35}$$

Where, x_d^e & x_q^e are the magnitudes along the respective d-axis and q-axis of rotating reference frame d^e & q^e as represented in the figure.3. (b). A relationship between magnitudes of functions x_d^s & x_q^s of stationary reference frame and x_d^e & x_q^e may be expressed as an equation given below.

$$\begin{bmatrix} x_d^e \\ x_q^e \end{bmatrix} = \begin{bmatrix} \cos\theta & -\sin\theta \\ \sin\theta & \cos\theta \end{bmatrix} \begin{bmatrix} x_d^s \\ x_q^s \end{bmatrix} \tag{2.36}$$

A generalized form of rotating reference frame functions may be expressed as,

$$x_{dqo}^e = T x_{dqo}^s \tag{2.37}$$

Where, 'T' is a time dependent matrix called as Park's transformation matrix,

$$T = \begin{bmatrix} \cos\theta & -\sin\theta \\ \sin\theta & \cos\theta \end{bmatrix} \tag{2.38}$$

For an unbalanced system, rotating reference frame functions may be expressed as,

$$\begin{bmatrix} x_d^e \\ x_q^e \\ x_o^e \end{bmatrix} = \begin{bmatrix} \cos\theta & -\sin\theta & 0 \\ \sin\theta & \cos\theta & 0 \\ 0 & 0 & 1 \end{bmatrix} \begin{bmatrix} x_d^s \\ x_q^s \\ x_o^s \end{bmatrix} \tag{2.39}$$

Rotating reference frame also called as synchronous reference frame if it rotates at system frequency. Thus, a set of functions in rotating reference frame are time-continuous, time-invariant or DC, and nonlinear in behavior. Small signal analysis [5] is performed on these functions to linearize the system which is not covered in this review. Large signal analysis is considered in this thesis to analyze the current regulation control strategies.

2.5. Filter Topologies

Output voltages and currents of a three-phase voltage source inverter/rectifier discussed in the previous sections are pulsating DC in behavior, consists of harmonics. A three-phase filter is required to filter out these harmonics. Different types of filters are employed depending up on the

application of the three-phase inverter. A simple inductive filter is used in motor control applications. Voltage source inverter with LC filter topology has been employed in applications of line interactive UPS or DVR where sensitive load voltage needs to be tracked while inductor or capacitor current will be the main feedback [12]. The current source inverter with CL filter topology has been employed in static synchronous compensators (STATCOM) to control the output current to track a specified current or power [13]. The voltage source inverter with LCL filter topology is employed to interface utility to the grid of distributed generation to control the power flow by regulating the output current [14, 15]. The output currents and voltages of the inverter will be smoothened further using an LCL filter.

Majority of the existing literature has been limited to the analysis of grid-tied inverter with simple inductive filter consists of a second-order transfer function. Few of the authors have extended this analysis to LC, CL, and LCL filter. However, the respective transfer functions of several filter topologies have been analyzed in a three-phase reference frame to avoid the complexity of transforming multiple variables associated with the LCL filter in a synchronous reference frame [15].

A battery-fed, three-phase inverter with an inductive filter for motor applications conists of a pair of cross coupling between d-axis and q-axis in synchronous reference frame. Thus, a system with a filter consisting of multiple enrgy storage elements results in multiple cross coupling between d-axis and q-axis in synchronous refernce frame. Thus, analysis of a grid-tied inverter with an LCL filter in synchronous reference frame becomes more complex. A system with energy storage elements poses the risk of the resonance at a frequency other than system frequency [16]. In addition to current control, a damping control strategy is required to be employed because the grid-tied inverter with an LCL may allow the signals into the grid at a frequency other than system

frequency due to energy storage elements [17]. Several ways to regulate the effects of the resonance caused by energy storage elements have been presented in the literature [17].

2.6. Current Regulation Strategies

The presence of steady-state error in a proportional-integral controller in a stationary reference frame has been discussed in the majority of the literature [18]. Steady-state error is imminent in the stationary reference frame since the feedback signals are time-varying and difficult to track [19]. Synchronous reference frame theory has been established to transform the time-variant feedback signals from the stationary reference frame to time-invariant signals. Time-invariant signals can be tracked easily without any steady-state error [20]. Thus, the current regulation strategy in the synchronous reference frame has been adopted widely.

A traditional proportional-integral current regulation strategy in the synchronous reference frame had been implemented for motor control application with a simple inductive filter consisting of two cross-couplings between the d-axis and q-axis [8]. However, analysis of the current regulation strategy in the synchronous reference frame becomes more complex because the application of this control strategy to grid-tied inverter establishes multiple cross-couplings if the system has a filter with multiple energy storage elements [21].

Another current regulation strategy proposed in [22] may be operated in a synchronous reference frame or stationary reference frame by altering the index matrices of current or voltages as proposed by the authors. This regulation strategy establishes cross-couplings either on the controller or plant side of the system depending on the mode of regulation strategy [22]. A proportional resonant current regulator in the stationary reference frame involves no cross-couplings either on the controller or plant side of the system [23]. This controller is required to be tuned precisely at grid frequency to operate at higher gains [24].

CHAPTER 3: DESCRIPTION & ANALYSIS OF CURRENT CONTROLLERS

3.1. Introduction

A detailed analysis of various current regulation strategies is presented in this chapter. State-space analysis of the circuit topology of the grid-tied inverter has been presented in Section 3.1. Analytical derivation of stationary reference frame proportional-integral controller (St-PI), synchronous reference frame proportional-integral controller (Sy-PI), stationary reference frame regulation of synchronous reference frame proportional-integral controller (St/Sy-PI), stationary reference frame proportional resonant controller has been presented in Section 3.2, Section 3.3, Section 3.4, and Section 3.5. A generalized current regulation strategy has been realized in Section 3.5.

3.1. State-space Analysis of Grid-Tied Inverter

A standard topology of an 800 V battery-fed three-phase inverter with an LCL filter tied to the grid has been considered. The nomenclature of various parameters listed in table.3.1 has been used to analyze the current regulation strategies. A simplified schematic of the circuit topology of a grid-tied inverter and controller hardware in the loop (CHIL) of the grid-tied inverter has been shown in the figure.3.1. Typhoon 604 has been used to emulate the power stage of the system. DSP microcontroller TMS320F28035 has been employed to implement control algorithms. State-space analysis of this topology has been presented in this section. The circuit topology of the grid-tied inverter consists of a filter with nine energy storage elements. Each phase has three energy storage elements inductor L_1, capacitor C, and inductor L_2.

TABLE .3.1:NOMENCLATURE

Parameter	*Explanation*
i_a, i_b, i_c	*Inverter output currents*
i_x, i_y, i_z	*Per phase grid currents*
v_a, v_b, v_c	*Per phase inverter output voltages*
e_a, e_b, e_c	*Per phase grid voltages*
v_{ca}, v_{cb}, v_{cc}	*Per phase voltages across capacitors*
d_a, d_b, d_c	*Per phase modulation depths*
L_1, L_2	*Per phase inductances of LCL filter*
R_1, R_2	*Resistance of inductors L_1 and L_2*
C	*Per phase capacitance of LCL filter*
C_{dc}	*DC link capacitor*
v_{dc}	*Input DC supply voltage*
i_{in}	*Input current form the DC source*
i_{dc}	*Input current to the inverter*
i_d^s, i_q^s & i_{gd}^s, i_{gq}^s	*Inverter and grid currents in the stationary frame*
i_d^e,i_q^e, & i_{gd}^e, i_{gq}^e	*Inverter and grid currents in the synchronous frame*
k_p, k_i	*Proportional constant and proportional gain*
k	*Damping proportional constant*
ω	*System frequency*

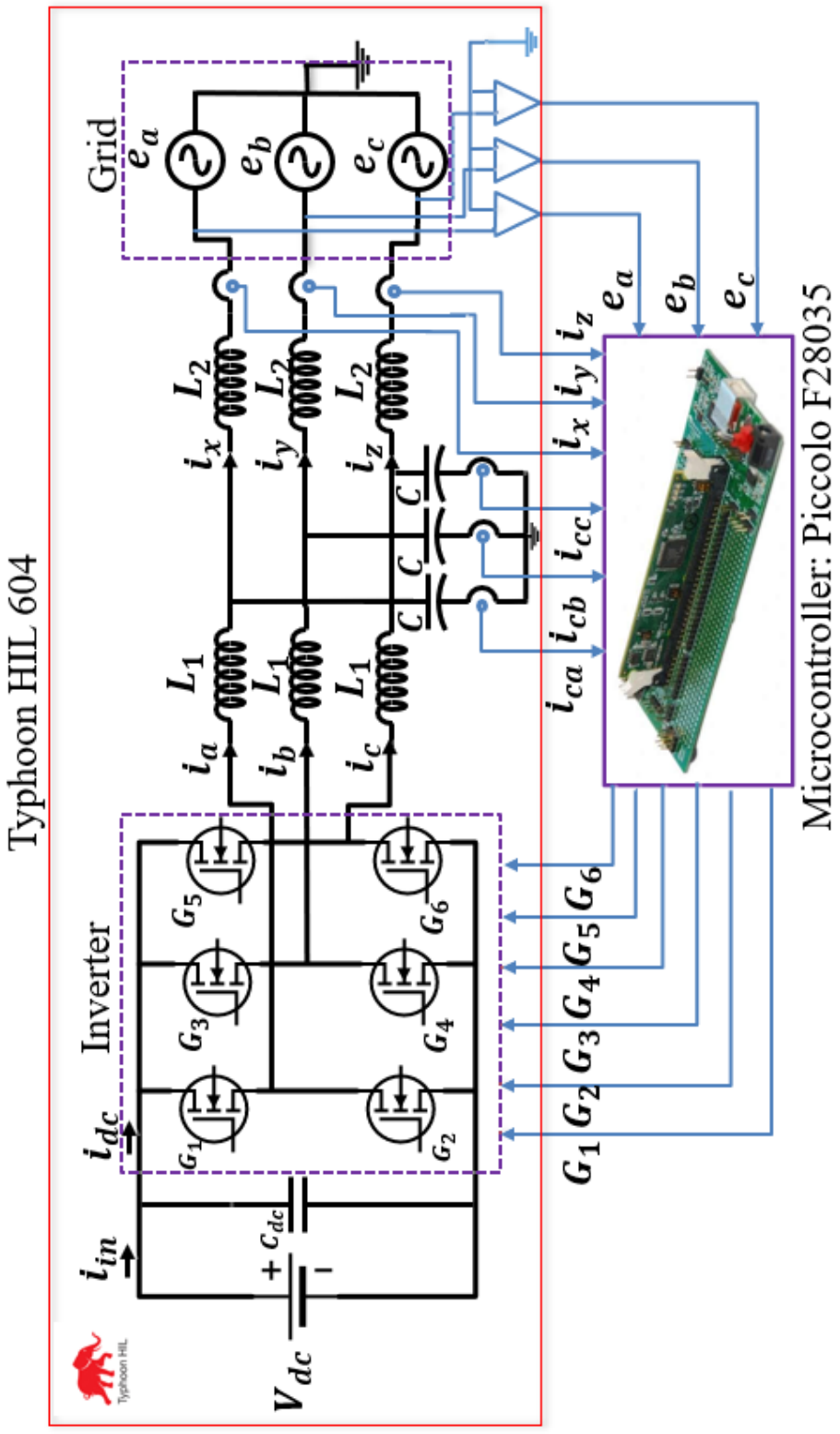

Figure.3.1. Simplified schematic of circuit topology and CHIL of the grid-tied inverter.

The per-phase voltage output of the three-phase inverter in figure.3.1 may be expressed in terms of modulation depths (switching functions averaged over a cycle) as given below,

$$v_a = 0.5V_{dc}d_a \tag{3.1}$$

$$v_b = 0.5V_{dc}d_b \tag{3.2}$$

$$v_c = 0.5V_{dc}d_c \tag{3.3}$$

Figure.3.2. shows an average model of a three-phase grid-tied inverter with an LCL filter [18-22]. A simplified per phase equivalent circuit of an average model is shown in the figure. 3.3. This circuit topology consists of three energy storage elements resulting in three state variables. These three state variables corresponding to phase a are current i_a through inductor L_1, voltage v_{ca} across capacitor C, and current i_x through inductor L_2. Thus, a three-phase grid-tied inverter system consists of nine state-space equations corresponding to nine state variables.

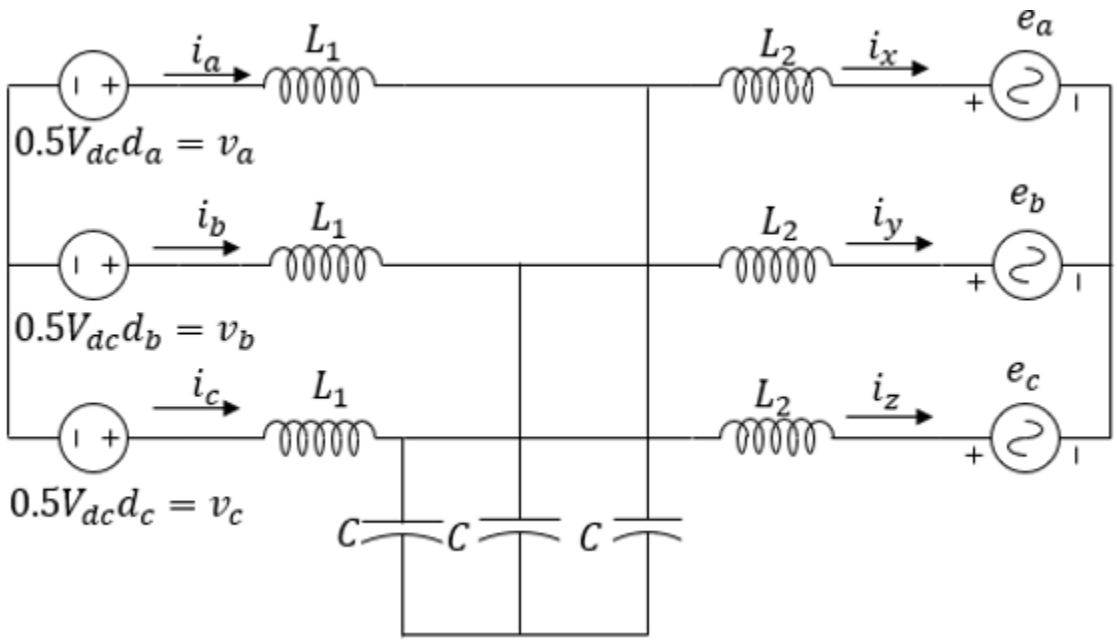

Figure.3.2. Simplified schematic of an average model of a three-phase grid-tied inverter with LCL filter.

It has been assumed that inductors L_1 and L_2 have a small value of resistances R_1 and R_2. Applying Kirchhoff's voltage law to loop 1, loop 2, and loop 3 in figure.3.3. results in the

equations (3.4) to (3.6). These equations are represented in a consolidated form (3.5) to account for state-space equations corresponding to three phases of the grid-tied inverter system. These equations have been transformed into respective reference frames in the frequency domain.

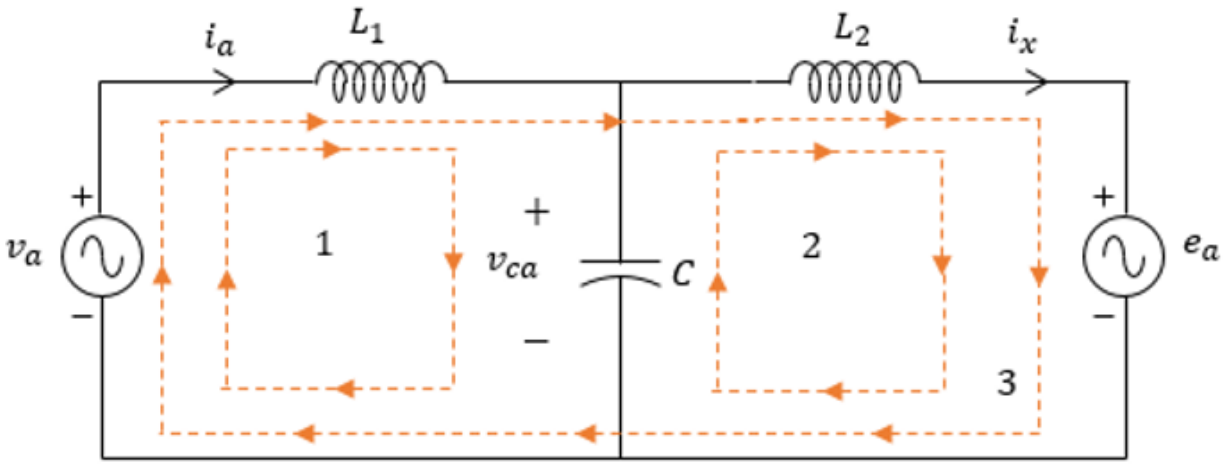

Figure.3.3. Schematic of per phase equivalent circuit of the simplified average model of grid-tied inverter with LCL filter.

$$\frac{d}{dt}(i_a) = \frac{1}{L_1}(v_a) - \frac{1}{L_1}(v_{ca}) - \frac{R_1}{L_1}(i_a) \tag{3.4}$$

$$\frac{d}{dt}(i_x) = \frac{1}{L_2}(v_{ca}) - \frac{1}{L_2}(e_a) - \frac{R_2}{L_2}(i_x) \tag{3.5}$$

$$\frac{d}{dt}(v_{ca}) = \frac{1}{C}(i_a) - \frac{1}{C}(i_x) \tag{3.6}$$

Thus, state-space equations corresponding to three-phases of the grid-tied inverter may be expressed as,

$$\frac{d}{dt}\begin{bmatrix} i_a \\ i_b \\ i_c \end{bmatrix} = \frac{1}{L_1}\begin{bmatrix} v_a \\ v_b \\ v_c \end{bmatrix} - \frac{1}{L_1}\begin{bmatrix} v_{ca} \\ v_{cb} \\ v_{cc} \end{bmatrix} - \frac{R_1}{L_1}\begin{bmatrix} i_a \\ i_b \\ i_c \end{bmatrix} \tag{3.7}$$

$$\frac{d}{dt}\begin{bmatrix} i_x \\ i_y \\ i_z \end{bmatrix} = \frac{1}{L_2}\begin{bmatrix} v_{ca} \\ v_{cb} \\ v_{cc} \end{bmatrix} - \frac{1}{L_2}\begin{bmatrix} e_a \\ e_b \\ e_c \end{bmatrix} - \frac{R_2}{L_2}\begin{bmatrix} i_x \\ i_y \\ i_z \end{bmatrix} \tag{3.8}$$

$$\frac{d}{dt}\begin{bmatrix} v_{ca} \\ v_{cb} \\ v_{cc} \end{bmatrix} = \frac{1}{C}\begin{bmatrix} i_a \\ i_b \\ i_c \end{bmatrix} - \frac{1}{C}\begin{bmatrix} i_x \\ i_y \\ i_z \end{bmatrix} \tag{3.9}$$

Thus, a plant model the three-phase grid tied inverter is realized by these three equations.

3.2. Stationary Reference Frame Proportional Integral Controller (St-PI)

In this section, transformation of three-phase state-space equations (3.7), (3.8), and (3.9) into stationary reference frame is presented. These three-state space equations in stationary reference frame are used to realize a plant transfer function. A proportional integral controller is embedded with plant transfer function to determine the forward path transfer function and the corresponding closed loop transfer function in the stationary reference frame. In addition to current control strategy, a damping control strategy is discussed to counter the effect of resonance due to energy storage elements.

Three-phase state-space equations may be transformed into stationary reference frame by applying the transformation shown in equations (3.9) and (3.10).

$$\begin{bmatrix} x_d^s \\ x_q^s \\ x_0^s \end{bmatrix} = T_{abc}\begin{bmatrix} x_a \\ x_b \\ x_c \end{bmatrix} \tag{3.9}$$

Where, T_{abc} is a Clarke's transformation matrix given below,

$$T_{abc} = \begin{bmatrix} \frac{2}{3} & -\frac{1}{3} & -\frac{1}{3} \\ 0 & \frac{1}{\sqrt{3}} & -\frac{1}{\sqrt{3}} \\ \frac{1}{3} & \frac{1}{3} & \frac{1}{3} \end{bmatrix} \tag{3.10}$$

Thus, by multiplying equations (3.7), (3.8), and (3.9) with a transformation matrix T_{abc} of constant elements result in the following expressions.

$$T_{abc}\frac{d}{dt}\begin{bmatrix} i_a \\ i_b \\ i_c \end{bmatrix} = \frac{1}{L_1}T_{abc}\begin{bmatrix} v_a \\ v_b \\ v_c \end{bmatrix} - \frac{1}{L_1}T_{abc}\begin{bmatrix} v_{ca} \\ v_{cb} \\ v_{cc} \end{bmatrix} - \frac{R_1}{L_1}T_{abc}\begin{bmatrix} i_a \\ i_b \\ i_c \end{bmatrix} \tag{3.11}$$

$$T_{abc}\cdot\frac{d}{dt}\begin{bmatrix} i_x \\ i_y \\ i_z \end{bmatrix} = \frac{1}{L_2}T_{abc}\cdot\begin{bmatrix} v_{ca} \\ v_{cb} \\ v_{cc} \end{bmatrix} - \frac{1}{L_2}T_{abc}\cdot\begin{bmatrix} e_a \\ e_b \\ e_c \end{bmatrix} - \frac{R_2}{L_2}T_{abc}\cdot\begin{bmatrix} i_x \\ i_y \\ i_z \end{bmatrix} \tag{3.12}$$

$$T_{abc}\cdot\frac{d}{dt}\begin{bmatrix} v_{ca} \\ v_{cb} \\ v_{cc} \end{bmatrix} = \frac{1}{C}T_{abc}\cdot\begin{bmatrix} i_a \\ i_b \\ i_c \end{bmatrix} - \frac{1}{C}T_{abc}\cdot\begin{bmatrix} i_x \\ i_y \\ i_z \end{bmatrix} \tag{3.13}$$

The transformation matrix T_{abc} of constant elements can be brought inside the derivative term because it has time independent elements. Thus, equations (3.11), (3.12), and (3.13) may be expressed in a modified form as given below,

$$\frac{d}{dt}\left[T_{abc}\cdot\begin{bmatrix} i_a \\ i_b \\ i_c \end{bmatrix}\right] = \frac{1}{L_1}\left[T_{abc}\cdot\begin{bmatrix} v_a \\ v_b \\ v_c \end{bmatrix}\right] - \frac{1}{L_1}\left[T_{abc}\cdot\begin{bmatrix} v_{ca} \\ v_{cb} \\ v_{cc} \end{bmatrix}\right] - \frac{R_1}{L_1}\left[T_{abc}\cdot\begin{bmatrix} i_a \\ i_b \\ i_c \end{bmatrix}\right] \tag{3.14}$$

$$\frac{d}{dt}\left[T_{abc}\cdot\begin{bmatrix} i_x \\ i_y \\ i_z \end{bmatrix}\right] = \frac{1}{L_2}\left[T_{abc}\cdot\begin{bmatrix} v_{ca} \\ v_{cb} \\ v_{cc} \end{bmatrix}\right] - \frac{1}{L_2}\left[T_{abc}\cdot\begin{bmatrix} e_a \\ e_b \\ e_c \end{bmatrix}\right] - \frac{R_2}{L_2}\left[T_{abc}\cdot\begin{bmatrix} i_x \\ i_y \\ i_z \end{bmatrix}\right] \tag{3.15}$$

$$\frac{d}{dt}\left[T_{abc}\cdot\begin{bmatrix} v_{ca} \\ v_{cb} \\ v_{cc} \end{bmatrix}\right] = \frac{1}{C}\left[T_{abc}\cdot\begin{bmatrix} i_a \\ i_b \\ i_c \end{bmatrix}\right] - \frac{1}{C}\left[T_{abc}\cdot\begin{bmatrix} i_x \\ i_y \\ i_z \end{bmatrix}\right] \tag{3.16}$$

Thus, the three-phase currents and voltages in the above state-space equations are in the form of (3.9) may be transformed into stationary reference frame as expressed below,

$$\frac{d}{dt}\begin{bmatrix} i_d^s \\ i_q^s \\ i_o^s \end{bmatrix} = \frac{1}{L_1}\begin{bmatrix} v_d^s \\ v_q^s \\ v_o^s \end{bmatrix} - \frac{1}{L_1}\begin{bmatrix} v_{cd}^s \\ v_{cq}^s \\ v_{co}^s \end{bmatrix} - \frac{R_1}{L_1}\begin{bmatrix} i_d^s \\ i_q^s \\ i_o^s \end{bmatrix} \tag{3.17}$$

$$\frac{d}{dt}\begin{bmatrix} i_{dg}^s \\ i_{qg}^s \\ i_{og}^s \end{bmatrix} = \frac{1}{L_2}\begin{bmatrix} v_{cd}^s \\ v_{cq}^s \\ v_{co}^s \end{bmatrix} - \frac{1}{L_2}\begin{bmatrix} e_d^s \\ e_q^s \\ e_o^s \end{bmatrix} - \frac{R_2}{L_2}\begin{bmatrix} i_{dg}^s \\ i_{qg}^s \\ i_{og}^s \end{bmatrix} \tag{3.18}$$

$$\frac{d}{dt}\begin{bmatrix} v_{cd}^{s} \\ v_{cq}^{s} \\ v_{co}^{s} \end{bmatrix} = \frac{1}{C}\begin{bmatrix} i_{d}^{s} \\ i_{q}^{s} \\ i_{o}^{s} \end{bmatrix} - \frac{1}{C}\begin{bmatrix} i_{dg}^{s} \\ i_{qg}^{s} \\ i_{og}^{s} \end{bmatrix} \tag{3.19}$$

Considering a balanced load condition and neglecting the zero-sequence component in the state-space equations (3.17), (3.18), and (3.19) result in the below expressions,

$$\frac{d}{dt}\begin{bmatrix} i_{d}^{s} \\ i_{q}^{s} \end{bmatrix} = \frac{1}{L_1}\begin{bmatrix} v_{d}^{s} \\ v_{q}^{s} \end{bmatrix} - \frac{1}{L_1}\begin{bmatrix} v_{cd}^{s} \\ v_{cq}^{s} \end{bmatrix} - \frac{R_1}{L_1}\begin{bmatrix} i_{d}^{s} \\ i_{q}^{s} \end{bmatrix} \tag{3.20}$$

$$\frac{d}{dt}\begin{bmatrix} i_{dg}^{s} \\ i_{qg}^{s} \end{bmatrix} = \frac{1}{L_2}\begin{bmatrix} v_{cd}^{s} \\ v_{cq}^{s} \end{bmatrix} - \frac{1}{L_2}\begin{bmatrix} e_{d}^{s} \\ e_{q}^{s} \end{bmatrix} - \frac{R_2}{L_2}\begin{bmatrix} i_{dg}^{s} \\ i_{qg}^{s} \end{bmatrix} \tag{3.21}$$

$$\frac{d}{dt}\begin{bmatrix} v_{cd}^{s} \\ v_{cq}^{s} \end{bmatrix} = \frac{1}{C}\begin{bmatrix} i_{d}^{s} \\ i_{q}^{s} \end{bmatrix} - \frac{1}{C}\begin{bmatrix} i_{dg}^{s} \\ i_{qg}^{s} \end{bmatrix} \tag{3.22}$$

The state variables and output parameters corresponding to theses state-space equations in time-domain are expressed in a generalized form in as shown in equation (3.24) and (3.25).

$$\dot{x} = Ax + Bu \tag{3.23}$$

$$y = Cx + Du \tag{3.24}$$

Thus, the plant model of the three-phase grid-tied inverter system is represented using two generalized equations (3.25) and (3.26). Output voltages of the three-phase inverter and voltage source of the grid have been considered as inputs to the plant model of the three-phase grid-tied inverter system in stationary reference frame. The focus of this thesis is to implement various current control strategies. Thus, stationary reference frame equivalent currents of three-phase grid source have been considered as the output of the plant model. A four input and two output system is realized using the equations (3.25) and (3.26) of the plant model. Thus, the state-space equations of this plant model are scripted in MATLAB to find the plant transfer functions of the four input and two output system.

$$\frac{d}{dt}\begin{bmatrix} i_d^s \\ i_q^s \\ i_{dg}^s \\ i_{qg}^s \\ v_{cd}^s \\ v_{cq}^s \end{bmatrix} = \begin{bmatrix} -\frac{R_1}{L_1} & 0 & 0 & 0 & -\frac{1}{L_1} & 0 \\ 0 & -\frac{R_1}{L_1} & 0 & 0 & 0 & -\frac{1}{L_1} \\ 0 & 0 & -\frac{R_2}{L_2} & 0 & \frac{1}{L_2} & 0 \\ 0 & 0 & 0 & -\frac{R_2}{L_2} & 0 & \frac{1}{L_2} \\ \frac{1}{C} & 0 & -\frac{1}{C} & 0 & 0 & 0 \\ 0 & \frac{1}{C} & 0 & -\frac{1}{C} & 0 & 0 \end{bmatrix} \begin{bmatrix} i_d^s \\ i_q^s \\ i_{dg}^s \\ i_{qg}^s \\ v_{cd}^s \\ v_{cq}^s \end{bmatrix}$$

$$+ \begin{bmatrix} \frac{1}{L_1} & 0 & 0 & 0 \\ 0 & \frac{1}{L_1} & 0 & 0 \\ 0 & 0 & -\frac{1}{L_2} & 0 \\ 0 & 0 & 0 & -\frac{1}{L_2} \\ 0 & 0 & 0 & 0 \\ 0 & 0 & 0 & 0 \end{bmatrix} \begin{bmatrix} v_d^s \\ v_q^s \\ e_d^s \\ e_q^s \end{bmatrix} \tag{3.25}$$

$$\begin{bmatrix} i_{dg}^s \\ i_{qg}^s \end{bmatrix} = \begin{bmatrix} 0 & 0 & 1 & 0 & 0 & 0 \\ 0 & 0 & 0 & 1 & 0 & 0 \end{bmatrix} \begin{bmatrix} i_d^s \\ i_q^s \\ i_{dg}^s \\ i_{qg}^s \\ v_{cd}^s \\ v_{cq}^s \end{bmatrix} + \begin{bmatrix} 0 & 0 & 0 & 0 \\ 0 & 0 & 0 & 0 \end{bmatrix} \begin{bmatrix} v_d^s \\ v_q^s \\ e_d^s \\ e_q^s \end{bmatrix} \tag{3.26}$$

These state-space equations of a three-phase grid-tied inverter are in the stationary reference frame and in time-domain. A plant model in s-domain may be realized by transforming state-space equations from time-domain to frequency domain. Thus, by applying Laplace transformation and readjusting the terms result in the equations (3.20) to (3.22).

$$\begin{bmatrix} I_d^s(s) \\ I_q^s(s) \end{bmatrix} = \frac{1}{(R_1 + L_1 s)} \begin{bmatrix} V_d^s(s) \\ V_q^s(s) \end{bmatrix} - \frac{1}{(R_1 + L_1 s)} \begin{bmatrix} V_{cd}^s(s) \\ V_{cq}^s(s) \end{bmatrix} \quad (3.27)$$

$$\begin{bmatrix} I_{dg}^s(s) \\ I_{qg}^s(s) \end{bmatrix} = \frac{1}{(R_2 + L_2 s)} \begin{bmatrix} V_{cd}^s(s) \\ V_{cq}^s(s) \end{bmatrix} - \frac{1}{(R_2 + L_2 s)} \begin{bmatrix} E_d^s(s) \\ E_q^s(s) \end{bmatrix} \quad (3.28)$$

$$\begin{bmatrix} V_{cd}^s(s) \\ V_{cq}^s(s) \end{bmatrix} = \frac{1}{Cs} \begin{bmatrix} I_d^s(s) \\ I_q^s(s) \end{bmatrix} - \frac{1}{Cs} \begin{bmatrix} I_{dg}^s(s) \\ I_{qg}^s(s) \end{bmatrix} \quad (3.29)$$

Thus, equations (3.27) to (3.29) have been used to realize the plant model shown in figure.3.4.

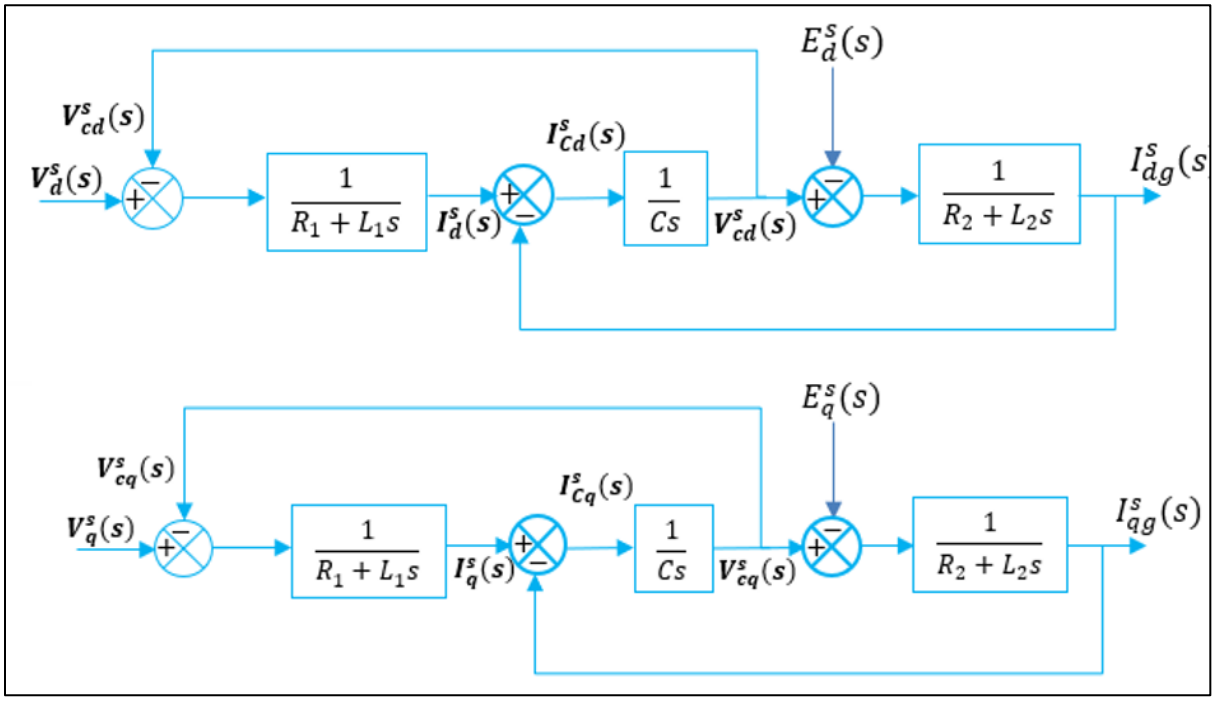

Figure.3.4. Schematic of plant model of the three-phase grid-tied inverter system in the stationary reference frame.

Thus, the plant transfer function from the plant model from the plant model shown in the figure.3.3 is expressed as,

$$\frac{I_{dg}^s(s)}{V_d^s(s)} = \frac{I_{dq}^s(s)}{V_q^s(s)} = \frac{1}{L_1 L_2 C s^3 + (R_1 L_2 + R_2 L_1) C s^2 + (R_1 R_2 C + L_1 + L_2) s + R_1 + R_2} \quad (3.30)$$

An approximation of the transfer function (3.30) by neglecting resistance of the inductors result in the equation (3.31).

$$\frac{I_{dg}^{s}(s)}{V_{d}^{s}(s)} = \frac{I_{dg}^{s}(s)}{V_{q}^{s}(s)} \approx \frac{1}{s\left(s^2 + \frac{L_1 + L_2}{L_1 L_2 C}\right)} \tag{3.31}$$

Thus, the transfer function of the plant with LCL filter is vulnerable to have a low impedance path at a resonance frequency as expressed below in equation (3.32).

$$Resonant\ Frequency,\ \omega_r = \sqrt{\frac{L_1 + L_2}{L_1 L_2 C}}\ rad/s \tag{3.32}$$

Thus, Bode plot of the transfer shown in figure.3.5 consists of a high gain in magnitude plot and a phase shift in the phase plot at a resonance frequency corresponding to the values of $L_1 = 8mH$, $L_2 = 2mH$, and $C = 15\mu F$.

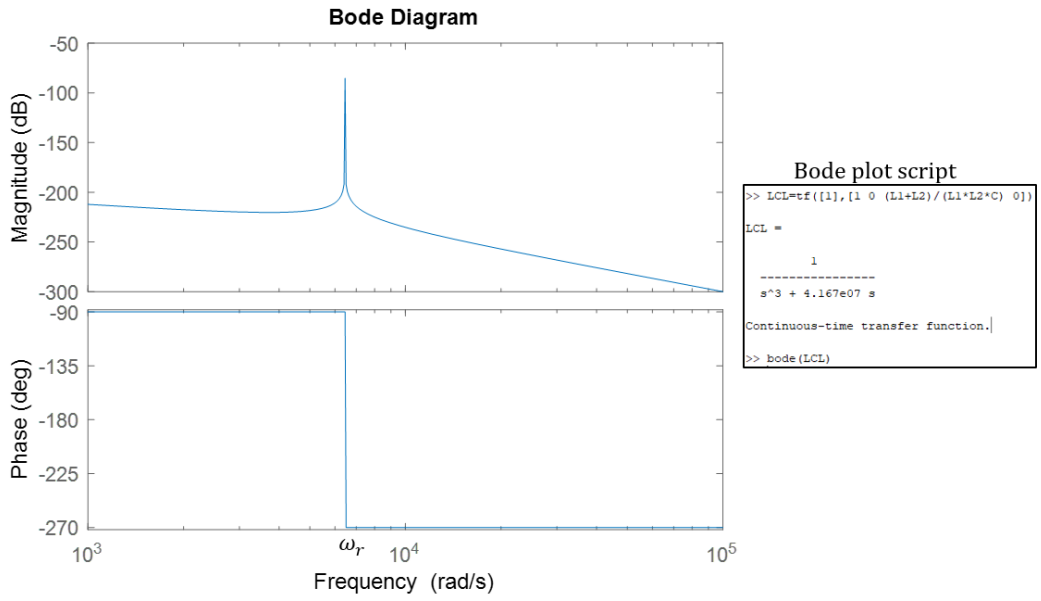

Figure.3.5. Bode plot of the LCL transfer function of the three-phase grid-tied inverter system in stationary reference frame.

A damping control strategy has been analyzed to damp the resonance caused by LCL parameters. A damping controller has been embedded with the plant model in the figure.3.4. The current through the capacitor has been controlled through a proportional controller as shown in the figure.3.6.

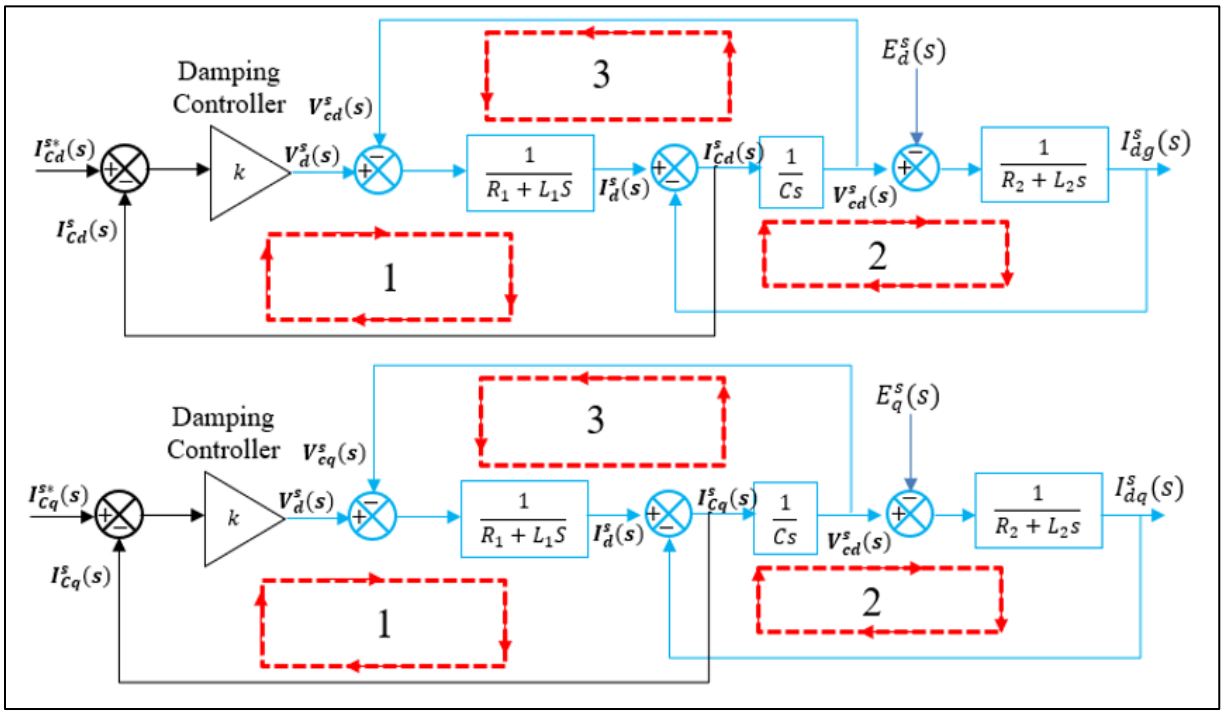

Figure.3.6. Schematic of damping controller embedded with plant model of the three-phase grid-tied inverter system in the stationary reference frame.

Thus, the transfer functions considering the damping controller in the figure.3.6 are expressed as,

$$\frac{I^s_{dg}(s)}{I^{s*}_{cd}(s)} = \frac{I^s_{dq}(s)}{I^{s*}_{cq}(s)} = \frac{k}{L_1 L_2 C s^3 + (kL_2 + R_1 L_2 + R_2 L_1) C s^2 + (R_1 R_2 C + kR_2 C + L_1 + L_2) s + R_1 + R_2} \tag{3.33}$$

$$\frac{I_{dg}^{s}(s)}{V_{d}^{s}(s)} = \frac{I_{dq}^{s}(s)}{V_{q}^{s}(s)} = \frac{1}{L_1L_2Cs^3 + (kL_2 + R_1L_2 + R_2L_1)Cs^2 + (R_1R_2C + kR_2C + L_1 + L_2)s + R_1 + R_2} \quad (3.34)$$

The Bode plot of the transfer function (3.34) with damping controller has been compared with the Bode plot of the LCL transfer function (3.31) as shown in figure.3.7.

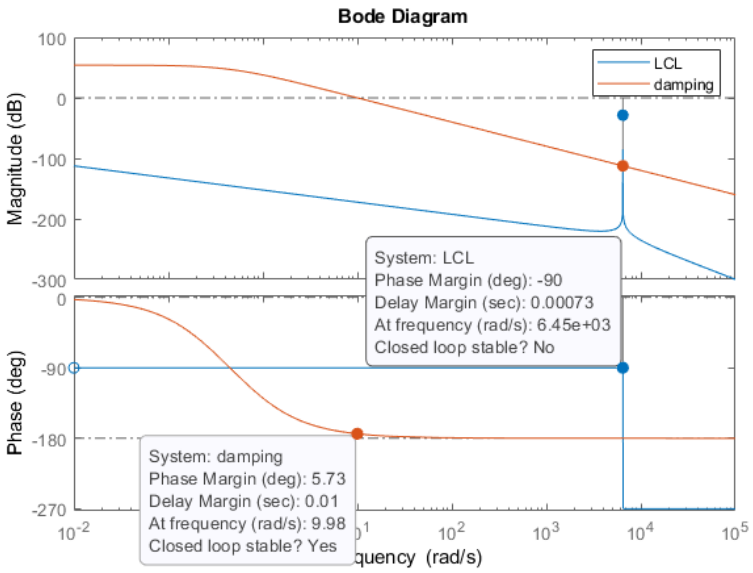

Figure.3.7. Bode plots of the plant model three-phase grid-tied inverter system with and without damping controller in the stationary reference frame.

A spike in gain due to the resonance may cause the system to operate in unstable mode. Thus, higher gain at frequencies other than grid frequencies is avoided by considering a damping control strategy. The plant transfer function with damping controller is embedded with a proportional-integral controller to implement a closed loop current control strategy in the stationary reference frame (St-PI) as shown in the figure.3.8. Considering the loop 1, loop 2, and loop 3 of the closed-loop control diagram, an open-loop transfer function is realized. This transfer function has been analyzed for different values of control parameters to identify the stability margins of the closed-

loop St-PI control strategy. This open-loop transfer function has been used to derive a closed-loop transfer function. The open-loop transfer function and closed-loop transfer function of the St-PI current control strategy are expressed in equations (3.35) and (3.36).

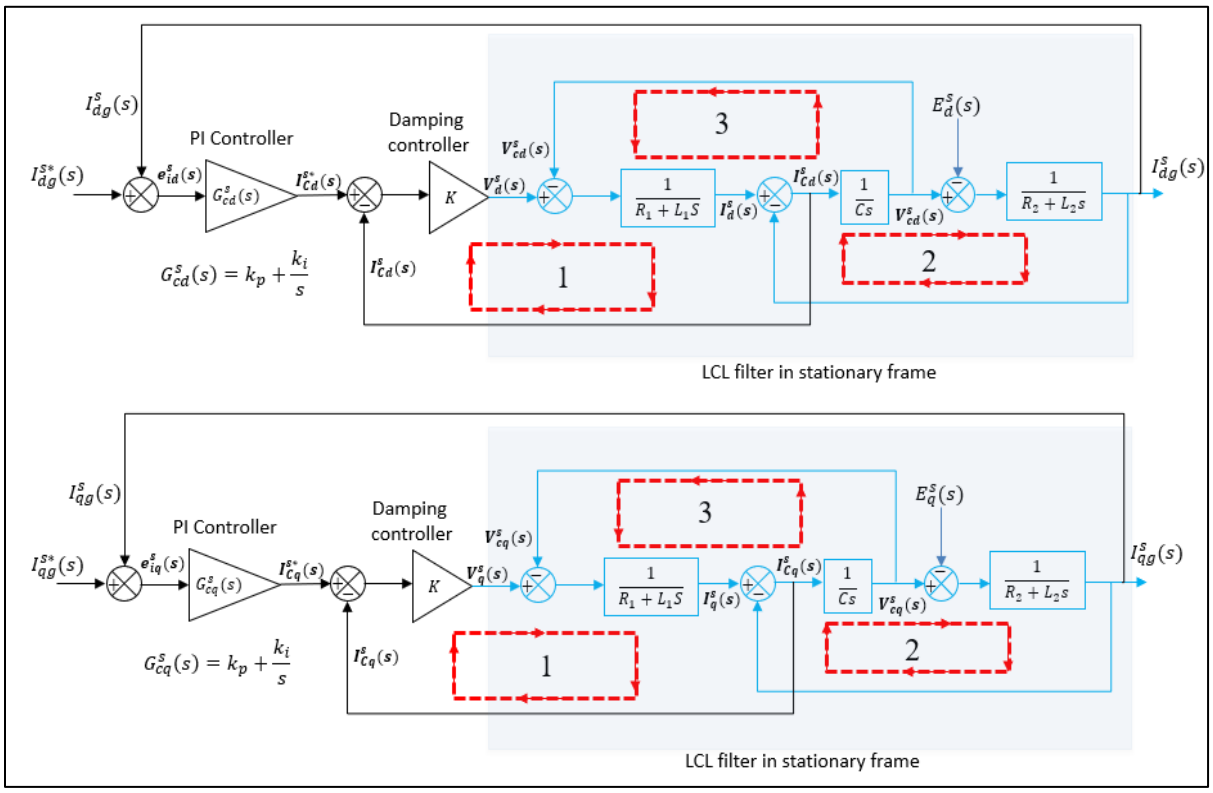

Figure.3.8. Schematic of the closed-loop St-PI current control strategy of a three-phase grid-tied inverter system.

Open-loop transfer function (OLTF) of the St-PI current control strategy has been expressed as,

$$\frac{e_{id}^{s}(s)}{I_{dg}^{s}(s)} = \frac{e_{iq}^{s}(s)}{I_{qg}^{s}(s)} = \frac{k_p k s + k_i k}{L_1 L_2 C s^3 + (kL_2 + R_1 L_2 + R_2 L_1) C s^2 + (R_1 R_2 C + k R_2 C + L_1 + L_2) s + R_1 + R_2} \quad (3.35)$$

Closed-loop transfer function (CLTF) of the St-PI current control strategy has been expressed as,

$$\frac{I_{dg}^{s}(s)}{I_{dg}^{s*}(s)} = \frac{\text{OLTF}}{1 + \text{OLTF}} \tag{3.36}$$

Bode plot of the transfer functions has been analyzed for the values of LCL and control parameters listed in table.3.2.

TABLE.3.1. SPECIFICATION OF LCL FILTER AND CONTROL PARAMETERS

L_1 (mH)	R_1 $(m\Omega)$	L_2 (mH)	R_2 $(m\Omega)$	C (μf)	k_p	k_i	k
8	1	2	1	15	0.5	50	1

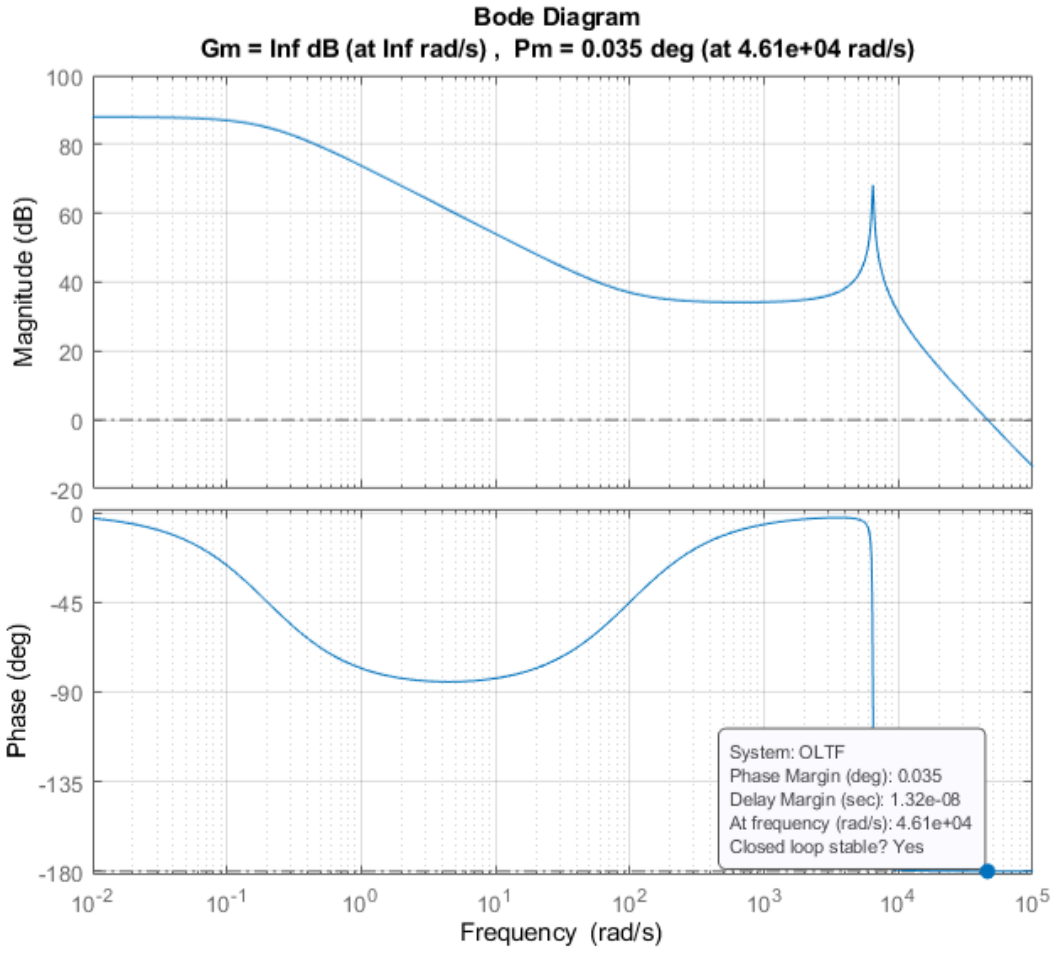

Figure.3.9. Bode plots of the plant model three-phase grid-tied inverter system with and without damping controller in the stationary reference frame.

Thus, closed-loop St-PI current control strategy has an infinite gain margin and a phase margin of 0.035 degrees. The phase-cross over frequency doesn't exists because of the phase never crossed the limit of -180 degrees which led to an infinite gain margin. Validation of the St-PI current regulation strategy using PSIM simulations and control hardware in loop is discussed in Chapter 5 and Chapter 6.

3.3. Synchronous Reference Frame Proportional Integral Controller (Sy-PI)

A closed-loop current control strategy employing synchronous reference frame proportional-integral controller (Sy-PI) is discussed in this section. The transformation of the three-phase functions into the stationary reference frame has been presented in the previous section. The voltage and current signals in the stationary reference frame are time-varying and difficult to track. Another transformation of these signals into a synchronous reference frame is presented in this section. Rotating reference frame is also called as synchronous reference frame by considering the rotation of the vectors at system frequency.

A generalized form of the synchronous reference frame functions may be expressed as,

$$\begin{bmatrix} x_d^s \\ x_q^s \end{bmatrix} = T^{-1} \begin{bmatrix} x_d^e \\ x_q^e \end{bmatrix} \tag{3.37}$$

Where, 'T' is a time dependent matrix called as Park's transformation matrix,

$$T = \begin{bmatrix} \cos\theta & -\sin\theta \\ \sin\theta & \cos\theta \end{bmatrix} \tag{3.38}$$

Thus, by applying generalized form of the synchronous reference frame equation (3.37) to the state-space equations of stationary reference frame in the time-domain (3.20) to (3.22) result in the following expressions,

$$\frac{d}{dt}\left[T^{-1} \cdot \begin{bmatrix} i_d^e \\ i_q^e \end{bmatrix}\right] = \frac{1}{L_1}\left[T^{-1} \cdot \begin{bmatrix} v_d^e \\ v_q^e \end{bmatrix}\right] - \frac{1}{L_1}\left[T^{-1} \cdot \begin{bmatrix} v_{cd}^e \\ v_{cq}^e \end{bmatrix}\right] - \frac{R_1}{L_1}\left[T^{-1} \cdot \begin{bmatrix} i_d^e \\ i_q^e \end{bmatrix}\right] \tag{3.39}$$

$$\frac{d}{dt}\left[T^{-1}\cdot\begin{bmatrix} i_{dg}^{e} \\ i_{qg}^{e}\end{bmatrix}\right]=\frac{1}{L_2}\left[T^{-1}\cdot\begin{bmatrix} v_{cd}^{e} \\ v_{cq}^{e}\end{bmatrix}\right]-\frac{1}{L_2}\left[T^{-1}\cdot\begin{bmatrix} e_{d}^{e} \\ e_{q}^{e}\end{bmatrix}\right]-\frac{R_2}{L_2}\left[T^{-1}\cdot\begin{bmatrix} i_{dg}^{e} \\ i_{qg}^{e}\end{bmatrix}\right] \tag{3.40}$$

$$\frac{d}{dt}\left[T^{-1}\cdot\begin{bmatrix} v_{cd}^{e} \\ v_{cq}^{e}\end{bmatrix}\right]=\frac{1}{C}\left[T^{-1}\cdot\begin{bmatrix} i_{d}^{e} \\ i_{q}^{e}\end{bmatrix}\right]-\frac{1}{C}\left[T^{-1}\cdot\begin{bmatrix} i_{dg}^{e} \\ i_{qg}^{e}\end{bmatrix}\right] \tag{3.41}$$

Multiplying the above equations (3.39) to (3.41) with the with the time-dependent transformation matrix T results in expressions (3.42) to (3.44) given below,

$$T\cdot\frac{d}{dt}\left[T^{-1}\cdot\begin{bmatrix} i_{d}^{e} \\ i_{q}^{e}\end{bmatrix}\right]=\frac{1}{L_1}\left[T\cdot T^{-1}\cdot\begin{bmatrix} v_{d}^{e} \\ v_{q}^{e}\end{bmatrix}\right]-\frac{1}{L_1}\left[T\cdot T^{-1}\cdot\begin{bmatrix} v_{cd}^{e} \\ v_{cq}^{e}\end{bmatrix}\right]-\frac{R_1}{L_1}\left[T\cdot T^{-1}\cdot\begin{bmatrix} i_{d}^{e} \\ i_{q}^{e}\end{bmatrix}\right] \tag{3.39}$$

$$T\cdot\frac{d}{dt}\left[T^{-1}\cdot\begin{bmatrix} i_{dg}^{e} \\ i_{qg}^{e}\end{bmatrix}\right]=\frac{1}{L_2}\left[T\cdot T^{-1}\cdot\begin{bmatrix} v_{cd}^{e} \\ v_{cq}^{e}\end{bmatrix}\right]-\frac{1}{L_2}\left[T\cdot T^{-1}\cdot\begin{bmatrix} e_{d}^{e} \\ e_{q}^{e}\end{bmatrix}\right]-\frac{R_2}{L_2}\left[T\cdot T^{-1}\cdot\begin{bmatrix} i_{dg}^{e} \\ i_{qg}^{e}\end{bmatrix}\right] \tag{3.40}$$

$$T\cdot\frac{d}{dt}\left[T^{-1}\cdot\begin{bmatrix} v_{cd}^{e} \\ v_{cq}^{e}\end{bmatrix}\right]=\frac{1}{C}\left[T\cdot T^{-1}\cdot\begin{bmatrix} i_{d}^{e} \\ i_{q}^{e}\end{bmatrix}\right]-\frac{1}{C}\left[T\cdot T^{-1}\cdot\begin{bmatrix} i_{dg}^{e} \\ i_{qg}^{e}\end{bmatrix}\right] \tag{3.41}$$

Multiplication of the matrix T by inverse of it results in identity matrix,

$$T\cdot T^{-1}=\begin{bmatrix}\cos\theta & -\sin\theta \\ \sin\theta & \cos\theta\end{bmatrix}\begin{bmatrix}\cos\theta & \sin\theta \\ -\sin\theta & \cos\theta\end{bmatrix}=\begin{bmatrix}1 & 0 \\ 0 & 1\end{bmatrix}=I \tag{3.42}$$

Thus, by replacing the term $T\cdot T^{-1}$ with an identity matrix in equations (3.39) to (3.41) result in the following expressions,

$$T\cdot\frac{d}{dt}\left[T^{-1}\cdot\begin{bmatrix} i_{d}^{e} \\ i_{q}^{e}\end{bmatrix}\right]=\frac{1}{L_1}\begin{bmatrix} v_{d}^{e} \\ v_{q}^{e}\end{bmatrix}-\frac{1}{L_1}\begin{bmatrix} v_{cd}^{e} \\ v_{cq}^{e}\end{bmatrix}-\frac{R_1}{L_1}\begin{bmatrix} i_{d}^{e} \\ i_{q}^{e}\end{bmatrix} \tag{3.39}$$

$$T\cdot\frac{d}{dt}\left[T^{-1}\cdot\begin{bmatrix} i_{dg}^{e} \\ i_{qg}^{e}\end{bmatrix}\right]=\frac{1}{L_2}\begin{bmatrix} v_{cd}^{e} \\ v_{cq}^{e}\end{bmatrix}-\frac{1}{L_2}\begin{bmatrix} e_{d}^{e} \\ e_{q}^{e}\end{bmatrix}-\frac{R_2}{L_2}\begin{bmatrix} i_{dg}^{e} \\ i_{qg}^{e}\end{bmatrix} \tag{3.40}$$

$$T\cdot\frac{d}{dt}\left[T^{-1}\cdot\begin{bmatrix} v_{cd}^{e} \\ v_{cq}^{e}\end{bmatrix}\right]=\frac{1}{C}\begin{bmatrix} i_{d}^{e} \\ i_{q}^{e}\end{bmatrix}-\frac{1}{C}\begin{bmatrix} i_{dg}^{e} \\ i_{qg}^{e}\end{bmatrix} \tag{3.41}$$

The transformation matrix T is a time-dependent matrix because$\theta = \omega t$. The time dependent terms in the derivative part of the equation have to be simplified. Thus, a generalized form of the term in left-hand side term of the equations (3.39) to (3.41) is expressed as,

$$T \cdot \frac{d}{dt}\left[T^{-1} \cdot \begin{bmatrix} x_d^e \\ x_q^e \end{bmatrix}\right] = T \cdot \frac{d}{dt}[T^{-1}] \cdot \begin{bmatrix} x_d^e \\ x_q^e \end{bmatrix} + T \cdot T^{-1} \frac{d}{dt}\begin{bmatrix} x_d^e \\ x_q^e \end{bmatrix} \tag{3.42}$$

Thus, by substituting the time dependent elements of the transformation matrix T result in the expression (3.43).

$$T \cdot \frac{d}{dt}\left[T^{-1} \cdot \begin{bmatrix} x_d^e \\ x_q^e \end{bmatrix}\right] = \begin{bmatrix} \cos\ \omega t & -\sin \omega t \\ \sin \omega t & \cos\ \omega t \end{bmatrix} \cdot \frac{d}{dt}\begin{bmatrix} \cos\ \omega t & \sin \omega t \\ -\sin \omega t & \cos\ \omega t \end{bmatrix} \cdot \begin{bmatrix} x_d^e \\ x_q^e \end{bmatrix} + \frac{d}{dt}\begin{bmatrix} x_d^e \\ x_q^e \end{bmatrix} \tag{3.43}$$

Thus, simplifying the equation (3.43) results in the expression (3.44).

$$T \cdot \frac{d}{dt}\left[T^{-1} \cdot \begin{bmatrix} x_d^e \\ x_q^e \end{bmatrix}\right] = \begin{bmatrix} 0 & \omega \\ -\omega & 0 \end{bmatrix}\begin{bmatrix} x_d^e \\ x_q^e \end{bmatrix} + \frac{d}{dt}\begin{bmatrix} x_d^e \\ x_q^e \end{bmatrix} \tag{3.44}$$

Applying the result of this generalized form to the equations (3.39) to (3.41) result in the expressions (3.45) to (3.47).

$$\frac{d}{dt}\begin{bmatrix} i_d^e \\ i_q^e \end{bmatrix} = \frac{1}{L_1}\begin{bmatrix} v_d^e \\ v_q^e \end{bmatrix} - \frac{1}{L_1}\begin{bmatrix} v_{cd}^e \\ v_{cq}^e \end{bmatrix} - \frac{R_1}{L_1}\begin{bmatrix} i_d^e \\ i_q^e \end{bmatrix} - \begin{bmatrix} 0 & \omega \\ -\omega & 0 \end{bmatrix}\begin{bmatrix} i_d^e \\ i_q^e \end{bmatrix} \tag{3.45}$$

$$\frac{d}{dt}\begin{bmatrix} i_{dg}^e \\ i_{qg}^e \end{bmatrix} = \frac{1}{L_2}\begin{bmatrix} v_{cd}^e \\ v_{cq}^e \end{bmatrix} - \frac{1}{L_2}\begin{bmatrix} e_d^e \\ e_q^e \end{bmatrix} - \frac{R_2}{L_2}\begin{bmatrix} i_{dg}^e \\ i_{qg}^e \end{bmatrix} - \begin{bmatrix} 0 & \omega \\ -\omega & 0 \end{bmatrix}\begin{bmatrix} i_{dg}^e \\ i_{qg}^e \end{bmatrix} \tag{3.46}$$

$$\frac{d}{dt}\begin{bmatrix} v_{cd}^e \\ v_{cq}^e \end{bmatrix} = \frac{1}{C}\begin{bmatrix} i_d^e \\ i_q^e \end{bmatrix} - \frac{1}{C}\begin{bmatrix} i_{dg}^e \\ i_{qg}^e \end{bmatrix} - \begin{bmatrix} 0 & \omega \\ -\omega & 0 \end{bmatrix}\begin{bmatrix} v_{cd}^e \\ v_{cq}^e \end{bmatrix} \tag{3.47}$$

Thus, the state variables of state-space equations in the synchronous reference frame result in a pair of cross couplings in each equation. These equations are expressed in a generalized form of (3.23) and (3.24) to realize a plant model of the three-phase grid-tied inverter system in the synchronous reference frame. The state-space equations of plant model in the synchronous reference frame have to be transformed from time-domain into frequency or s-domain to realize

the schematic of the plant model. This plant model in the synchronous reference frame is used to analyze the current control strategy. Thus, the generalized form of the plant model of the three-phase grid-tied inverter is expressed as,

$$\frac{d}{dt}\begin{bmatrix} i_d^e \\ i_q^e \\ i_{dg}^e \\ i_{qg}^e \\ v_{cd}^e \\ v_{cq}^e \end{bmatrix} = \begin{bmatrix} -\frac{R_1}{L_1} & -\omega & 0 & 0 & -\frac{1}{L_1} & 0 \\ \omega & -\frac{R_1}{L_1} & 0 & 0 & 0 & -\frac{1}{L_1} \\ 0 & 0 & -\frac{R_2}{L_2} & -\omega & \frac{1}{L_2} & 0 \\ 0 & 0 & \omega & -\frac{R_2}{L_2} & 0 & \frac{1}{L_2} \\ \frac{1}{C} & 0 & -\frac{1}{C} & 0 & 0 & -\omega \\ 0 & \frac{1}{C} & 0 & -\frac{1}{C} & \omega & 0 \end{bmatrix} \begin{bmatrix} i_d^e \\ i_q^e \\ i_{dg}^e \\ i_{qg}^e \\ v_{cd}^e \\ v_{cq}^e \end{bmatrix} + \begin{bmatrix} \frac{1}{L_1} & 0 & 0 & 0 \\ 0 & \frac{1}{L_1} & 0 & 0 \\ 0 & 0 & -\frac{1}{L_2} & 0 \\ 0 & 0 & 0 & -\frac{1}{L_2} \\ 0 & 0 & 0 & 0 \\ 0 & 0 & 0 & 0 \end{bmatrix} \begin{bmatrix} v_d^e \\ v_q^e \\ e_d^e \\ e_q^e \end{bmatrix} \tag{3.48}$$

$$\begin{bmatrix} i_{dg}^e \\ i_{qg}^e \end{bmatrix} = \begin{bmatrix} 0 & 0 & 1 & 0 & 0 & 0 \\ 0 & 0 & 0 & 1 & 0 & 0 \end{bmatrix} \begin{bmatrix} i_d^e \\ i_q^e \\ i_{dg}^e \\ i_{qg}^e \\ v_{cd}^e \\ v_{cq}^e \end{bmatrix} + \begin{bmatrix} 0 & 0 & 0 & 0 \\ 0 & 0 & 0 & 0 \end{bmatrix} \begin{bmatrix} v_d^e \\ v_q^e \\ e_d^e \\ e_q^e \end{bmatrix} \tag{3.49}$$

Transforming the state-space equations (3.45), (3.46), and (3.47) into s-domain result in the equations (3.50), (3.51), and (3.52).

$$s\begin{bmatrix} I_d^e(s) \\ I_q^e(s) \end{bmatrix} = \frac{1}{L_1}\begin{bmatrix} V_d^e(s) \\ V_q^e(s) \end{bmatrix} - \frac{1}{L_1}\begin{bmatrix} V_{cd}^e(s) \\ V_{cq}^e(s) \end{bmatrix} - \frac{R_1}{L_1}\begin{bmatrix} I_d^e(s) \\ I_q^e(s) \end{bmatrix} - \begin{bmatrix} 0 & \omega \\ -\omega & 0 \end{bmatrix}\begin{bmatrix} I_d^e(s) \\ I_q^e(s) \end{bmatrix} \tag{3.50}$$

$$s\begin{bmatrix} I_{dg}^{e}(s) \\ I_{qg}^{e}(s) \end{bmatrix} = \frac{1}{L_2}\begin{bmatrix} V_{cd}^{e}(s) \\ V_{cq}^{e}(s) \end{bmatrix} - \frac{1}{L_2}\begin{bmatrix} E_{d}^{e}(s) \\ E_{q}^{e}(s) \end{bmatrix} - \frac{R_2}{L_2}\begin{bmatrix} I_{dg}^{e}(s) \\ I_{qg}^{e}(s) \end{bmatrix} - \begin{bmatrix} 0 & \omega \\ -\omega & 0 \end{bmatrix}\begin{bmatrix} I_{dg}^{e}(s) \\ I_{qg}^{e}(s) \end{bmatrix} \tag{3.51}$$

$$s\begin{bmatrix} V_{cd}^{e}(s) \\ V_{cq}^{e}(s) \end{bmatrix} = \frac{1}{C}\begin{bmatrix} I_{d}^{e}(s) \\ I_{q}^{e}(s) \end{bmatrix} - \frac{1}{C}\begin{bmatrix} I_{dg}^{e}(s) \\ I_{qg}^{e}(s) \end{bmatrix} - \begin{bmatrix} 0 & \omega \\ -\omega & 0 \end{bmatrix}\begin{bmatrix} V_{cd}^{e}(s) \\ V_{cq}^{e}(s) \end{bmatrix} \tag{3.52}$$

These equations (3.50), (3.51), and (3.52) in s-domain are synthesized into individual equations (3.53) to (3.58) to realize the plant model. Thus, the state-space equations corresponding to each state-variable of plant model are expressed as,

$$I_{d}^{e}(s) = \frac{1}{R_1 + L_1 s}\Big(\Big(V_{d}^{e}(s) - V_{q}^{e}(s)\Big) - \omega L_1 I_{q}^{e}(s)\Big) \tag{3.53}$$

$$I_{q}^{e}(s) = \frac{1}{R_1 + L_1 s}\Big(\Big(V_{d}^{e}(s) - V_{q}^{e}(s)\Big) + \omega L_1 I_{d}^{e}(s)\Big) \tag{3.54}$$

$$I_{dg}^{e}(s) = \frac{1}{R_2 + L_2 s}\Big(\Big(V_{cd}^{e}(s) - E_{d}^{e}(s)\Big) - \omega L_2 I_{qg}^{e}(s)\Big) \tag{3.55}$$

$$I_{qg}^{e}(s) = \frac{1}{R_2 + L_2 s}\Big(\Big(V_{cq}^{e}(s) - E_{q}^{e}(s)\Big) + \omega L_2 I_{dg}^{e}(s)\Big) \tag{3.56}$$

$$V_{cd}^{e}(s) = \frac{1}{Cs}\Big(\Big(I_{d}^{e}(s) - I_{dg}^{e}(s)\Big) - \omega C V_{cq}^{e}(s)\Big) \tag{3.57}$$

$$V_{cq}^{e}(s) = \frac{1}{Cs}\Big(\Big(I_{q}^{e}(s) - I_{qg}^{e}(s)\Big) - \omega C V_{cd}^{e}(s)\Big) \tag{3.58}$$

A plant model is realized from the state-space equations (3.53) to (3.58) is shown in the figure.3.10. The schematic of plant model shown in the figure.3.9 consists of three parts derived from the equations (3.53) & (3.54), (3.57) & (3.58), and (3.55) & (3.56). Thus, the three-phase grid-tied inverter with an LCL filter in synchronous reference frame consists of multiple cross couplings. The plant model is a four input and two output system. A damping controller consists of capacitor current as feedback is required to be embedded with this plant transfer function to provide high impedance path to the signals at the resonance frequency due to energy storage

elements. Thus, a proportional-integral controller is embedded with the model consists of a plant and damping controller as shown in the figure.3.11.

Thus, Sy-PI current control strategy for a grid-tied inverter with an LCL filter consists of multiple cross-couplings in the plant model. Realization of the overall transfer function in this form is complex because it is a four-input and two output closed-loop control system with multiple cross-couplings in the plant model. The plant model in the stationary reference frame as shown in figure.3.12 consists of no cross-couplings. A simple approach to realizing Sy-PI control is by transforming the proportional-integral controller from a synchronous reference frame to a stationary reference frame. Thus, stationary reference frame equivalence of proportional-integral controller in synchronous reference frame may be embedded with damping controller and plant model with no cross-couplings in the stationary reference frame.

The proportional-integral controller in the closed-loop schematic of the figure.3.10 may be expressed as,

$$G_c^e(s) = \begin{bmatrix} G_{cd}^e(s) & 0 \\ 0 & G_{cq}^e(s) \end{bmatrix} = \begin{bmatrix} k_p + k_i/s & 0 \\ 0 & k_p + k_i/s \end{bmatrix} \tag{3.59}$$

This proportional-integral controller transfer function is in the synchronous reference frame. Any transfer function of s-domain in the synchronous reference frame may be transformed into stationary reference frame by applying the following expression [25].

$$G_c^s(s) = \frac{1}{2}\begin{bmatrix} G_{cd}^e(s+j\omega) + G_{cd}^e(s-j\omega) & jG_{cd}^e(s+j\omega) - jG_{cd}^e(s-j\omega) \\ -jG_{cd}^e(s+j\omega) + jG_{cd}^e(s-j\omega) & G_{cq}^e(s+j\omega) + G_{cd}^e(s-j\omega) \end{bmatrix} \tag{3.60}$$

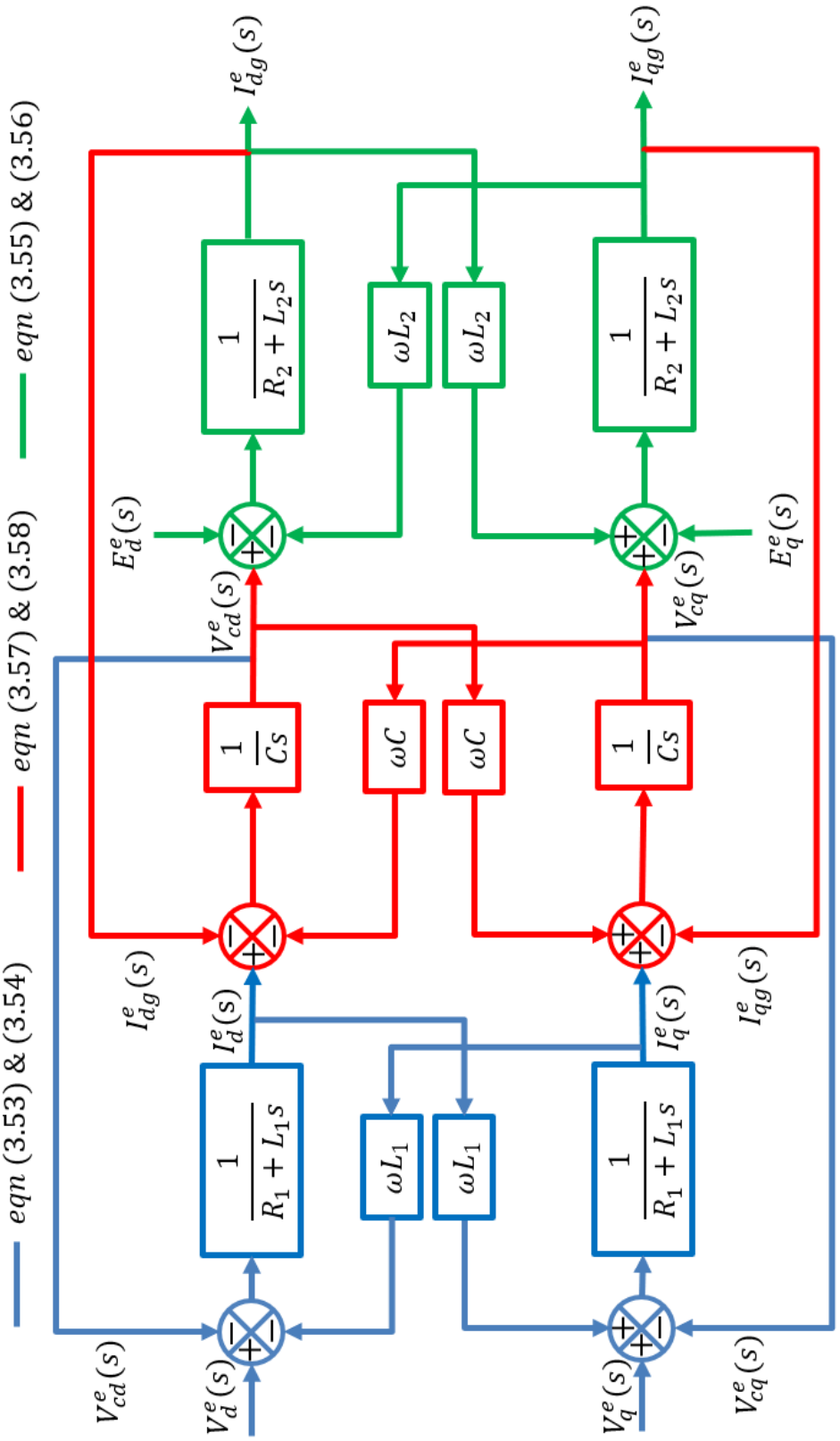

Figure.3.10. Schematic of the plant model of a grid-tied inverter with LCL filter in synchronous reference frame.

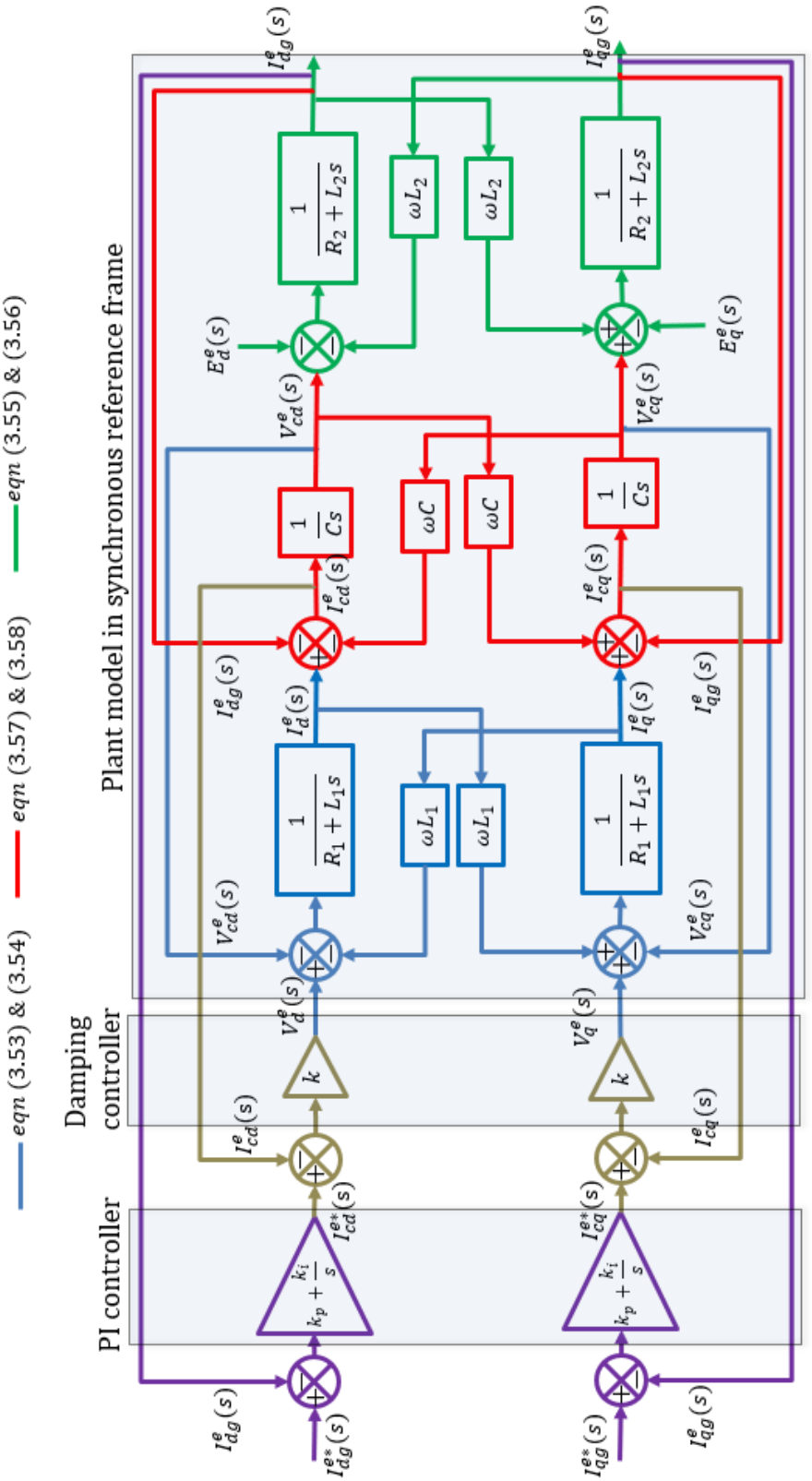

Figure.3.11. Schematic of control block diagram of proportional integral controller, damping controller, and plant model of a grid-tied inverter with LCL filter in synchronous reference frame.

Thus, Thus, substituting $(s+j\omega)$ and $(s-j\omega)$ terms in (3.59) and by applying (3.60) result in the following expression.

$$G_c^s(s)=\frac{1}{2}\begin{bmatrix} k_p+\frac{k_i}{s+j\omega}+k_p+\frac{k_i}{s-j\omega} & k_p+\frac{k_i}{s+j\omega}-k_p-\frac{k_i}{s-j\omega} \\ k_p+\frac{k_i}{s+j\omega}-k_p-\frac{k_i}{s-j\omega} & k_p+\frac{k_i}{s+j\omega}+k_p+\frac{k_i}{s-j\omega} \end{bmatrix} \tag{3.61}$$

A simplified form of the above expression (3.60) result in an expression with no zero elements inside the matrix of controller transfer function.

$$G_c^s(s)=\begin{bmatrix} G_{cdd}^s(s) & G_{cdq}^s(s) \\ G_{cqd}^s(s) & G_{cqq}^s(s) \end{bmatrix}=\begin{bmatrix} k_p+k_i\frac{s}{s^2+\omega^2} & k_i\frac{s}{s^2+\omega^2} \\ -k_i\frac{s}{s^2+\omega^2} & k_p+k_i\frac{s}{s^2+\omega^2} \end{bmatrix} \tag{3.62}$$

Therefore, a stationary reference frame equivalence of Sy-PI current control strategy consists of cross-couplings in the controller section and no cross-couplings in the plant model as shown in the figure.3.12. The forward path transfer function and cross-coupling transfer function of the stationary reference frame equivalence of Sy-PI current control strategy may be expressed as,

$$\frac{I_{dg}^s(s)}{e_{id}^s(s)}=\frac{I_{qg}^s(s)}{e_{iq}^s(s)}=\frac{k_pks^2+k_iks+k_pk\omega^2}{b_5s^5+b_4s^4+b_3s^3+b_2s^2+b_1s+b_0} \tag{3.63}$$

$$\frac{I_{dg}^s(s)}{e_{iq}^s(s)}=-\frac{I_{qg}^s(s)}{e_{id}^s(s)}=\frac{k_iks}{b_5s^5+b_4s^4+b_3s^3+b_2s^2+b_1s+b_0} \tag{3.64}$$

Where,

$$\mathrm{b}_5=L_1L_2C \tag{3.65}$$

$$\mathrm{b}_4=L_1CR_2+L_2C(R_1+k) \tag{3.66}$$

$$\mathrm{b}_3=L_1+L_2+CR_2(R_1+k)+L_1L_2C\omega^2 \tag{3.67}$$

$$\mathrm{b}_2=R_1+R_2+(L_1CR_2+L_2C(R_1+k))\omega^2 \tag{3.68}$$

$$\mathrm{b}_1=(L_1+L_2+CR_2(R_1+k))\omega^2 \tag{3.69}$$

$$\mathrm{b}_0=(R_1+R_2)\,\omega^2 \tag{3.70}$$

The stability analysis for the forwardpath tarnsfer functions is discussed in the section 3.6.

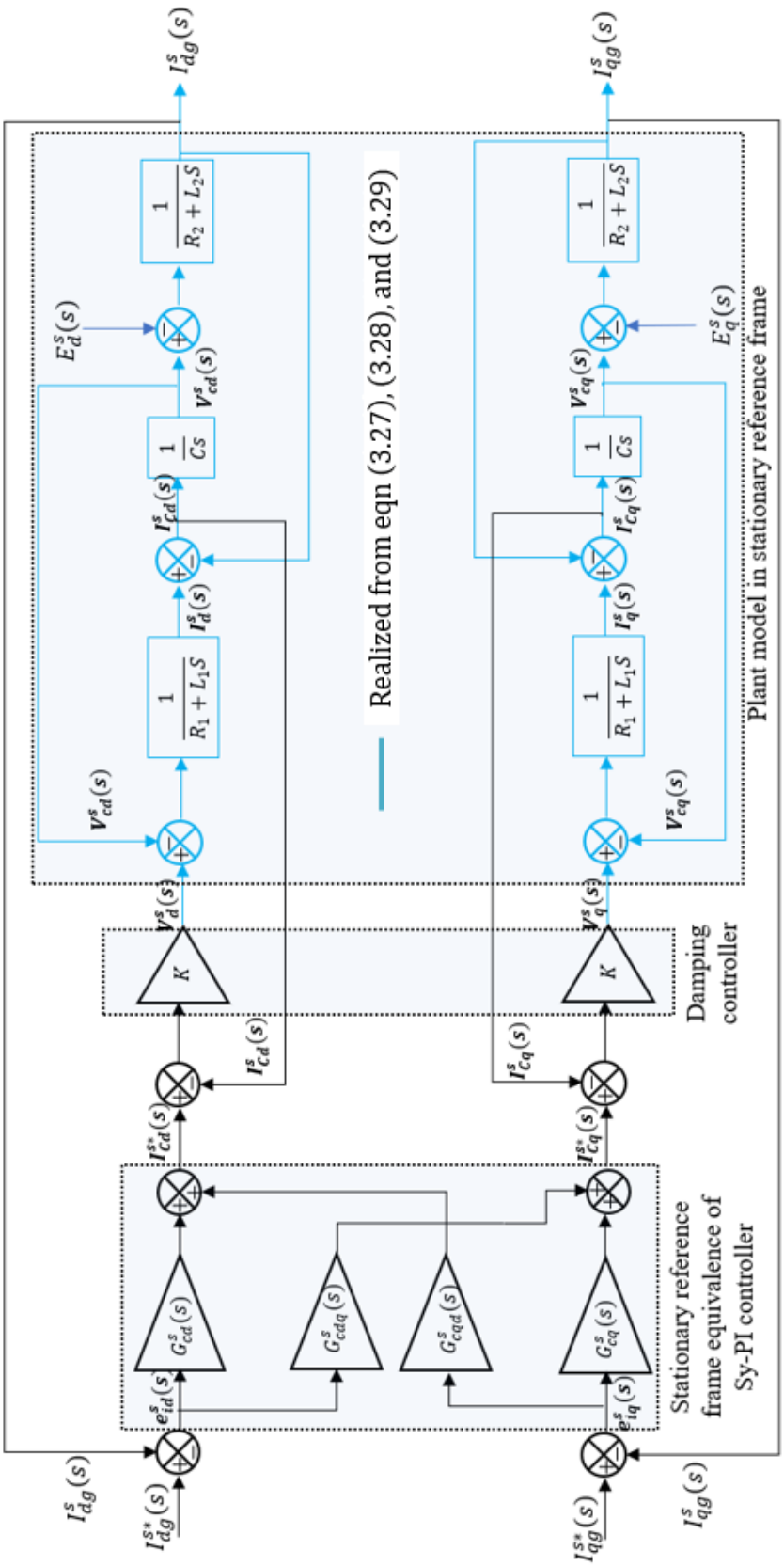

Figure.3.12. Schematic of stationary reference frame equivalence of Sy-PI controller, damping controller, and plant model of the grid-tied inverter with LCL filter.

3.4. Stationary Reference Frame Regulation of Synchronous Reference Frame Proportional Integral Controller (St/Sy-PI)

A PI current control strategy in [22] for motor control applications has a blend of synchronous reference frame current controller and stationary reference frame current controller. Index matrices $T_I(\theta)$ and $T_V(\theta)$ have to be set in a specific syntax to operate in a respective reference frame. In this section, this same control strategy has been applied to a grid-tied inverter with an LCL filter to a grid-tied inverter. A schematic of this control strategy is shown in the figure.3.13. The configuration of index matrices of the respective reference frames employing the current control strategy has been listed in the table.3.2.

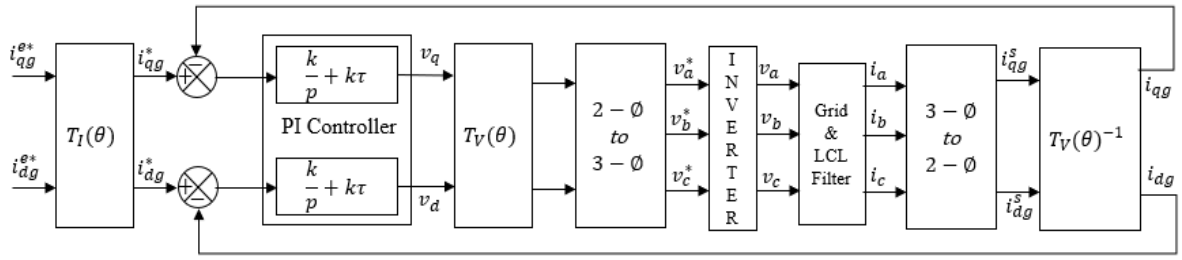

Figure.3.13. Schematic of closed loop St/Sy-PI current control strategy for a grid tied inverter with an LCL filter.

TABLE 3.2:CONFIGURATION OF INDEX MATRICES

	Stationary Regulator	Synchronous Regulator
$T(\theta)$	$\begin{bmatrix} cos\theta & sin\theta \\ -sin\theta & cos\theta \end{bmatrix}$	
$T_I(\theta)$	$T(\theta)^{-1}$	$\begin{bmatrix} 1 & 0 \\ 0 & 1 \end{bmatrix}$
$T_V(\theta)$	$\begin{bmatrix} 1 & 0 \\ 0 & 1 \end{bmatrix}$	$T(\theta)^{-1}$

Where, $\theta = \omega t$. Considering the closed-loop current control strategy as shown in the figure.3.13, generalized q-axis and d-axis voltages may be expressed in the time-domain for a stationary or synchronous current regulator may be expressed as,

$$\begin{bmatrix} v_q \\ v_d \end{bmatrix} = \left(k\tau + \frac{k}{p}\right)\begin{bmatrix} i_{qg}^{*} - i_{qg} \\ i_{dg}^{*} - i_{dg} \end{bmatrix} \tag{3.71}$$

Where, $'p'$ is a differential operator. Synchronous reference frame q-axis and d-axis voltages may be expressed as,

$$\begin{bmatrix} v_q^e \\ v_d^e \end{bmatrix} = \left(k\tau + \frac{k}{p}\right)\begin{bmatrix} i_{qg}^{\mathrm{e}*} - i_{qg}^{\mathrm{e}} \\ i_{dg}^{\mathrm{e}*} - i_{dg}^{\mathrm{e}} \end{bmatrix} \tag{3.72}$$

The equation (3.72) is modified to express in term of a generalized auxiliary function as in the equation (3.73)

$$\begin{bmatrix} v_q^e \\ v_d^e \end{bmatrix} = k\tau\begin{bmatrix} i_{qg}^{\mathrm{e}*} - i_{qg}^{\mathrm{e}} \\ i_{dg}^{\mathrm{e}*} - i_{dg}^{\mathrm{e}} \end{bmatrix} + \frac{k}{p}\begin{bmatrix} i_{qg}^{\mathrm{e}*} - i_{qg}^{\mathrm{e}} \\ i_{dg}^{\mathrm{e}*} - i_{dg}^{\mathrm{e}} \end{bmatrix} = (k\tau)\frac{1}{k}p\begin{bmatrix} x_q^e \\ x_d^e \end{bmatrix} + \begin{bmatrix} x_q^e \\ x_d^e \end{bmatrix} \tag{3.73}$$

Where, x_{qd}^e is called an auxiliary equation as given below,

$$\begin{bmatrix} x_q^e \\ x_d^e \end{bmatrix} = \frac{k}{p}\begin{bmatrix} i_{qg}^{\mathrm{e}*} - i_{qg}^{\mathrm{e}} \\ i_{dg}^{\mathrm{e}*} - i_{dg}^{\mathrm{e}} \end{bmatrix} \; or \; px_{qd}^e = k\begin{bmatrix} i_{qg}^{\mathrm{e}*} - i_{qg}^{\mathrm{e}} \\ i_{dg}^{\mathrm{e}*} - i_{dg}^{\mathrm{e}} \end{bmatrix} \tag{3.74}$$

Thus, voltage equation may be expressed as,

$$\begin{bmatrix} v_q^e \\ v_d^e \end{bmatrix} = (I + \tau p)\begin{bmatrix} x_q^e \\ x_d^e \end{bmatrix} \tag{3.75}$$

Synchronous reference frame q-axis and d-axis currents in equation (3.74) may be represented in stationary reference frame by applying the transformation shown in equation (3.76).

$$\begin{bmatrix} x_q^s \\ x_d^s \end{bmatrix} = T(\theta)\begin{bmatrix} x_q^e \\ x_d^e \end{bmatrix} \text{ or } T(\theta)^{-1}\begin{bmatrix} x_q^s \\ x_d^s \end{bmatrix} = \begin{bmatrix} x_q^e \\ x_d^e \end{bmatrix} \tag{3.76}$$

Thus, equation (3.74) is expressed as,

$$p\left(T(\theta)^{-1} \cdot \begin{bmatrix} x_q^s \\ x_d^s \end{bmatrix}\right) = kT(\theta)^{-1} \cdot \begin{bmatrix} i_{qg}^{\mathrm{s}*} - i_{qg}^{s} \\ i_{dg}^{\mathrm{s}*} - i_{dg}^{s} \end{bmatrix} \tag{3.77}$$

The matrix $T(\theta)$ is a time-dependent function. Thus,

$$[p(T(\theta)^{-1})] \cdot \begin{bmatrix} x_q^s \\ x_d^s \end{bmatrix} + T(\theta)^{-1} \cdot p\begin{bmatrix} x_q^s \\ x_d^s \end{bmatrix} = \; kT(\theta)^{-1} \cdot \begin{bmatrix} i_{qg}^{\mathrm{s}*} - i_{qg}^{s} \\ i_{dg}^{\mathrm{s}*} - i_{dg}^{s} \end{bmatrix} \tag{3.78}$$

Multiplying equation (3.78) by the transformation matrix $T(\theta)$ results in the following

equation,

$$[T(\theta)\cdot p(T(\theta)^{-1})]\cdot\begin{bmatrix}x_q^s\\x_d^s\end{bmatrix}+p\begin{bmatrix}x_q^s\\x_d^s\end{bmatrix}=\ k\begin{bmatrix}i_{qg}^{s*}-i_{qg}^{s}\\i_{dg}^{s*}-i_{dg}^{s}\end{bmatrix} \tag{3.79}$$

Thus,

$$\left(\begin{bmatrix}cos\theta & sin\theta\\-sin\theta & cos\theta\end{bmatrix}\cdot\frac{d}{dt}\begin{bmatrix}cos\ \theta & sin\,\theta\\-sin\,\theta & cos\ \theta\end{bmatrix}\right)\cdot\begin{bmatrix}x_q^s\\x_d^s\end{bmatrix}+\frac{d}{dt}\begin{bmatrix}x_q^s\\x_d^s\end{bmatrix}=\ k\begin{bmatrix}i_{qg}^{s*}-i_{qg}^{s}\\i_{dg}^{s*}-i_{dg}^{s}\end{bmatrix} \tag{3.80}$$

Simplifying the equation (3.80) results in the expression (3.81).

$$\begin{bmatrix}0 & \omega\\-\omega & 0\end{bmatrix}\cdot\begin{bmatrix}x_q^s\\x_d^s\end{bmatrix}+\frac{d}{dt}\begin{bmatrix}x_q^s\\x_d^s\end{bmatrix}=\ k\begin{bmatrix}i_{qg}^{s*}-i_{qg}^{s}\\i_{dg}^{s*}-i_{dg}^{s}\end{bmatrix} \tag{3.81}$$

Similarly, synchronous reference frame q-axis and d-axis voltages in equation (3.75) may be represented in stationary reference frame by applying the transformation shown in equation (3.76).

$$T(\theta)^{-1}\cdot\begin{bmatrix}v_q^s\\v_d^s\end{bmatrix}=(I+\tau p)T(\theta)^{-1}\cdot\begin{bmatrix}x_q^s\\x_d^s\end{bmatrix} \tag{3.82}$$

A detailed form of the equation (3.82) is expressed as,

$$T(\theta)^{-1}\cdot\begin{bmatrix}v_q^s\\v_d^s\end{bmatrix}=T(\theta)^{-1}\cdot\begin{bmatrix}x_q^s\\x_d^s\end{bmatrix}+\tau\left[\left[p(T(\theta)^{-1})\cdot\begin{bmatrix}x_q^s\\x_d^s\end{bmatrix}\right]+\left[T(\theta)^{-1}\cdot p\begin{bmatrix}x_q^s\\x_d^s\end{bmatrix}\right]\right] \tag{3.83}$$

Multiplying equation (3.83) by the transformation matrix $T(\theta)$ results in the following equation,

$$\begin{bmatrix}v_q^s\\v_d^s\end{bmatrix}=\begin{bmatrix}x_q^s\\x_d^s\end{bmatrix}+\tau\left[\left[T(\theta)\cdot p(T(\theta)^{-1})\cdot\begin{bmatrix}x_q^s\\x_d^s\end{bmatrix}\right]+\left[p\begin{bmatrix}x_q^s\\x_d^s\end{bmatrix}\right]\right] \tag{3.84}$$

Thus,

$$\begin{bmatrix}v_q^s\\v_d^s\end{bmatrix}=\begin{bmatrix}x_q^s\\x_d^s\end{bmatrix}+\tau\left[\left[\begin{bmatrix}cos\theta & sin\theta\\-sin\theta & cos\theta\end{bmatrix}\cdot\frac{d}{dt}\begin{bmatrix}cos\ \theta & sin\,\theta\\-sin\,\theta & cos\ \theta\end{bmatrix}\cdot\begin{bmatrix}x_q^s\\x_d^s\end{bmatrix}\right]+\frac{d}{dt}\begin{bmatrix}x_q^s\\x_d^s\end{bmatrix}\right] \tag{3.85}$$

Simplifying the equation (3.85) results in the expression (3.86).

$$\begin{bmatrix} v_q^s \\ v_d^s \end{bmatrix} = \begin{bmatrix} x_q^s \\ x_d^s \end{bmatrix} + \tau \left[\begin{bmatrix} 0 & -\omega \\ \omega & 0 \end{bmatrix} \cdot \begin{bmatrix} x_q^s \\ x_d^s \end{bmatrix} + \frac{d}{dt} \begin{bmatrix} x_q^s \\ x_d^s \end{bmatrix} \right] \tag{3.86}$$

Equation (3.81) is substituted in the equation (3.86) to obtain the following expression,

$$\begin{bmatrix} v_q^s \\ v_d^s \end{bmatrix} = \begin{bmatrix} x_q^s \\ x_d^s \end{bmatrix} + k\tau \begin{bmatrix} i_{qg}^{s*} - i_{qg}^s \\ i_{dg}^{s*} - i_{dg}^s \end{bmatrix} \tag{3.87}$$

Thus, a controller is realized by synthesizing expressions (3.81) and (3.87) result in the following expressions (3.88) to (3.91).

$$\omega x_d^s + \frac{dx_q^s}{dt} = k(i_{qg}^{s*} - i_{qg}^s) \tag{3.88}$$

$$-\omega x_q^s + \frac{dx_d^s}{dt} = k(i_{dg}^{s*} - i_{dg}^s) \tag{3.89}$$

$$v_q^s = x_q^s + k\tau(i_{qg}^{s*} - i_{qg}^s) \tag{3.90}$$

$$v_d^s = x_d^s + k\tau(i_{dg}^{s*} - i_{dg}^s) \tag{3.91}$$

Transforming the expressions (3.88) to (3.91) into s-domain results in the expressions (3.92) to (3.95).

$$X_q^s(s) = \frac{k\left(I_{qg}^{s*}(\mathrm{s}) - I_{qg}^s(\mathrm{s})\right) - \omega X_d^s(s)}{s} \tag{3.92}$$

$$X_d^s(s) = \frac{k\left(I_{dg}^{s*}(\mathrm{s}) - I_{dg}^s(\mathrm{s})\right) + \omega X_q^s(s)}{s} \tag{3.93}$$

$$V_q^s(s) = X_q^s(s) + k\tau\left(I_{qg}^{s*}(\mathrm{s}) - I_{qg}^s(\mathrm{s})\right) \tag{3.94}$$

$$V_d^s(s) = X_d^s(s) + k\tau\left(I_{dg}^{s*}(\mathrm{s}) - I_{dg}^s(\mathrm{s})\right) \tag{3.95}$$

The auxiliary state equations (3.92) & (3.93) and voltage equations (3.94) & (3.95) have been used to realize the stationary reference frame equivalence of synchronous proportional-integral controller (St/Sy-PI) as shown in the figure.3.14. The control structure of the St/Sy-PI current controller consists of two individual loops and a cross-coupling loop.

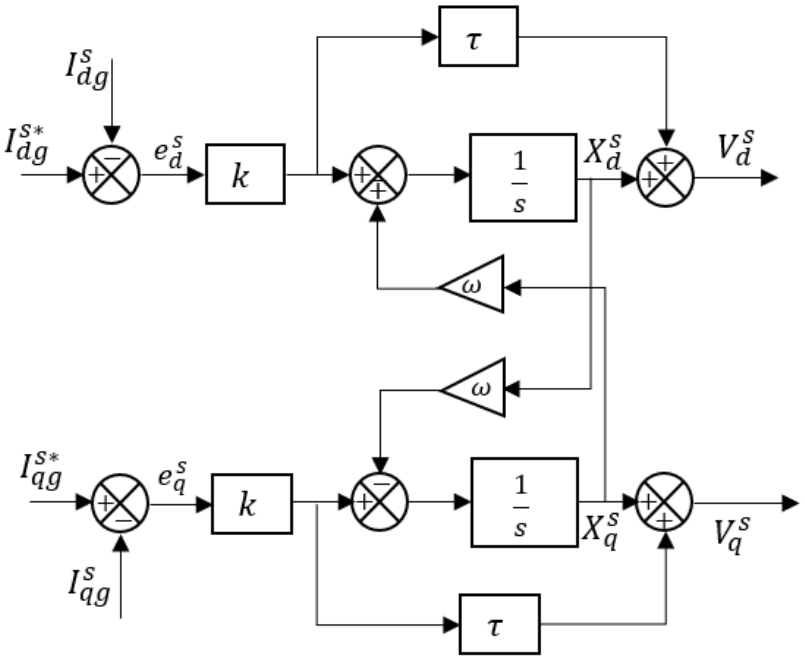

Figure.3.14. Schematic of stationary reference frame equivalence of generalized PI (St/Sy-PI) current controller.

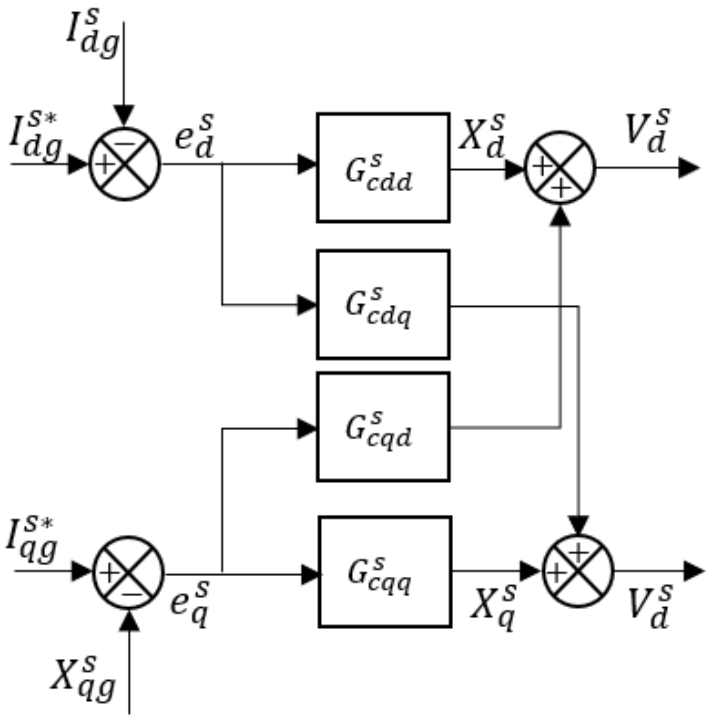

Figure.3.15. Simplified schematic of St/Sy-PI current controller.

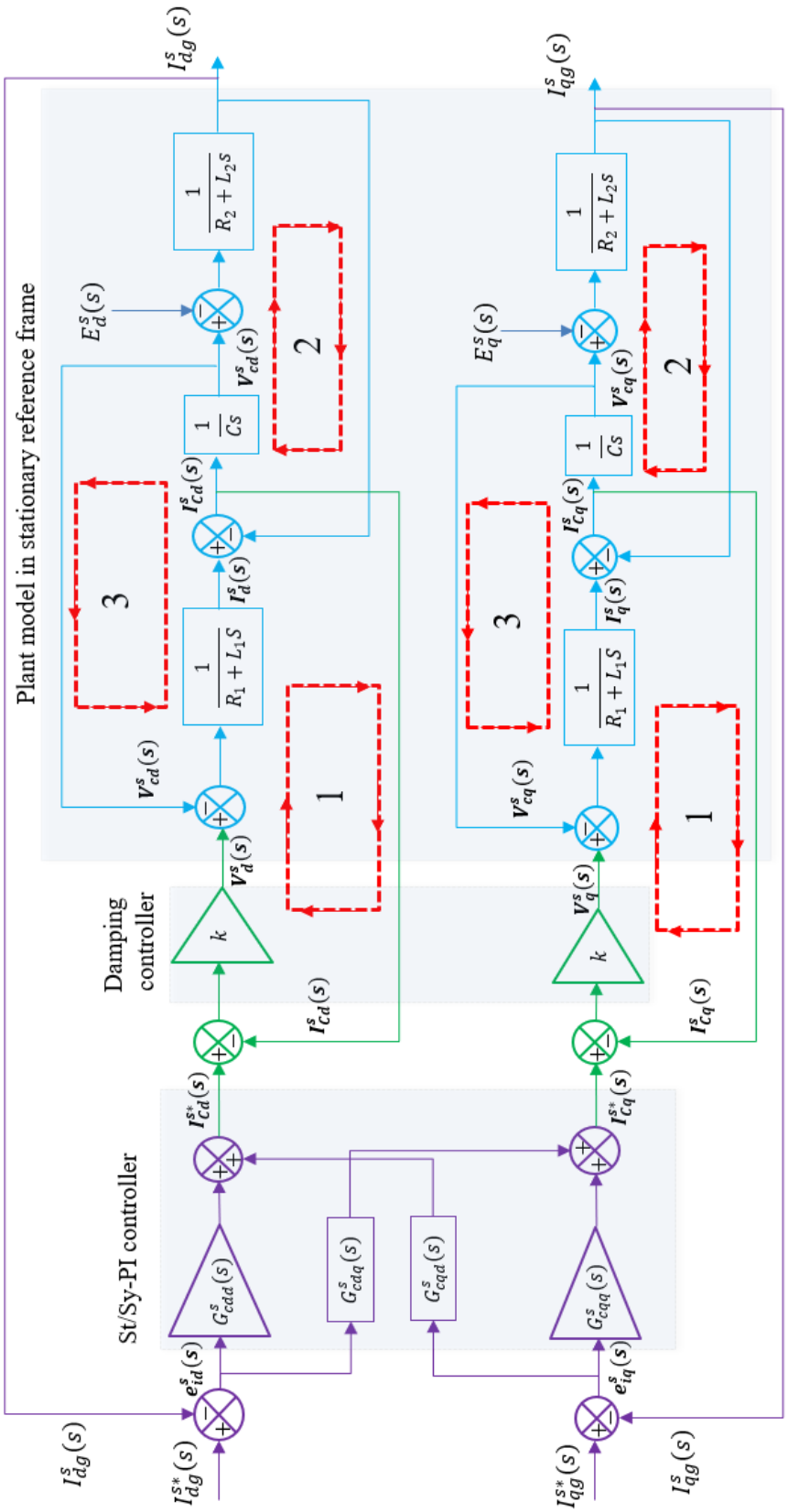

Figure.3.16. Schematic of control block diagram of St/Sy-PI controller, damping controller, and plant model of a grid-tied inverter with LCL filter in stationary reference frame.

An overall closed-loop current control schematic of the St/Sy-PI current control strategy is shown in the figure.3.16. The St/Sy-PI current controller has been embedded with damping controller and plant model of the three-phase grid-tied inverter in stationary reference frame. This control structure of St/Sy-PI in the figure.3.14 is simplified by applying Mason's gain formula. Thus, a simplified form of St/Sy-PI current controller is obtained as shown in the figure.3.13. The resultant forward path and cross-coupling transfer functions of the St/Sy-PI controller are expressed as,

$$G_c^s(s) = \begin{bmatrix} G_{cdd}^s(s) & G_{cdq}^s(s) \\ G_{cqd}^s(s) & G_{cqq}^s(s) \end{bmatrix} = \begin{bmatrix} \dfrac{k\tau s^2 + ks + k\tau\omega_e^2}{s^2 + \omega_e^2} & \dfrac{\omega_e k}{s^2 + \omega_e^2} \\ \dfrac{-\omega_e k}{s^2 + \omega_e^2} & \dfrac{k\tau s^2 + ks + k\tau\omega_e^2}{s^2 + \omega_e^2} \end{bmatrix} \tag{3.96}$$

Therefore, equations (3.96) and (3.62) are identical with $k_p = k\tau \; and \; k_i = k$. Thus, the overall closed-loop control schematic of the St/Sy-PI current controller for a grid-tied inverter with an LCL filter is identical to the schematic as shown in the figure.3.12. The forward-path and cross-coupling transfer functions (3.63) and (3.64) apply to St/Sy-PI current controller because the controller schematics are identical. Thus, the St/Sy-PI current controller and stationary reference frame equivalence of Sy-PI current controller consists of resonant elements in the forward path and cross-coupling path. The analysis of these controllers is complex because of existence of the cross-couplings.

3.5. Stationary Reference Frame Proportional Resonant Controller (St-PR)

The analytical outcome of stationary reference frame equivalence of Sy-PI current controller and St/Sy-PI current controller results in an identical control structure. A proportional resonant controller in the forward path and a resonant controller in the cross-coupling path have been identified in the control schematic as shown in the figure.3.16. Therefore, a proportional resonant

controller in the stationary reference frame (St-PR) may be realized by making cross-coupling elements as zero in equation (3.96) or (3.62).

$$G_c^s(s) = \begin{bmatrix} G_{cdd}^s(s) & G_{cdq}^s(s) \\ G_{cqd}^s(s) & G_{cqq}^s(s) \end{bmatrix} = \begin{bmatrix} k_p + k_i \dfrac{s}{s^2+\omega^2} & 0 \\ 0 & k_p + k_i \dfrac{s}{s^2+\omega^2} \end{bmatrix} \tag{3.97}$$

Thus, the closed-loop current control schematic of the St-PR current controller is similar to the figure.3.16. or figure.3.12 except for no cross-couplings exist between the d-axis and q-axis as shown in the figure.3.15. and figure.3.16. The overall closed-loop current control schematic of St-PR current control strategy consists of a St-PR controller embedded with damping controller and plant model of the three-phase grid-tied inverter in the stationary reference frame. One of the merits of St-PR is no cross-coupling exists between d-axis and q-axis of the plant model and controller. The St-PR controller is required to be tuned precisely at the grid frequency or else the system is vulnerable to unstable operation at frequencies other than grid frequency.

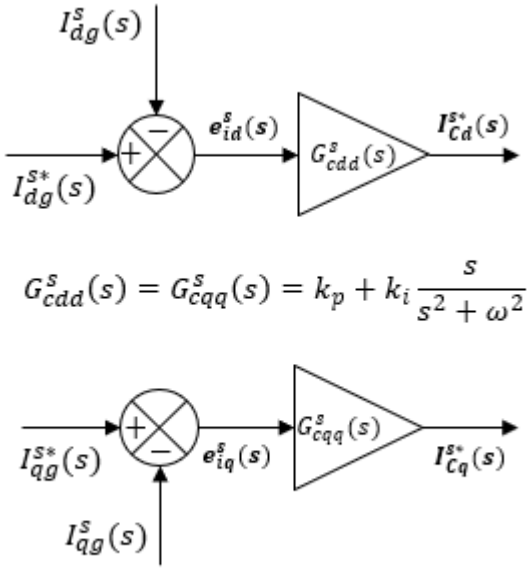

Figure.3.17. Schematic of St-PR current controller.

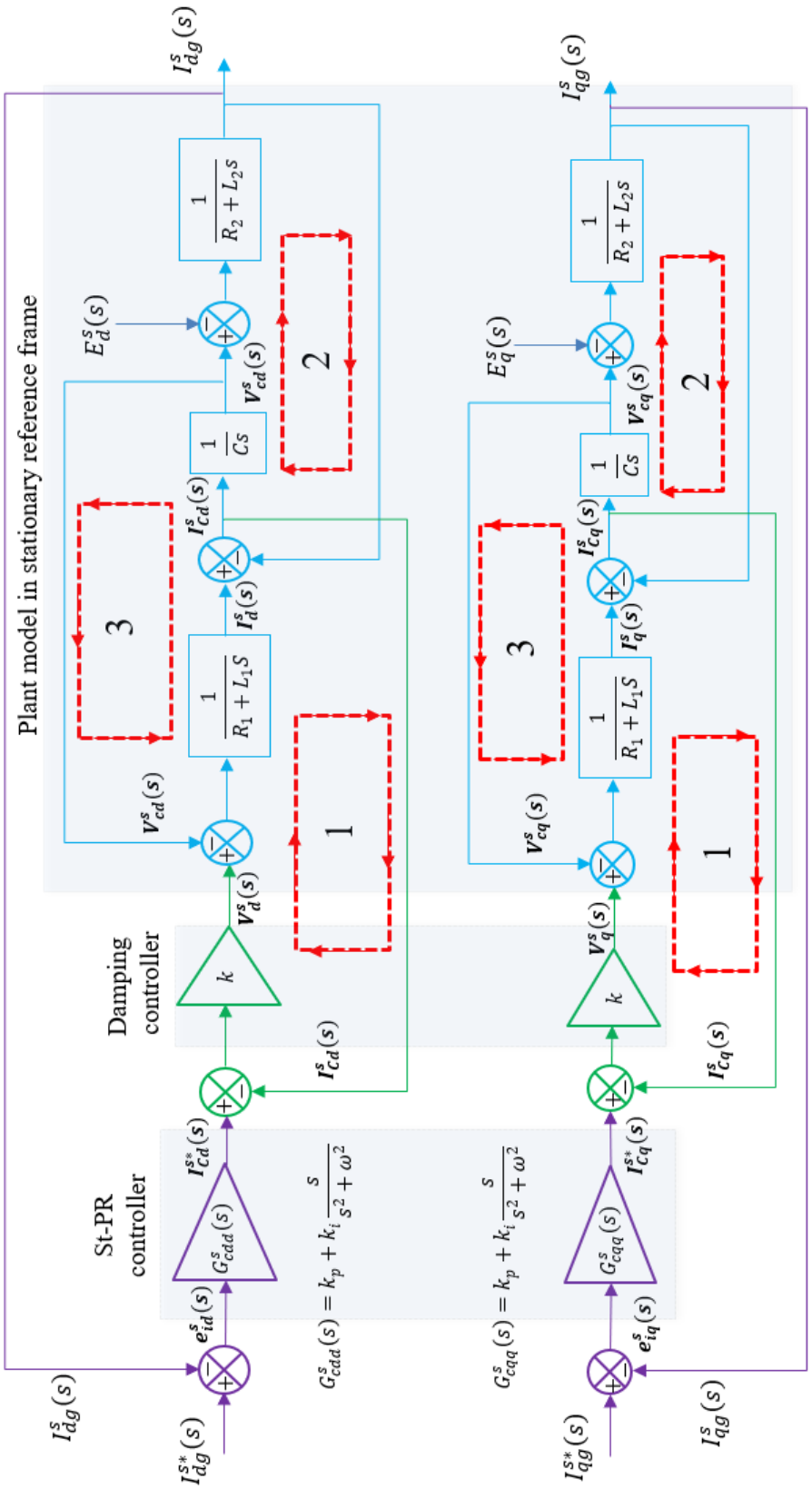

Figure.3.18. Schematic of control block diagram of St-PR controller, damping controller, and plant model of a grid-tied inverter with LCL filter in stationary reference frame.

3.5. Generalized Current Regulation Strategy

The Sy-PI current controller transfer function $G_c^e(s)$ consists of no cross-couplings and the plant model consists of multiple cross-couplings in the synchronous reference frame. The St/Sy-PI current controller transfer function $G_c^s(s)$ consists of cross-couplings and the plant model consists of no-cross couplings in the stationary reference frame. The St-PR controller transfer function and plant model consist of no cross-couplings in the stationary reference frame.

Thus, a generalized controller consisting of Sy-PI, St/Sy-PI, and St-PR has been established using the equations (3.59), (3.96), and (3.97). A schematic of generalized current control strategy for a three-phase grid-tied inverter is shown in figure.3.19. The configuration of index and controller matrices is shown in table 3.3. The index matrices have been set to realize the Sy-PI, St/Sy-PI, and St-PR current control strategies in the respective reference frames as discussed in sections 3.2 to 3.4.

TABLE 3.3: CONFIGURATION OF INDEX AND CONTROL MATRICES

	Sy-PI	St/Sy-PI	St-PR
$T_I(\theta)$	$T(\theta)^{-1}$	$\begin{bmatrix}1 & 0\\0 & 1\end{bmatrix}$	$\begin{bmatrix}1 & 0\\0 & 1\end{bmatrix}$
$T_V(\theta)$	$\begin{bmatrix}1 & 0\\0 & 1\end{bmatrix}$	$T(\theta)^{-1}$	$T(\theta)^{-1}$
$G_c^*(s)$	$\begin{bmatrix}G_{cd}^e(s) & 0\\0 & G_{cq}^e(s)\end{bmatrix}$	$\begin{bmatrix}G_{cdd}^s(s) & G_{cdq}^s(s)\\G_{cqd}^s(s) & G_{cqq}^s(s)\end{bmatrix}$	$\begin{bmatrix}G_{cdd}^s(s) & 0\\0 & G_{cqq}^s(s)\end{bmatrix}$

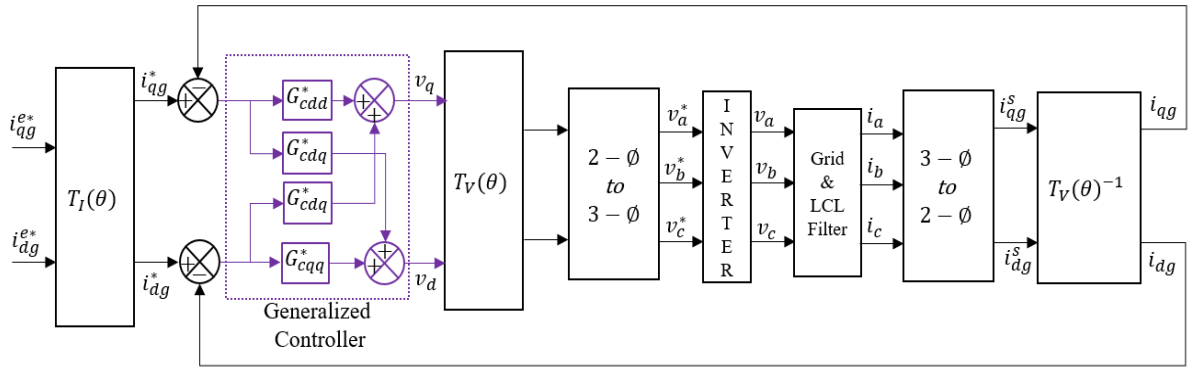

Figure.3.19. Control schematic of generalized closed-loop current control strategy consisting of Sy-PI, St/Sy-PI, and St-PR for a grid-tied inverter with an LCL filter.

It may be noted that this generalized current control strategy can also be applied to realize stationary reference frame PI current control by setting $\omega = 0$.

3.5. Stability Analysis

Stability analysis for Sy-PI, St/Sy-PI, and St-PR current controller strategies has been discussed in this section. The closed-loop control structure of the stationary reference frame equivalence of Sy-PI and St/Sy-PI are identical and similar to St-PR is similar except for no cross-couplings exists between d-axis and q-axis. Thus, The same forward-path transfer function applies to Sy-PI, St/Sy-PI, and St-PR current control strategies because of their similarity in control structure as discussed in previous sections. Range of control parameters $k_p, k_{i,}$ and k has been determined from the stability analysis. A battery voltage of 800V_{dc}, three-phase grid voltage of 208V at a grid frequency of 60Hz with the following grid specifications as shown in table 3.3 have been considered for this analysis.

TABLE 3.3: SPECIFICATION OF LCL FILTER AND CONTROL PARAMETERS FOR SY-PI, ST/SY-PI, AND ST-PR CONTROL STRATEGIES

L_1 (mH)	R_1 $(m\Omega)$	L_2 (mH)	R_2 $(m\Omega)$	C (μf)	k_p	k_i	k
8	1	2	1	15	$0.1 - 0.5$	50	$1 - 10$

The Bode plot has been shown in the figure.3.20 consists of multiple plots for different values of damping factor k. The system has been observed to be in stable mode for low values of damping factor ($k = 1, 5, \text{and } 2.5$) and unstable for higher values of the damping factor ($k = 10$) . A gain margin of 7.95 dB and a phase margin of 36.8° has been observed at $k_p = 0.5$, $k_i = 50$, and $k = 5$. The magnitude of gain is high at system frequency. A small spike in the magnitude of gain is due to the resonance of LCL parameters. A sudden drop in the phase has been observed at system frequency and resonant frequency. The root locus diagram of the system has been shown in the figure.3.21. The system has five poles and two zeros. Location of the pole-zeros has been observed

to be on the left side of the pole-zero plot for lower values of proportional gain constant k_p. The system has been observed to be stable for $0.1 < k_p < 1.5$. The discrete equivalents of these control parameters have been used in simulation and experimental validation.

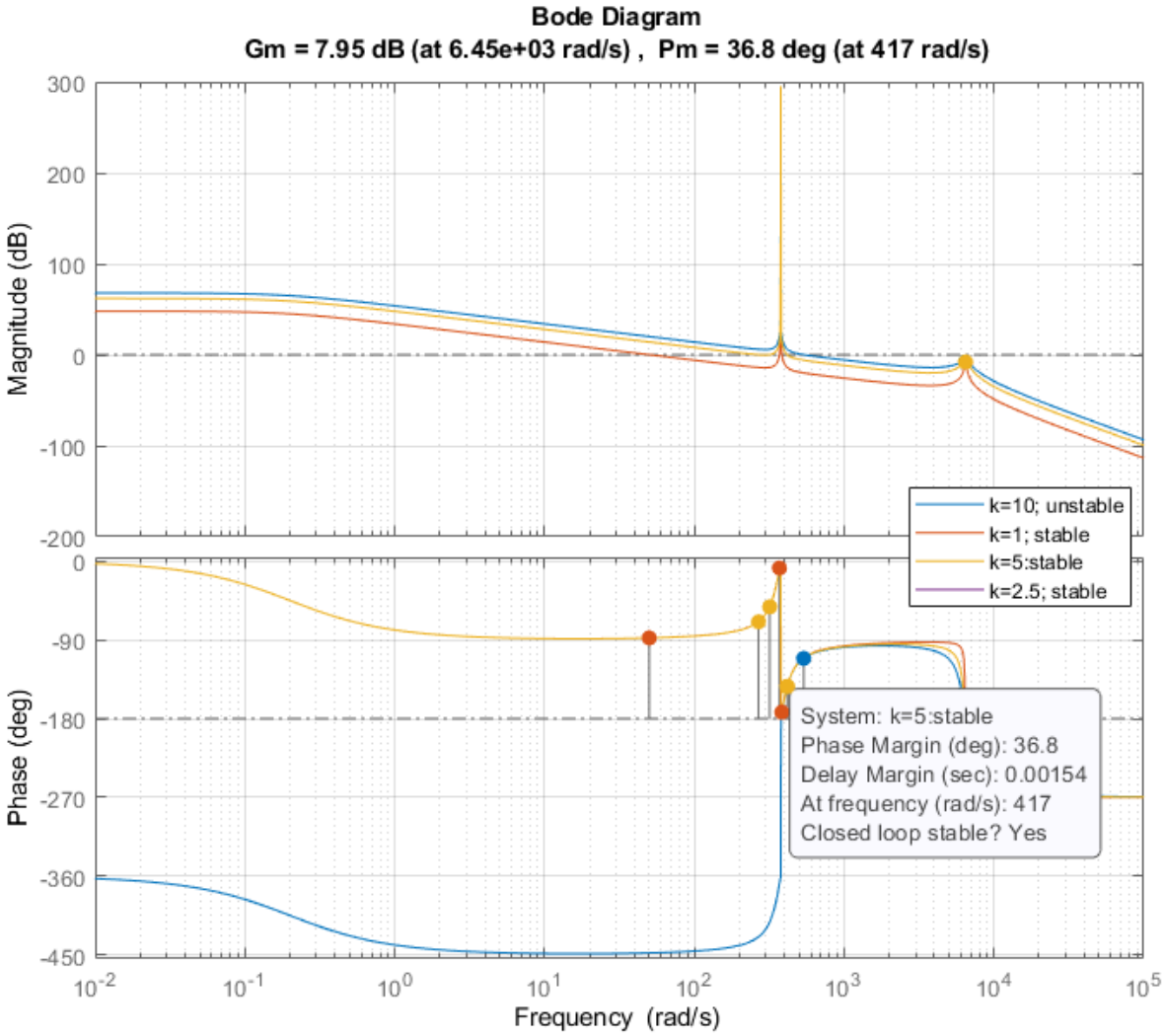

Figure.3.20. Bode plot of the forward-path transfer function of stationary reference frame equivalence of Sy-PI controller (also valid for St/Sy-PI and St-PR) for a grid-tied inverter with an LCL filter.

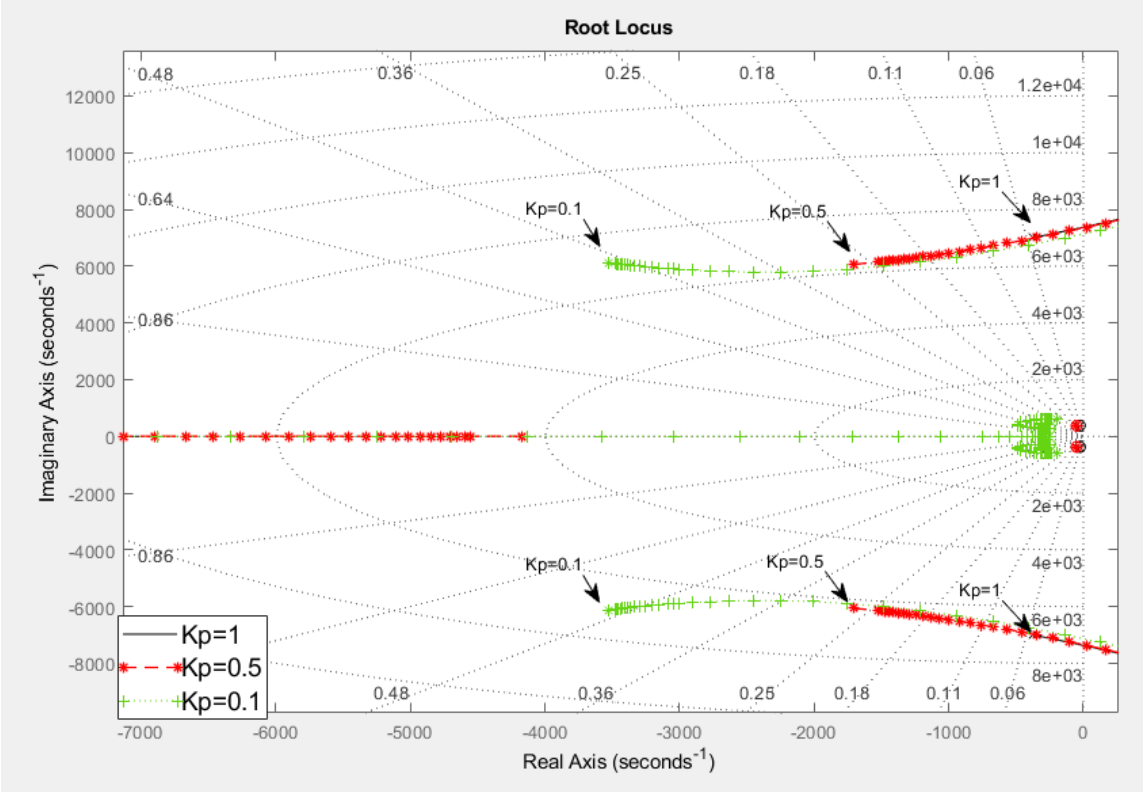

Figure.3.21. Root locus diagram of the forward-path transfer function of stationary reference frame equivalence of Sy-PI controller (also valid for St/Sy-PI and St-PR) for a grid-tied inverter with an LCL filter.

CHAPTER 4: MODELING & SIMULATION

4.1. Introduction

Modeling and simulation of various current controller strategies have been discussed in this Chapter. An introduction to the modeling and simulation of the grid-tied inverter is presented in Section 4.1. Common PSIM simulation modules used in various control strategies are presented in section 4.2. PSIM Simulation models of St-PI, Sy-PI, St/Sy-PI, and St-PR have been presented in Section 4.3, Section 4.4, Section 4.5, and Section 4.6.

PSIM simulation platform has been used to verify the analysis of the current control strategies discussed in the chapter 3. PSIM simulation control has been set to implement control algorithms compatible with the targeted hardware TI DSP Piccolo TMS320F28035. Modeling of the current control of the three-phase grid-tied inverter consists of different modules. Each module consists of different elements to perform a specific task. These elements have been chosen from the PSIM library are discrete in behavior and generate code in a specific syntax compatible with the TI DSP Piccolo TMS320F28035. A DSP clock has been set to operate DSP at $60\ MHz$ and external clock at $10\ MHz$.

4.2. Common Modules in Modeling of Grid-Tied Inverter

The simulation model of the three-phase grid-tied inverter consists of the power stage, signal conditioning, phase-locked loop (PLL), three-phase to stationary reference frame transformation, three-phase to synchronous reference frame transformation, current controller, and sinusoidal pulse-width modulation. Power stage, signal conditioning, PLL, and sinusoidal pulse-width modulation (SPWM) are common simulation modules for St-PI, Sy-PI, St/Sy-PI, and St-PR current control strategies. PLL consists of transformation of the three-phase grid voltages into the stationary reference frame. Three-phase grid voltages have been considered as reference to

generate the phase angle that is required to perform the synchronous transformation of the three-phase currents and voltages of the grid. The stationary reference transformation module has been used to implement St-PI, Sy-PI, and St-PR current control strategies. The synchronous reference frame transformation module has been used to implement Sy-PI's current control strategy.

4.2.1. Power Stage

The schematics of simulation models of common modules are discussed in this section. The power stage of the grid-tied inverter system consists of a three-phase inverter, LCL filter, three-phase grid, three current sensors, and three voltage sensors. The three-phase inverter consists of six Insulated-Gate Bipolar Transistors IGBT switches $Q1$ to $Q6$ arranged in a specific sequence as shown in figure.4.1. A diode has been connected across each IGBT in antiparallel to enable synchronous rectifier mode of operation. This arrangement of the diodes and IGBTs in the specified topology permits the system to have bidirectional power flow. DC side of the three-phase inverter is powered by a battery of 800Vdc. The IGBTs receive the gate signals from the sinusoidal pulse-width module. AC side of the three-phase inverter is connected to a three-phase LCL filter. The LCL filter consists of six inductors and three capacitors. Each phase of the three-phase inverter has been connected to an LCL filter in a specific topology as shown in the figure.4.1. A small value of resistance has been considered in each inductor. A three-phase grid of 208Vac has been connected to another end of the three-phase LCL filter.

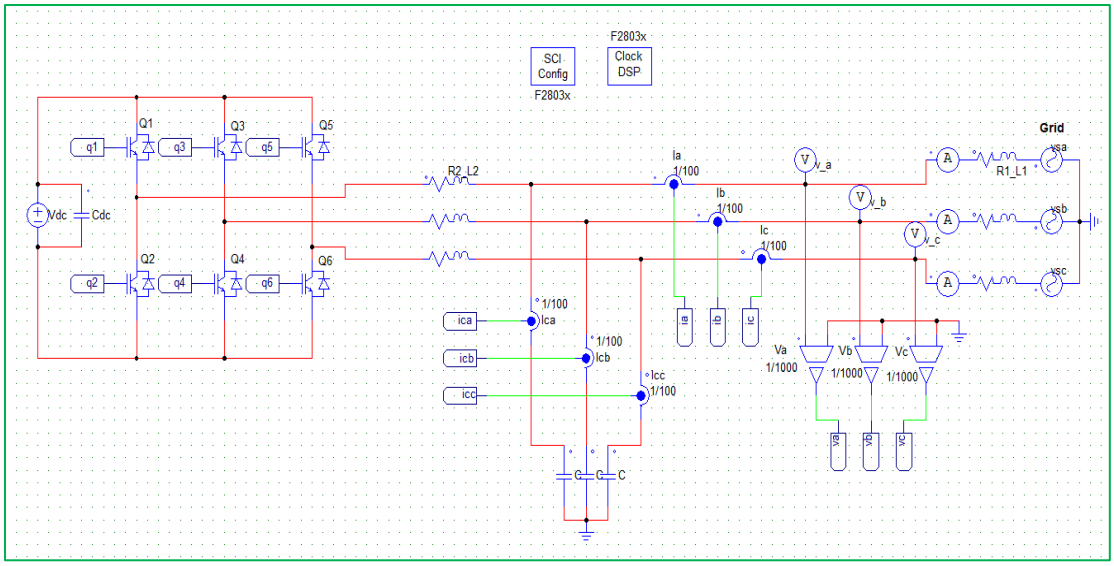

Figure.4.1. PSIM simulation schematic of power stage module of the three-phase grid-tied inverter with LCL filter.

4.2.2. Analog to Digital Conversion

The outputs of the three-phase current sensors and voltage sensors of the grid-tied inverter are required to be scaled to a compatible level of analog to digital conversion (ADC) input port pins of the TI DSP Piccolo TMS320F28035. A schematic of the signal conditioning module is shown in the figure.4.2. The ADC input port pins of the TI DSP Piccolo TMS320F28035 are compatible with unipolar signals of 0 to 3.3 V. Thus, the magnitude of the currents and voltages sensed by the current and voltage sensors have been scaled by a factor of $1/100$ and $1/1000$. These scaled currents and voltages are bipolar sinusoidal in shape. Thus, an offset of 1.65 has been added to each signal to shift the amplitude levels between 0 to 3.3 V. ADC module has been set in DC mode with a gain of 1 because the signals have been conditioned externally. Thus, ADC performs analog to digital conversion. The digitalized or discretized version of the currents and voltages have been sampled at a frequency of 10 kHz.

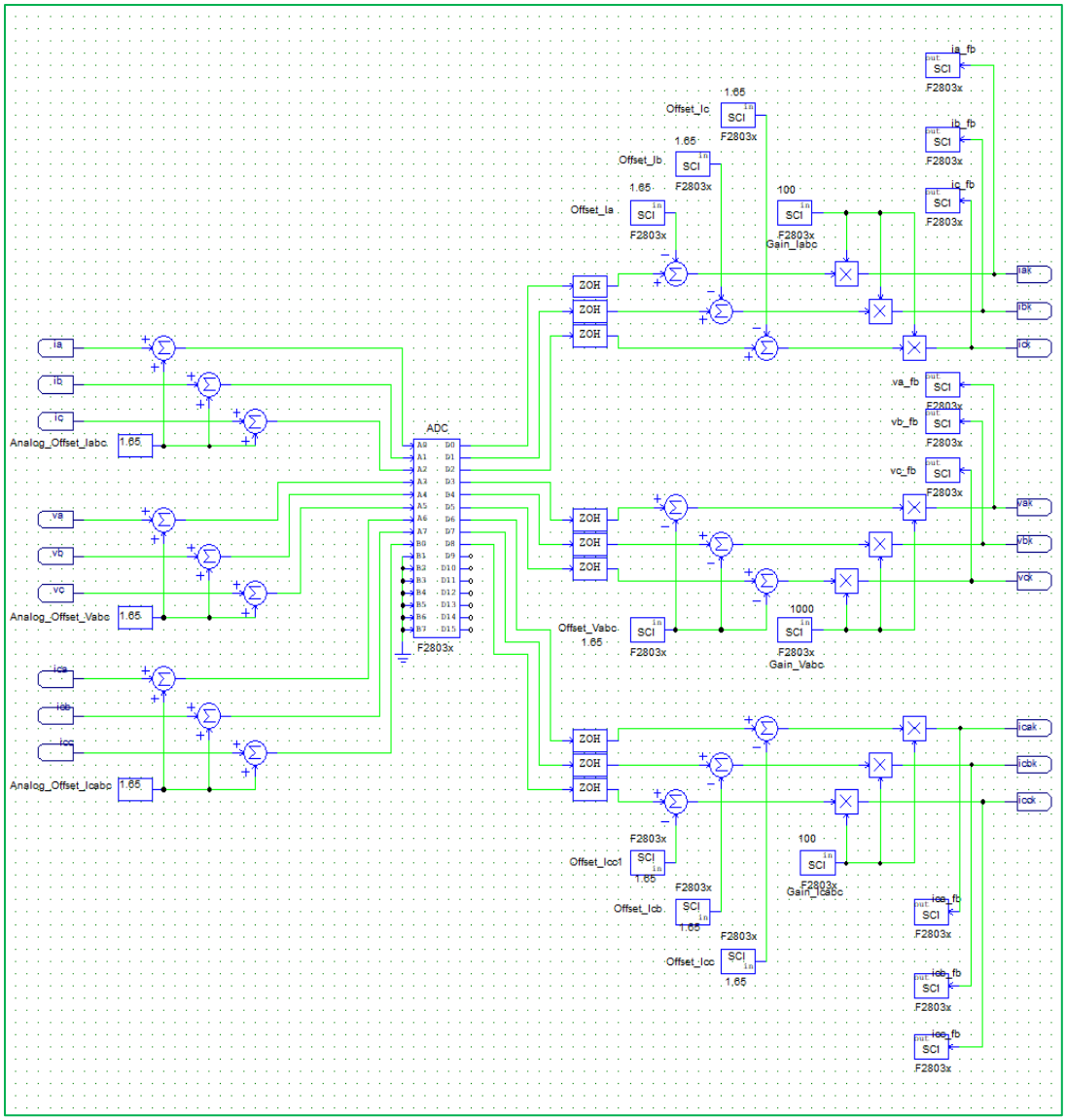

Figure.4.2. Schematic of signal condition module consists of scaling, offset, sample & hold (ZOH), and ADC blocks.

The discretized currents and voltage signals are unipolar. These unipolar signals are required to be transformed inside the microcontroller to replicate the original signals of bipolar sinusoidal in shape. Thus, an offset of -1.65 has been added to each signal to make them bipolar sinusoidal in shape. These signals have been rescaled by a factor of 100 for currents and 1000 for voltage

signals. These offset and scaling inputs inside the microcontroller are accessed externally by enabling the serial communication interface (SCI) feature.

4.2.3. Phase-Locked Loop

The three-phase voltages of the grid are considered as a reference to generate a phase angle to perform the transformation in respective reference frames as discussed in the previous section. A schematic of the PLL is shown in figure.4.3. The three-phase currents have been transformed into stationary reference frame by employing Clarke's transformation block. A trigonometric math operation of arc tan has been performed on the ratio of voltage signals in the stationary reference frame to generate a phase of sawtooth shape.

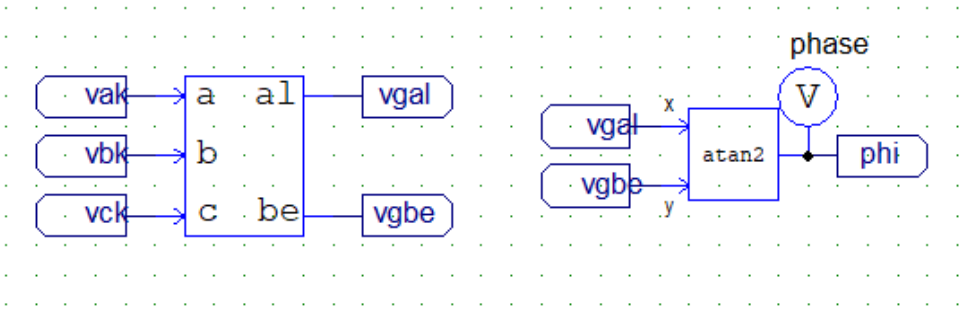

Figure.4.3. PSIM simulation schematic of three-phase PLL module.

4.2.4. Sinusoidal Pulse Width Modulation

Sinusoidal pulse width modulation (SPWM) technique has been chosen to generate gate signals required to operate IGBT switches in the three-phase inverter. A schematic of SPWM module and its settings have been shown in the figure.4.4. SPWM has been set to operate at a switching frequency of 10 kHz with a dead band of 4 μs. Input signals to the SPWM have been normalized to have a peak-to-peak magnitude of 2 V. Thus, the triangular carrier wave has been set to have a peak to peak of 2 V.

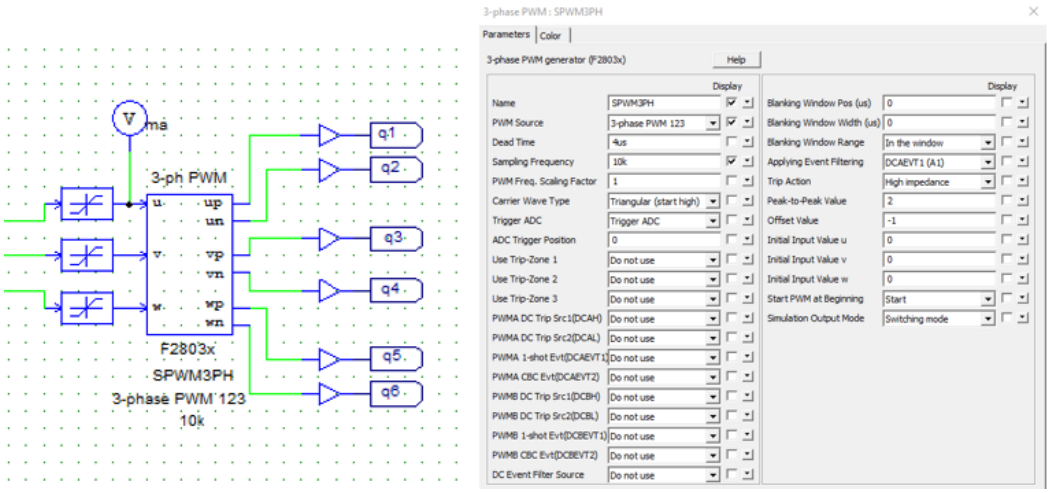

Figure.4.4. PSIM simulation schematic of the SPWM module and its specifications.

4.3. Modeling of Stationary Reference Frame Proportional Integral Controller (St-PI)

Modeling of the St-PI current control strategy has been discussed in this section. A PSIM simulation schematic of the St-PI current control strategy is shown in the figure.4.5. The schematic of St-PI current control strategy consists of a reference current generation module in addition to the common modules discussed in the previous sections. The Serial communication interface (SCI) feature of the microcontroller has been employed to set the reference values of currents in the stationary reference frame. A PSIM simulation schematic of the reference current generation is shown in figure.4.6. This schematic consists of PLL to generate the shape of the reference signals, and three-phase to stationary reference frame transformation of the grid and capacitor currents. The closed-loop current control schematic of the St-PI regulator is shown in figure.4.7. The current control schematic consists of an outer loop of grid currents, an inner loop of the capacitor currents, and grid voltages as feed-forward in the stationary reference frame. The output of the current controllers has been normalized by a factor of $1/0.5V_{dc}$. The simulation results of the St-PI current control strategy have been discussed in Chapter 5.

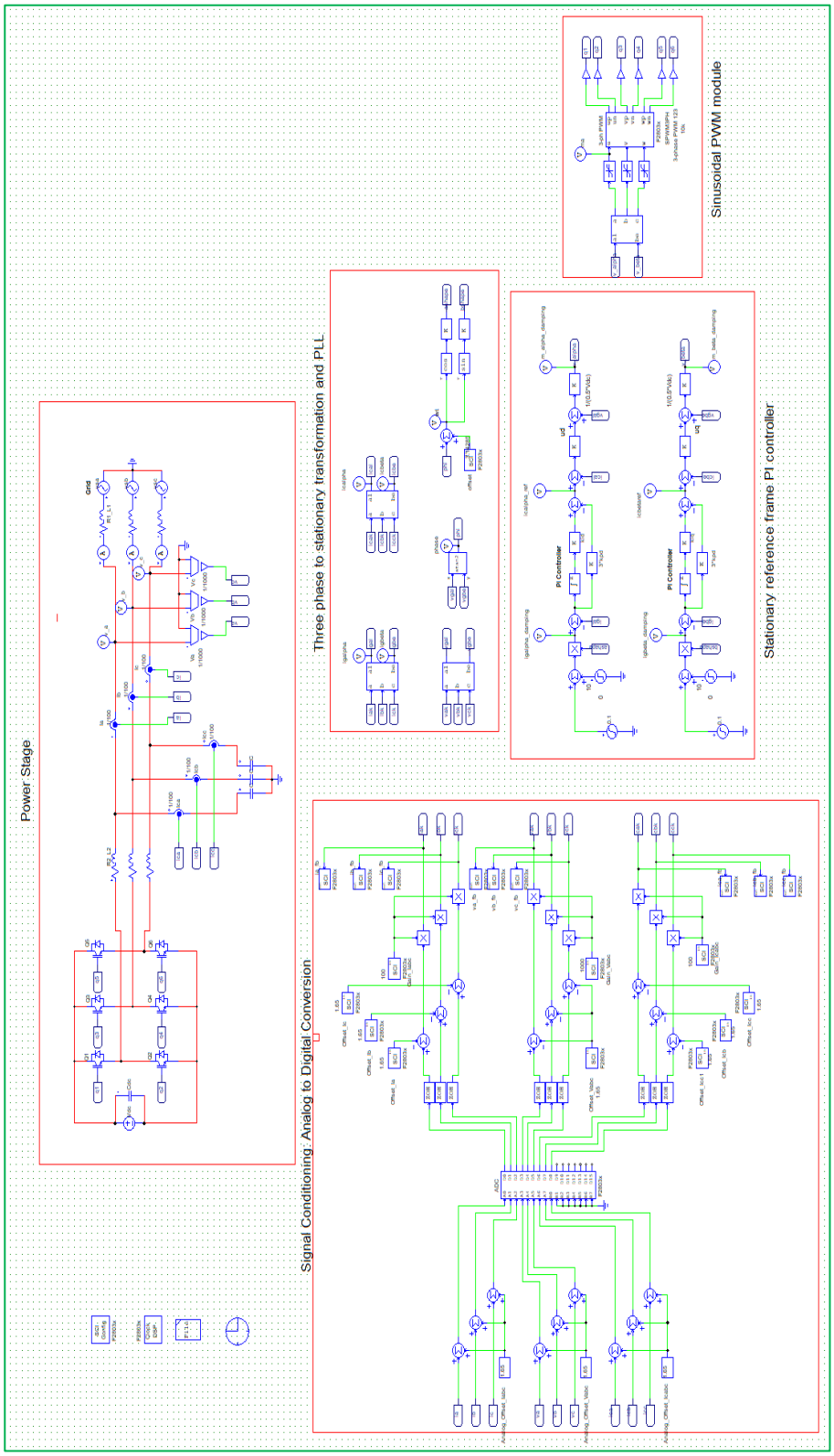

Figure.4.5. PSIM simulation schematic of the closed loop St-PI current control strategy of the three-phase grid tied inverter with LCL filter.

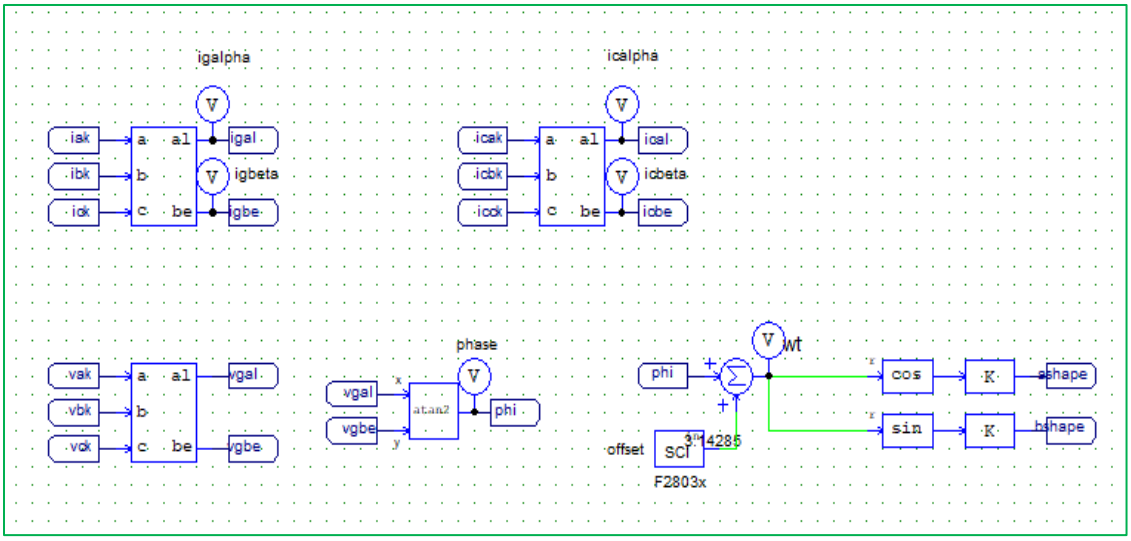

Figure.4.6. PSIM simulation schematic of the shape of reference current generation and transformation of grid and capacitor currents in the stationary reference frame.

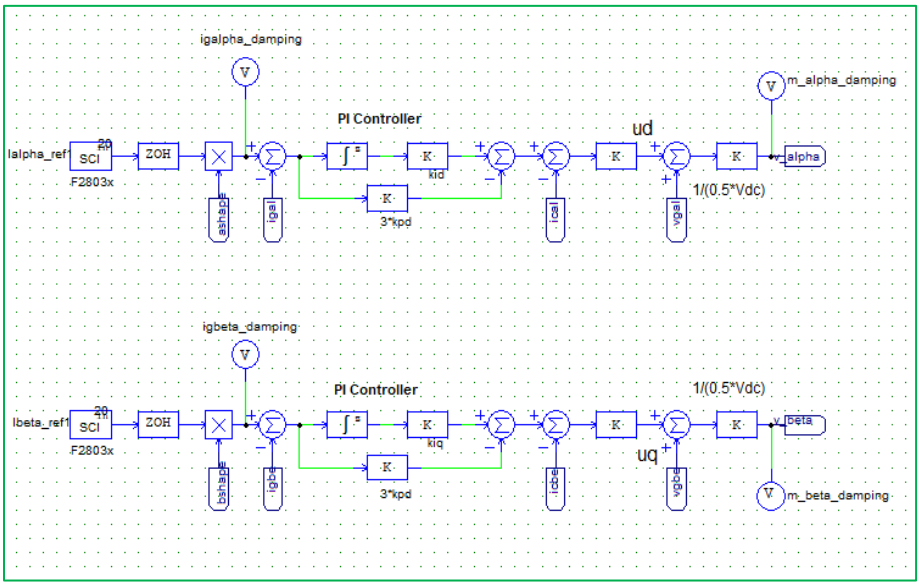

Figure.4.7. PSIM simulation schematic of the St-PI current controller.

4.4. Modeling of Synchronous Reference Frame Proportional Integral Controller (Sy-PI)

Modeling and simulation of the Sy-PI current control strategy are discussed in this section. A PSIM simulation schematic of the three-phase to the synchronous transformation of the voltages and currents is shown in figure.4.8.

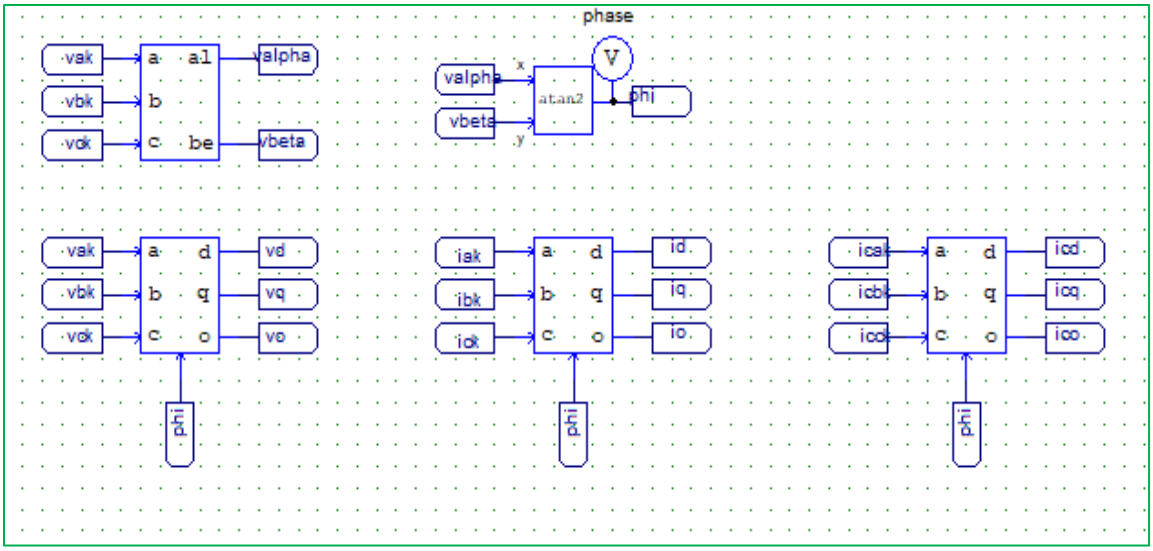

Figure.4.8. PSIM simulation schematic of the transformation of voltages and currents into the synchronous reference frame.

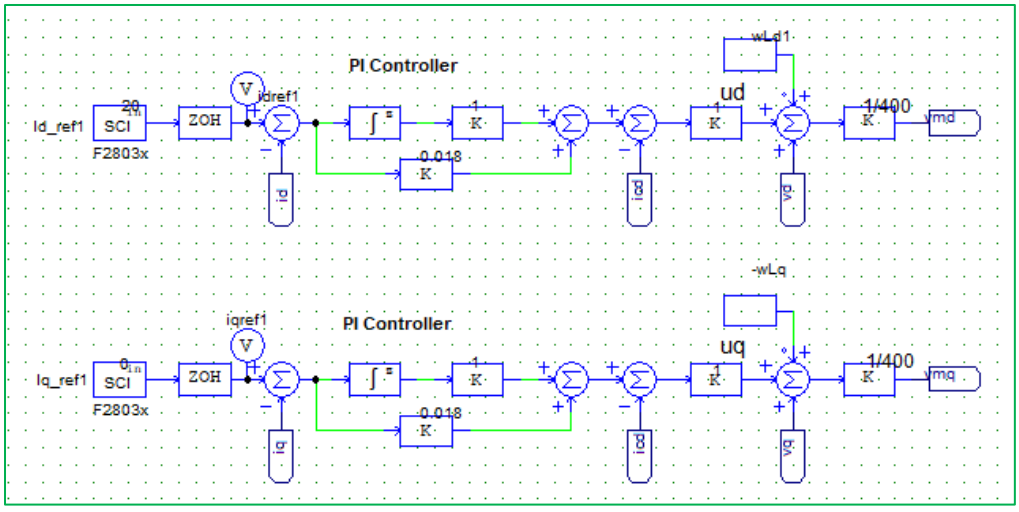

Figure.4.9. PSIM simulation schematic of the St-PI current controller.

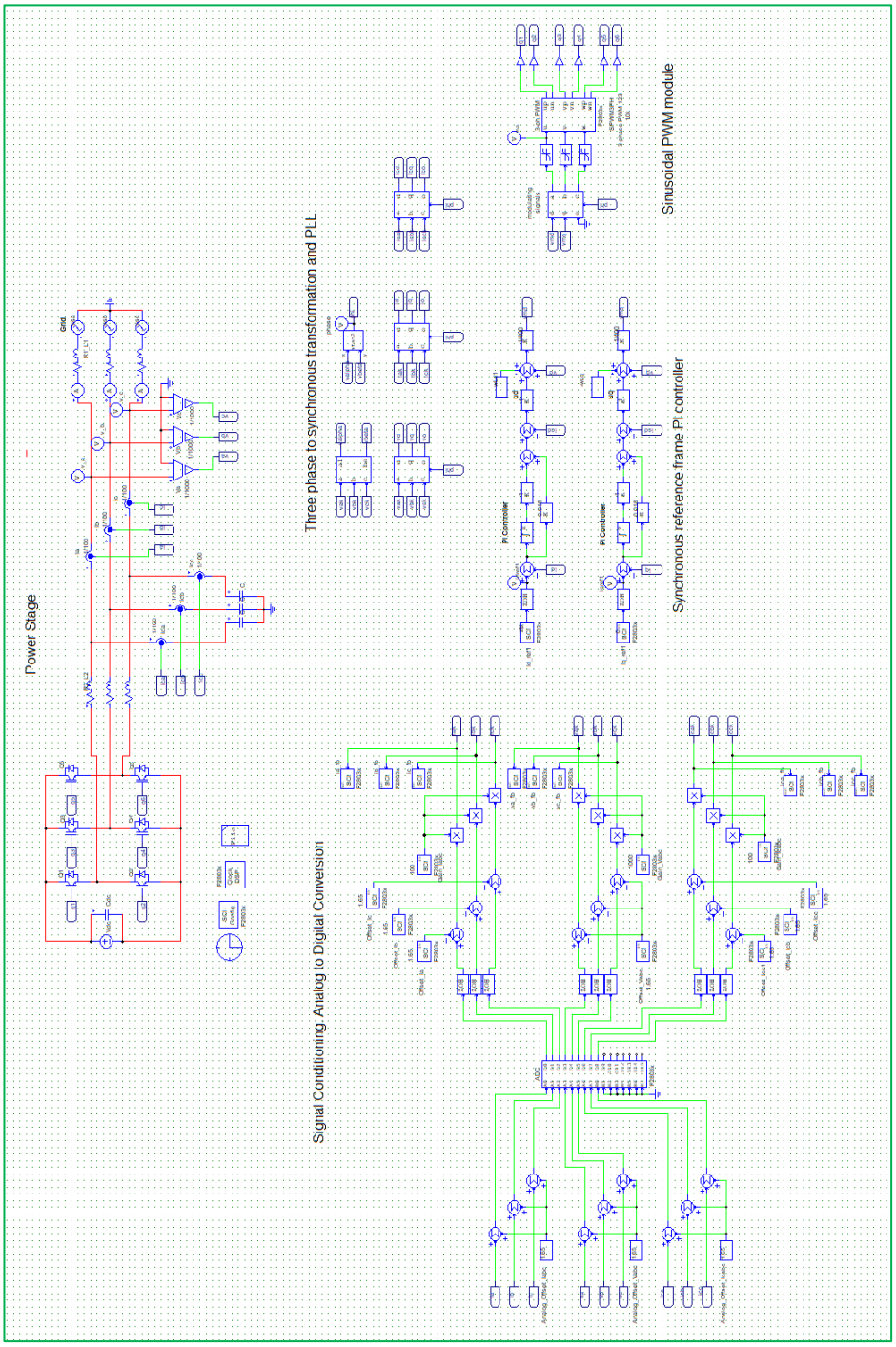

Figure.4.10. PSIM simulation schematic of the closed loop Sy-PI current control strategy of the three-phase grid tied inverter with LCL filter.

A PSIM simulation schematic of the closed-loop Sy-PI current control strategy is shown in figure.4.10. The schematic of this control strategy consists of the transformation of grid and capacitor currents in the synchronous reference frame in addition to the common modules discussed in the previous sections. The serial communication interface (SCI) feature of the microcontroller has been employed to set the reference values of currents in the synchronous reference frame. The simulation results of the Sy-PI current control strategy have been discussed in Chapter 5.

4.5. Modeling of Stationary Reference Frame Regulation of Synchronous Reference Frame Controller (St/Sy-PI)

Modeling and simulation of the St/Sy-PI current control strategy are discussed in this section. A PSIM simulation schematic of the three-phase to stationary reference frame transformation of the voltages, currents, and is shown in figure.4.6. This schematic consists of PLL to generate the shape of the reference signals, and three-phase to stationary reference frame transformation of the grid and capacitor currents.

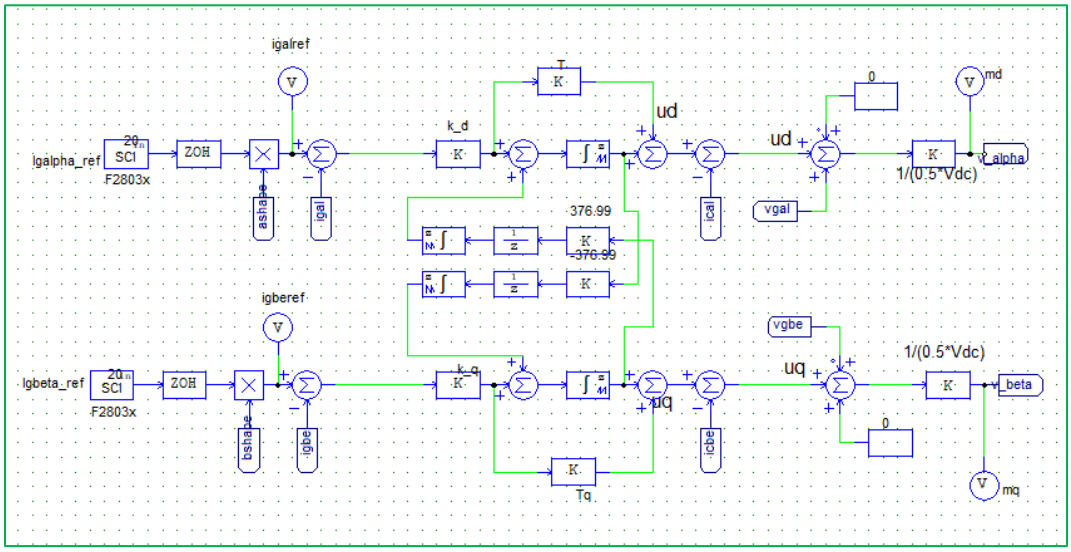

Figure.4.11. PSIM simulation schematic of the St/Sy-PI current controller.

A schematic of the St/Sy-PI regulator is shown in the figure.4.11. The peak amplitude of the reference current is multiplied by the shape of the reference current in the stationary reference frame. The current control schematic consists of an outer loop of grid currents, an inner loop of the capacitor currents, and grid voltages as feed-forward in the stationary reference frame. This module consists of cross-couplings between the d-axis and q-axis of the controller in the stationary reference frame. The output of the St/Sy-PI controllers has been normalized by a factor of $1/0.5V_{dc}$.

A PSIM simulation schematic of the closed-loop St/Sy-PI current control strategy is shown in figure.4.12. The schematic of this control strategy consists of the transformation of grid and capacitor currents into the stationary reference frame in addition to the common modules discussed in the previous sections. The serial communication interface (SCI) feature of the microcontroller has been employed to set the reference values of currents in the stationary reference frame. The simulation results of the St/Sy-PI current control strategy have been discussed in Chapter 5.

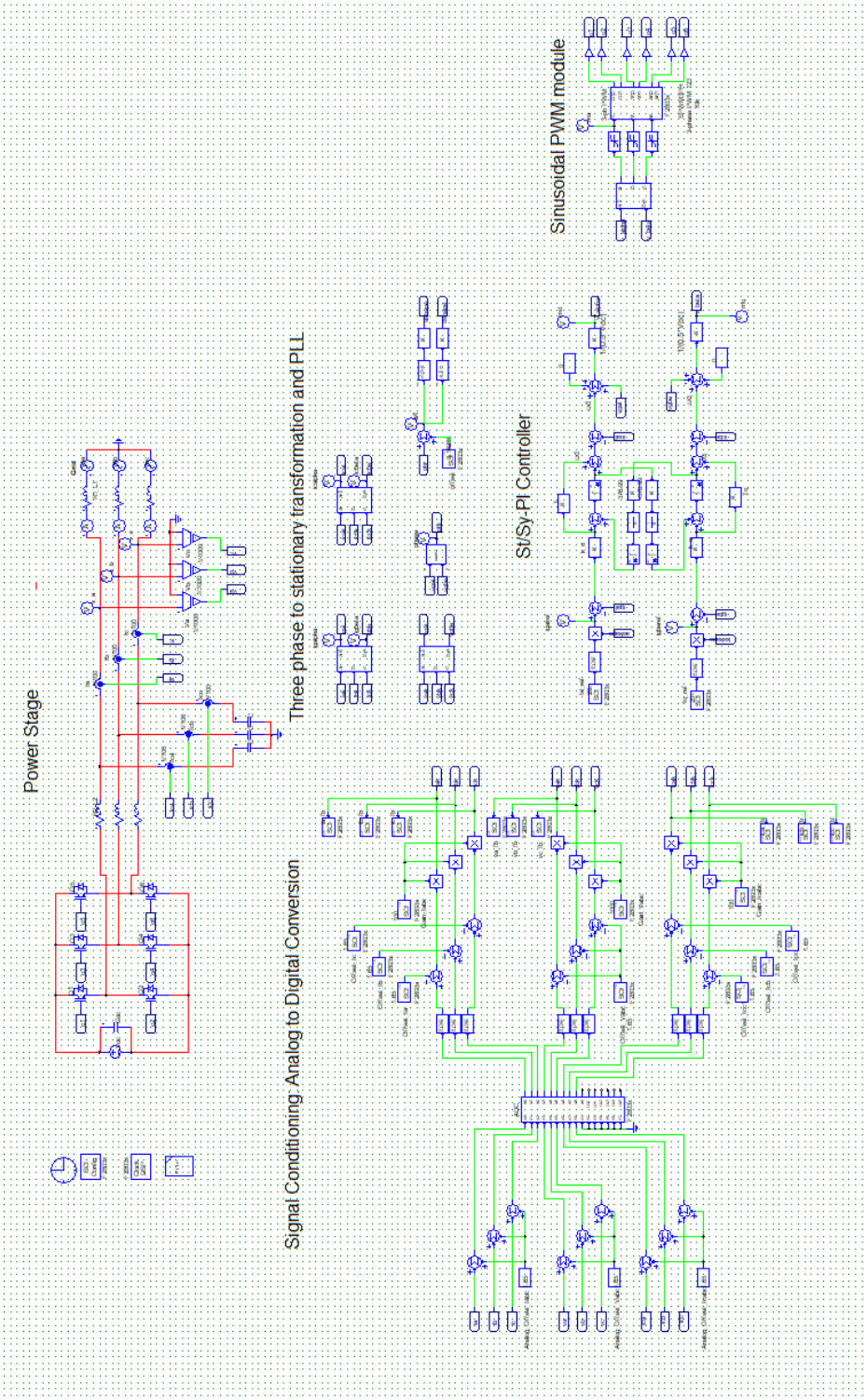

Figure.4.12. PSIM simulation schematic of the closed-loop St/Sy-PI current control strategy of the three-phase grid tied inverter with LCL filter.

4.6. Modeling of Stationary Reference Frame Proportional Resonant Controller (St-PR)

Modeling and simulation of the St -PR current control strategy is discussed in this section. The PLL and the generation of the shape of the reference currents as shown in figure.4.6 have been discussed in the previous section of the stationary reference frame controllers. A schematic of the St -PR regulator is shown in the figure.4.13. The peak amplitude of the reference current is multiplied with the shape of the reference current in the stationary reference frame. Double integrator technique has been applied to implement the St-PR control strategy [26]. The current control schematic consists of an outer loop of grid currents, an inner loop of the capacitor currents, and grid voltages as feed-forward in the stationary reference frame. This module has no cross-couplings between the d-axis and q-axis of the controller in the stationary reference frame. The output of the St/Sy-PI controllers has been normalized by a factor of $1/0.5V_{dc}$. A PSIM simulation schematic of the closed-loop St/Sy-PI current control strategy is shown in figure.4.14. The simulation results of the St -PR current control strategy have been discussed in Chapter 5.

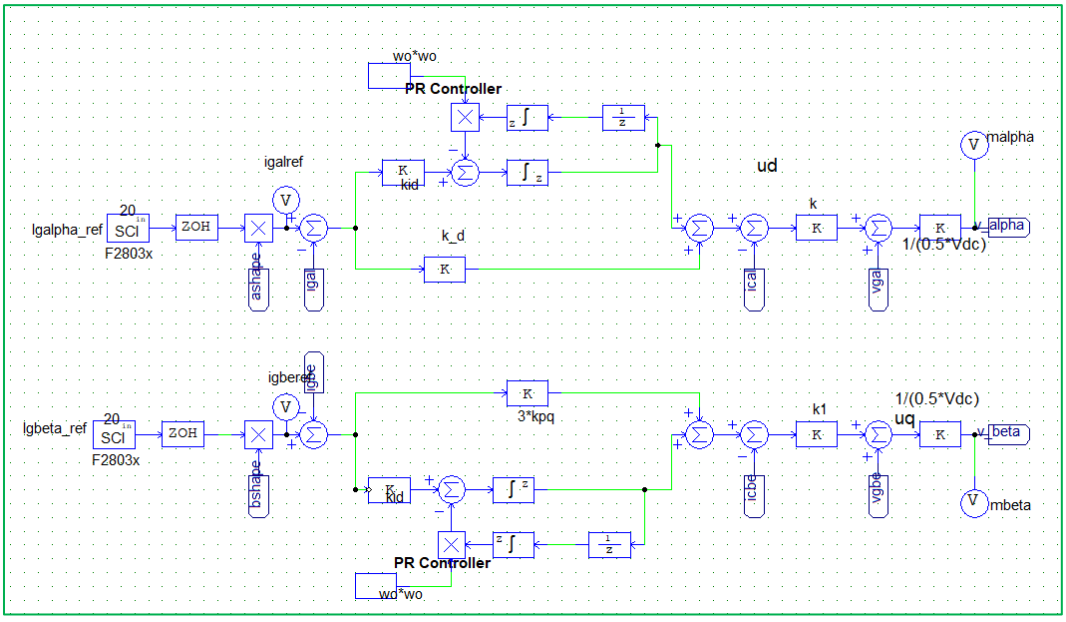

Figure.4.13. PSIM simulation schematic of the St-PR current controller.

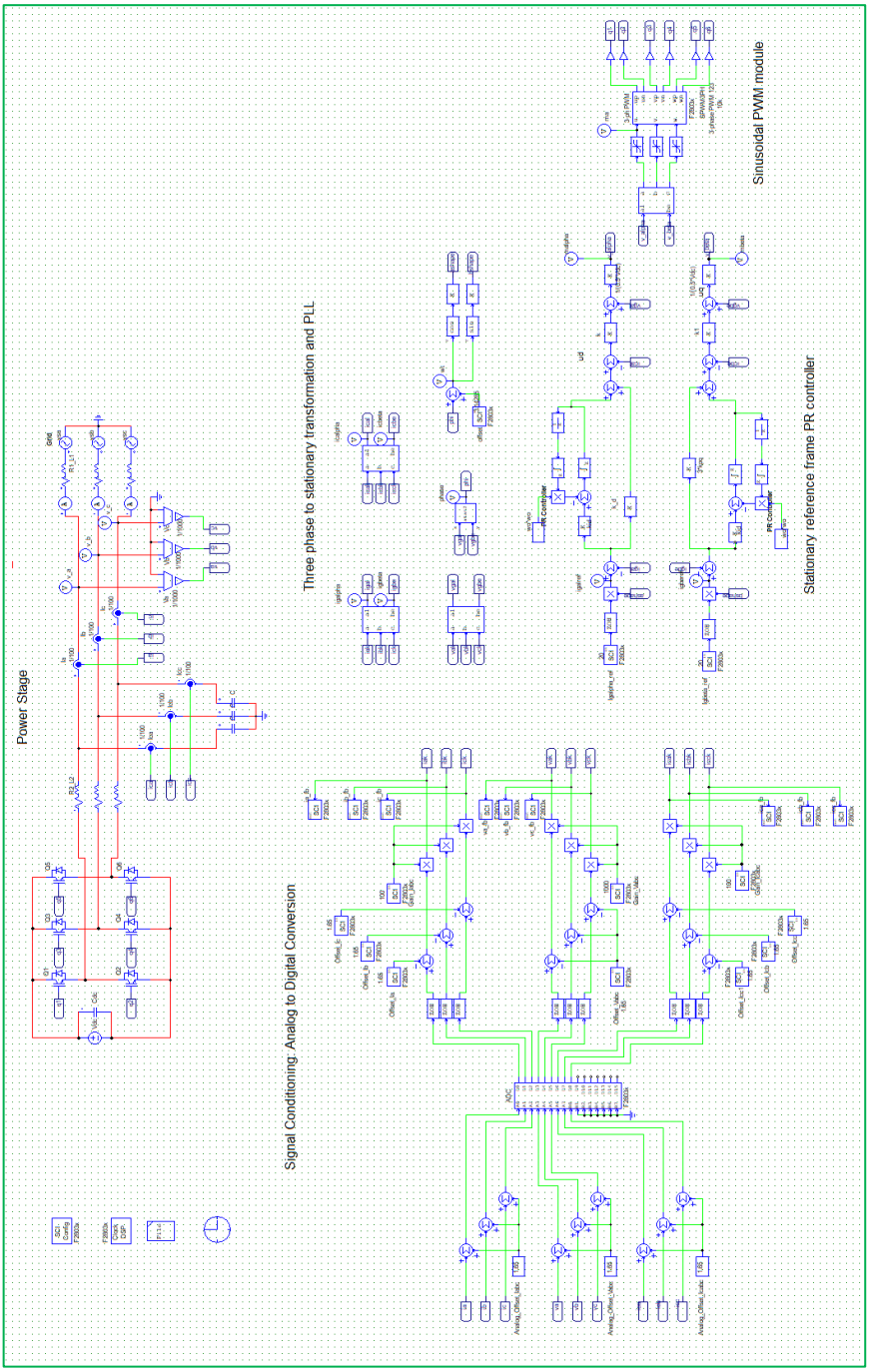

Figure.4.14. PSIM simulation schematic of the closed-loop St-PR current control strategy of the three-phase grid tied inverter with LCL filter.

CHAPTER 5: SIMULATION RESULTS

5.1. Introduction

This chapter is focused on presenting the simulation results of the various current control strategies. An introduction and current regulation scenario detailing the consideration of reference currents in respective reference frames is presented in Section 5.1 and Section 5.2. Simulation results of St-PI, Sy-PI, St/Sy-PI, and St-PR have been presented in Section 5.3.1, Section 5.3.2, Section 5.3.3, and Section 5.3.4. These simulation results are discussed in Section 5.4.

5.2. Current Regulation Scenario

Current regulators in the stationary reference frame i.e., St-PI, St/Sy-PI, and St-PR have a sinusoidal response because the reference currents and feedback currents are in sinusoidal shape in the stationary reference frame. The feedback signals are time-varying and difficult to track. An offset has been added to the phase angle output of the PLL to generate the shape of reference currents i_{dg}^{s} and i_{qg}^{s} to match with the phase of the grid voltages e_{d}^{s} and e_{q}^{s} the grid frame as shown in the figure.4.5.

The current regulator in the synchronous reference frame i.e., Sy-PI has a step response because the feedback currents and reference currents are time-invariant in the synchronous reference frame. The time-invariant feedback signals are easy to track. Reference currents have been set in a way to have three-phase currents and voltages are in phase.

5.3. Simulation Results

Simulation results of the various current control strategy consist of a set of the reference currents in the stationary reference frame and synchronous reference frame, three-phase

grid currents, and three-phase grid voltages. A change in the reference currents has been introduced to observe the response of the controller.

5.3.1. Stationary Reference Frame Proportional Integral Controller (St-PI)

Simulation results of St-PI current control strategy are discussed in this section. A change in peak of the reference currents i_{dgpeak}^{s*} and i_{qgpeak}^{s*} has been introduced. The feedback currents i_{dg}^{s} and i_{qg}^{s} are able to track the change in reference currents as shown in figure.5.1. The change in the reference currents is also reflected in the three-phase grid current currents. These currents are in phase with the three-phase grid voltages because of the identical change in the peak of reference currents from 10 A to 25A.

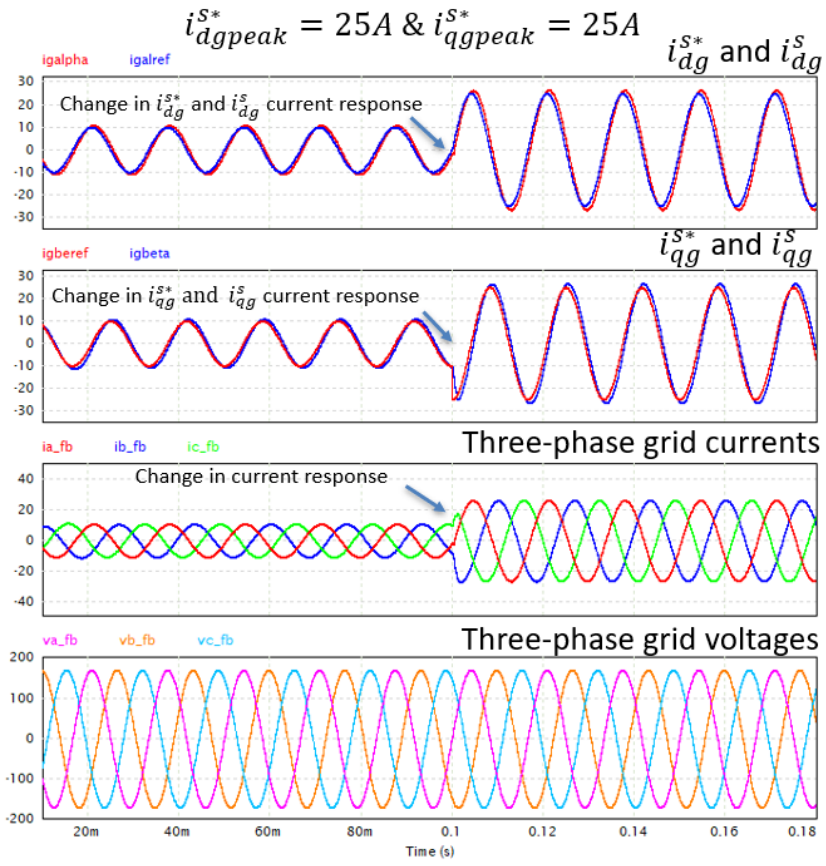

Figure.5.1. PSIM simulation results of the grid currents & voltages of the St- PI current control strategy.

5.3.2. Synchronous Reference Frame Proportional Integral Controller (Sy-PI)

The PSIM simulation results of Sy-PI current control strategy are discussed in this section. A change in the reference currents i_{dg}^{e*} and i_{qg}^{e*} has been introduced. The feedback currents i_{dg}^{e} and i_{qg}^{e} are tracking the change in reference currents as shown in figure.5.2. The change in the reference currents is also reflected in the three-phase grid current currents. These currents are in phase with the three-phase grid voltages because of the current references $i_{dg}^{e*} = 40$ and $i_{qg}^{e*} = 0$. A small overshoot has been observed during a transient phase of change in reference current.

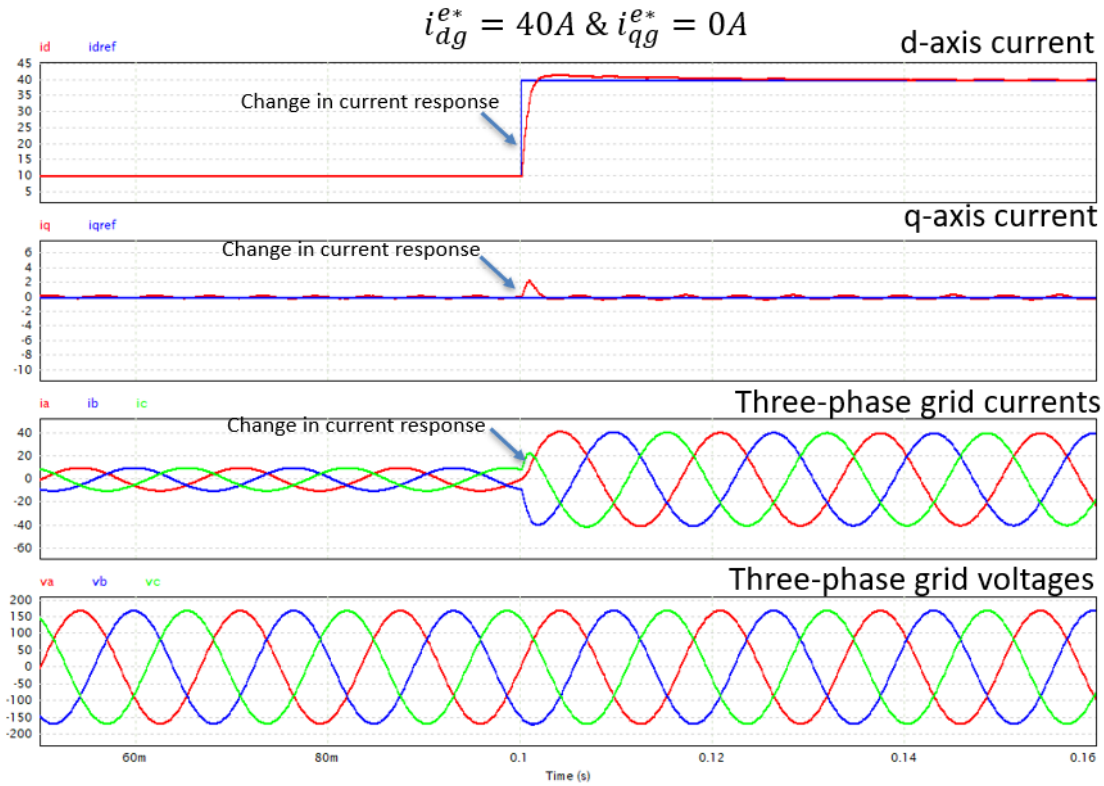

Figure.5.2. PSIM simulation results of the grid currents & voltages of the Sy- PI current control strategy.

5.3.3. Stationary Reference Frame Regulation of Synchronous Reference Frame Controller (St/Sy-PI)

Simulation results of St/Sy-PI current control strategy are discussed in this section. A change in the reference currents i_{dgpeak}^{S*} and i_{qgpeak}^{S*} has been introduced. The feedback currents i_{dg}^{S} and i_{qg}^{S} are tracking the change in reference currents as shown in figure.5.3. The change in the reference current also reflected in the three-phase grid current currents. These currents are in phase with the three-phase grid voltages because of an identical change in the peak of reference currents from 10 A to 20A. A small overshoot in the feedback signals has been observed during the transient phase of change in the reference currents.

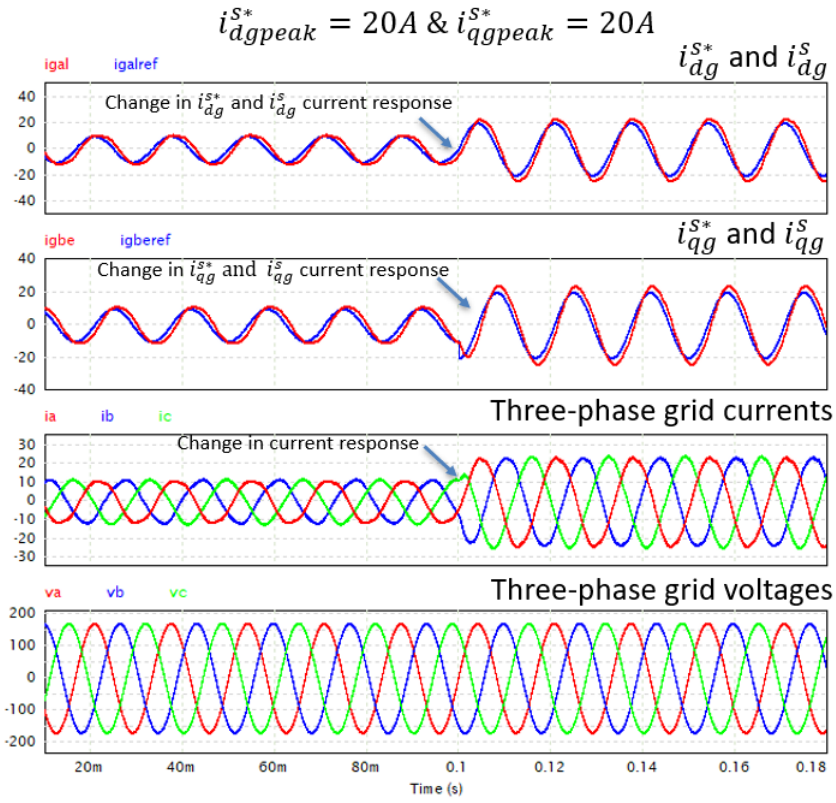

Figure.5.3. PSIM simulation results of the grid currents & voltages of the St/Sy- PI current control strategy.

5.3.4. Stationary Reference Frame Proportional Resonant Controller (St-PR)

Simulation results of St -PR current control strategy are discussed in this section. A change in the reference currents i_{dgpeak}^{S*} and i_{qgpeak}^{S*} has been introduced. The feedback currents i_{dg}^{S} and i_{qg}^{S} are able to track the change in reference currents as shown in figure.5.4. The change in the reference current also reflected in the three-phase grid current currents. These currents are in phase with the three-phase grid voltages because of an identical change in the peak of reference currents from 20 A to 40A. An overshoot in the feedback signals has been observed but it smaller compared to St-PI and St/Sy-PI current control strategies.

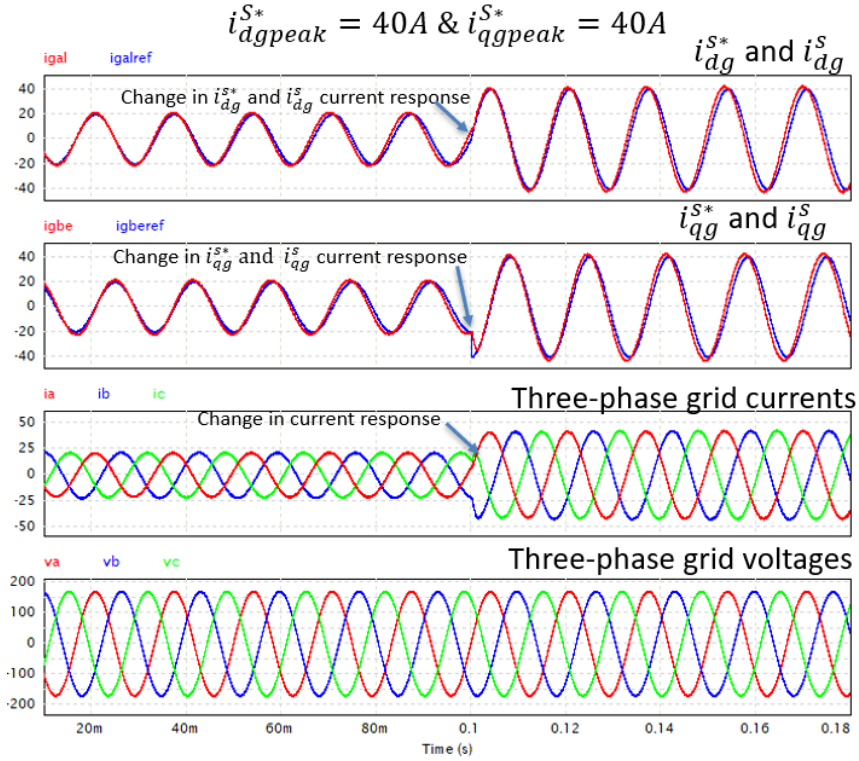

Figure.5.4. PSIM simulation results of the grid currents & voltages of the St- PR current control strategy.

5.4. Discussion

The simulation results of the current control strategies are observed to be satisfactory. A small overshoot has been observed in the feedback signals during the transient phase of change in the reference currents. The three-phase feedback currents are in phase with the three-phase grid voltages. A change in phase may be observed by altering the values of q-axis or d-axis reference currents in the respective reference frame. Thus, the theoretical analysis presented in the Chapter 3 has been verified by the results obtained PSIM simulations.

CHAPTER 6: EXPERIMENTAL VALIDATION OF CURRENT REGULATION STRATEGIES

6.1. Introduction

This chapter has been allotted to detail experimental setup and to report experimental results. An introduction to the experimental setup is presented in Section 6.1. Different stages of controller hardware in the loop (C-HIL) have been discussed in Section 6.2. Details of the power stage, analog to digital conversion and a serial communication interface to process the reference signals have been discussed in Section 6.2.1, Section 6.2.2, and Section 6.2.3. Experimental setup and experimental results have been presented in Section 6.3. and Section 6.4. A discussion on experimental validation is presented in Section 6.5.

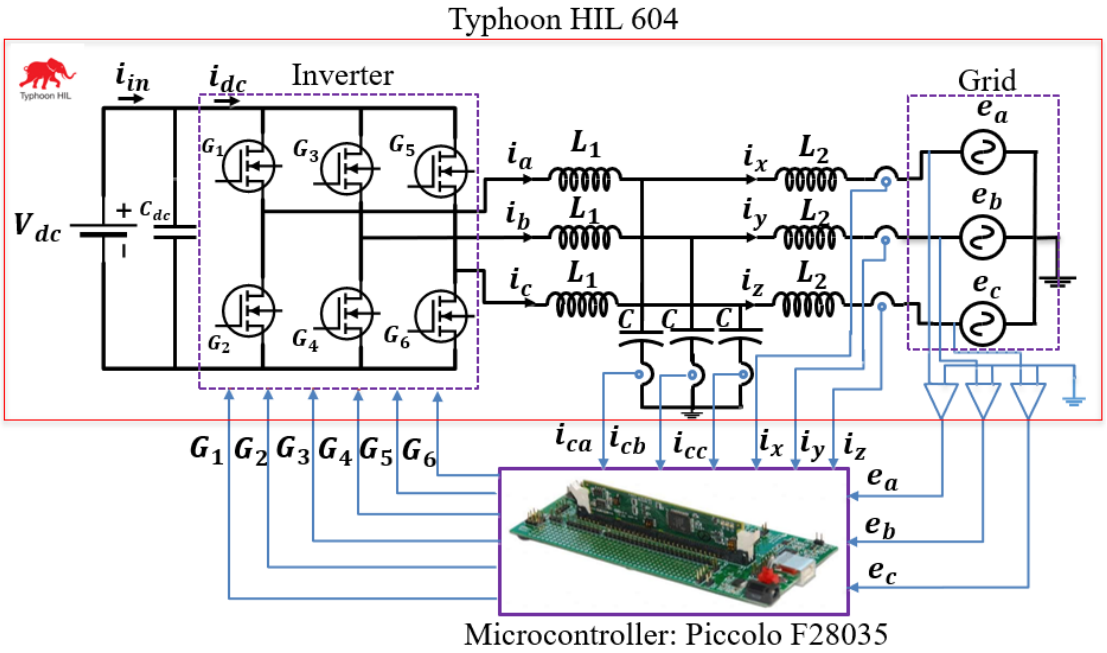

Figure.6.1. Simplified schematic of circuit topology and CHIL of the grid-tied inverter.

6.2. Controller Hardware in The Loop

A standard topology of an 800 V battery-fed three-phase inverter with an LCL filter tied to the grid has been considered. A simplified schematic of the circuit topology of a grid-tied inverter and controller hardware in the loop (CHIL) of the grid-tied inverter has been shown in the figure.6.1.

The controller hardware in the loop (C-HIL) system consists of a virtual power stage and a microcontroller is connected externally to control the desired parameters of the system. PSIM simulation platform has been used to generate the code for St-PI, Sy-PI, St/Sy-PI, and St-PR current control strategies. This code is deployed into the microcontroller TI DSP Piccolo TMS320F28035. Typhoon HIL 604 has been used to emulate the power stage consisting of a battery, voltage source inverter (VSI), LCL filter, and a three-phase grid. Thus, TI DSP Piccolo TMS320F28035 has been employed to implement the control algorithms externally to control the system parameters inside the Typhoon HIL 604.

6.2.1. Power Stage

Typhoon HIL control center consists of a schematic editor and HIL SCADA. The schematic editor has been used to model the power stage of the three-phase grid-tied inverter as shown in figure.6.2. The SCADA has been used to access the analog outputs of currents, voltages from the grid and battery, and digital inputs to the switches of VSI. The model settings inside the SCADA are used to perform the signal conditioning of analog currents and voltages compatible with the ADC input port requirements of the TI DSP Piccolo TMS320F28035. Analog output currents and voltages from the power stage, and

digital PWM outputs from the TI DSP Piccolo TMS320F28035 (inputs to the VSI of the power stage) have been accessed through a breakout board.

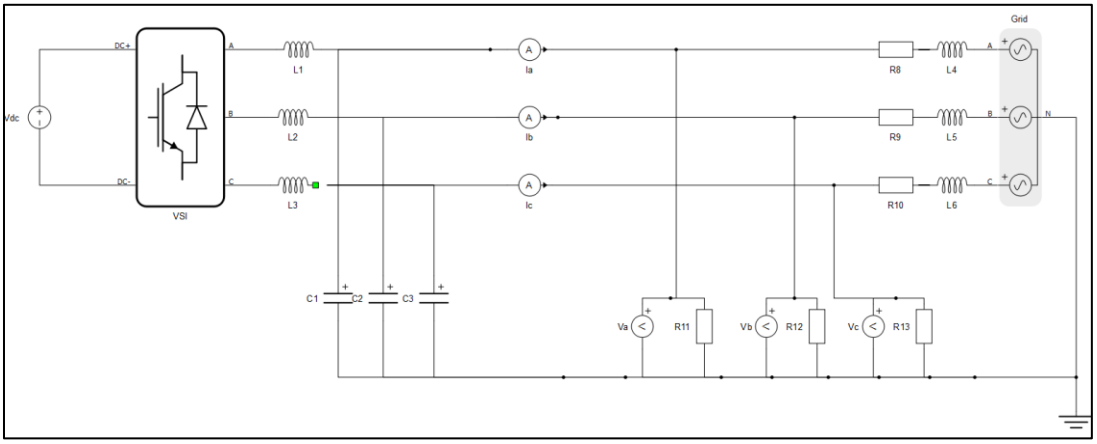

Figure.6.2. Power stage of the experimental setup of C-HIL employing HIL 604 and TI DSP Piccolo TMS320F28035.

6.2.2. Analog to Digital Conversion

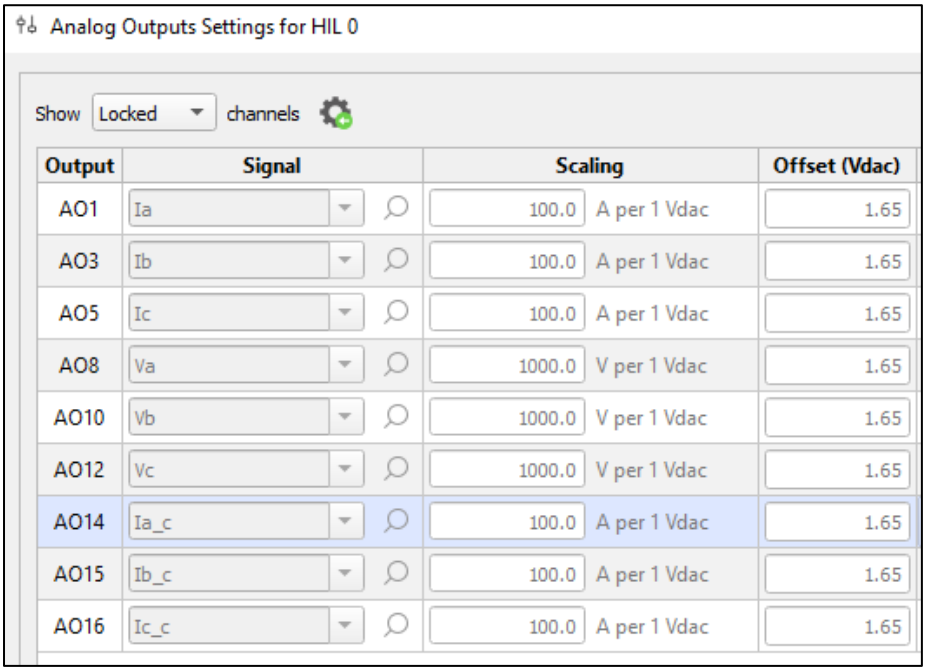

Output	Signal	Scaling	Offset (Vdac)
AO1	Ia	100.0 A per 1 Vdac	1.65
AO3	Ib	100.0 A per 1 Vdac	1.65
AO5	Ic	100.0 A per 1 Vdac	1.65
AO8	Va	1000.0 V per 1 Vdac	1.65
AO10	Vb	1000.0 V per 1 Vdac	1.65
AO12	Vc	1000.0 V per 1 Vdac	1.65
AO14	Ia_c	100.0 A per 1 Vdac	1.65
AO15	Ib_c	100.0 A per 1 Vdac	1.65
AO16	Ic_c	100.0 A per 1 Vdac	1.65

Figure.6.3. Signal conditioning of analog outputs of the power stage of the C-HIL system.

Analog outputs from the power stage or Typhoon HIL setup have been scaled with an appropriate offset of 0 to 3.3V inside the model settings of the SCADA panel as shown in figure.6.3. These analog outputs from the breakout board of Typhoon HIL 604 have been fed to an analog to digital (ADC) input ports of the TI DSP Piccolo TMS320F28035.

6.2.3. Pulse Width Modulation

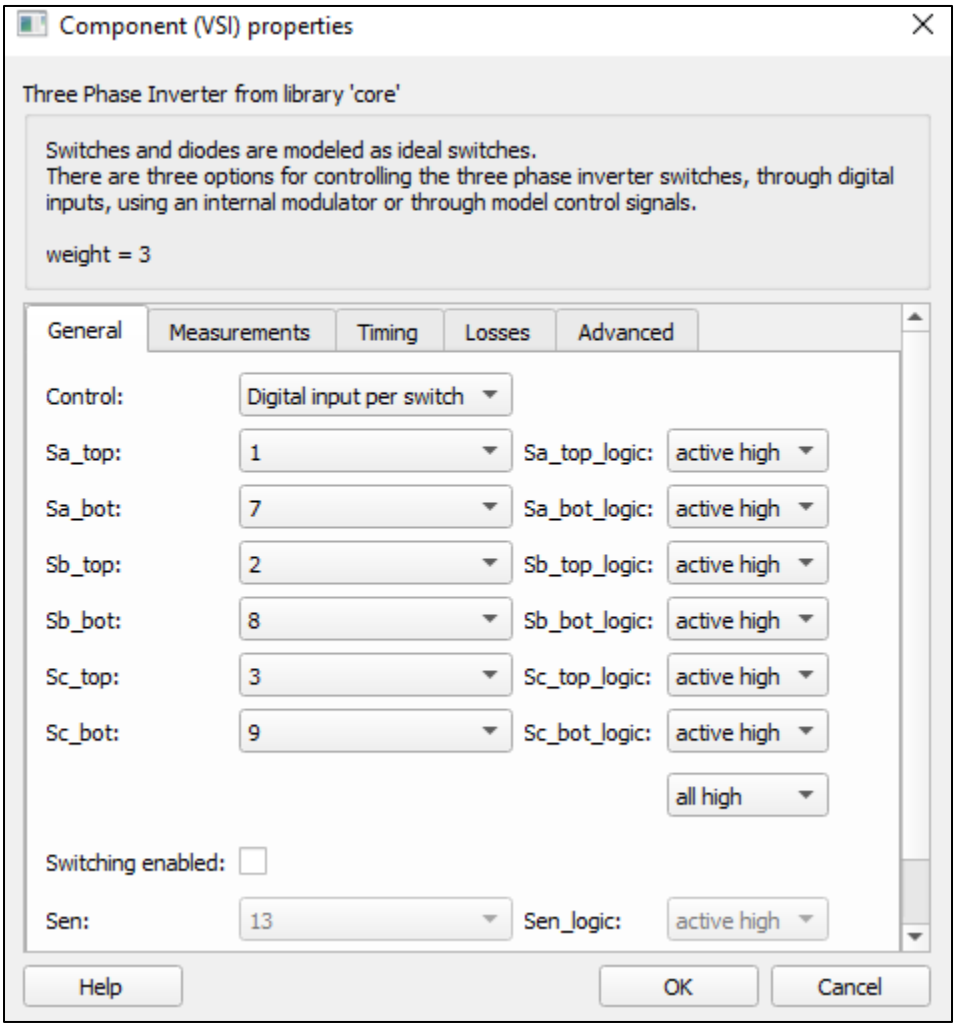

Figure.6.4. Configuration of digital inputs to the three-phase VSI of the power stage of the C-HIL.

PWM port outputs of the TI DSP Piccolo TMS320F28035 have been interfaced with digital inputs of the Typhoon HIL breakout board. These digital inputs are PWM input

signals to the switches of the three-phase VSI of the power stage of the three-phase grid-tied inverter as shown in the figure.6.4.

6.2.4. Serial Communication Interface

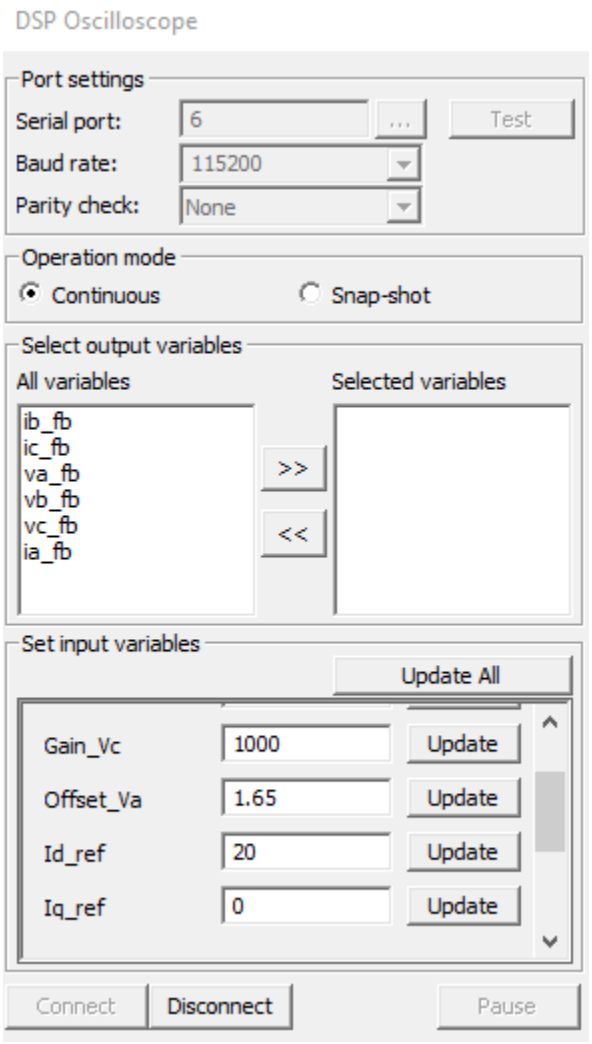

Figure.6.5. PSIM simulation schematic of SCI panel to change the controller settings.

Serial communication has been enabled to get access to the reference currents, ADC offset and scaling settings, and to monitor the feedback currents through digital oscilloscope inside the PSIM simulation software as shown in the figure.6.5. Reference currents to the controller are changed online through this serial communication panel.

6.3. Experimental Setup

have been considered for the experimental validation. The experimental setup of C-HIL consists of a power stage inside the HIL 604, SCADA panel, and TI DSP Piccolo TMS320F28035 is shown in figure.6.6.

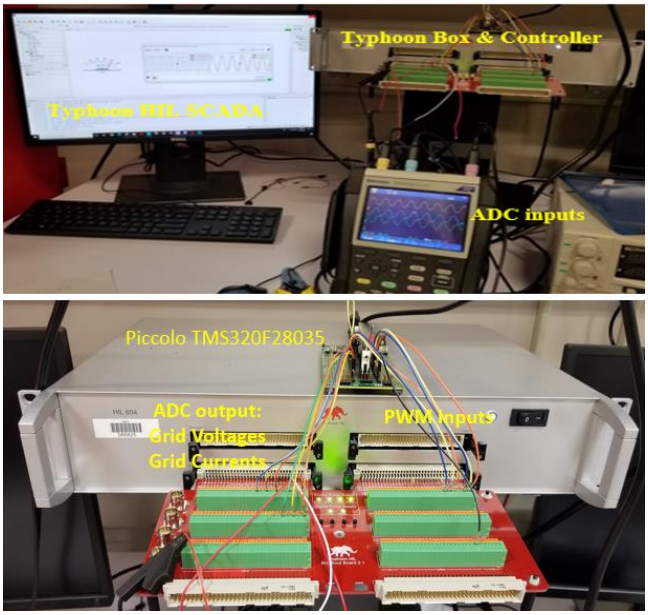

Figure.6.6. Picture of the experimental setup showing controller-hardware in loop (C-HIL) implementation of the grid-tied inverter employing Typhoon HIL 604 and Piccolo TMS320F28035.

A battery voltage of 800V_{dc}, three-phase grid voltage of 208V at a grid frequency of 60Hz with the following grid specifications as shown in table 4.0

TABLE 3:SPECIFICATION OF LCL FILTER AND CONTROL PARAMETERS

L_1 (mH)	R_1 $(m\Omega)$	L_2 (mH)	R_2 $(m\Omega)$	C (μf)	k_p	k_i	k
8	1	2	1	15	0.5	50	5

6.4. Experimental Results

6.4.1. Stationary Reference Frame Proportional Integral Controller (St-PI)

Experimental results of St-PI current control strategy employing C-HIL are discussed in this section. A change in peak of the reference currents i_{dgpeak}^{s*} and i_{qgpeak}^{s*} has been introduced.

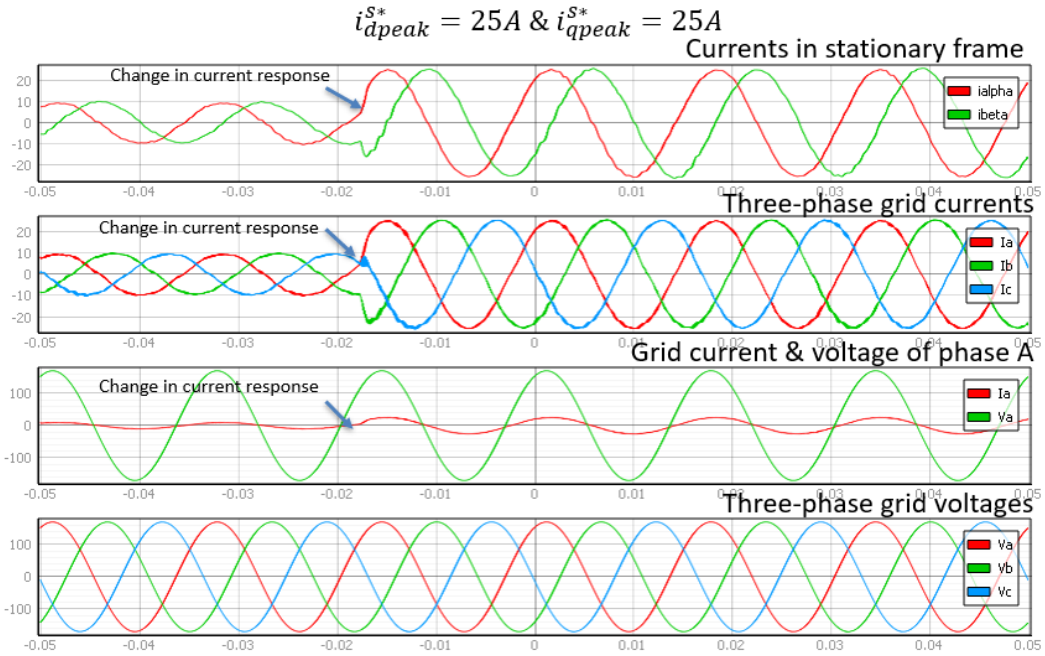

Figure.6.7. Experimental results of the grid currents & voltages of the St-PI current control strategy employing Typhoon CHIL system.

The feedback currents i_{dg}^{s} and i_{qg}^{s} are tracking the change in reference currents as shown in figure.6.7. The change in the reference currents is also reflected in the three-phase grid current currents. These currents are in phase with the three-phase grid voltages because of the identical change in the peak of reference currents from 10 A to 25A. These results are identical to the PSIM simulation results of the St-PI current control strategy presented in the Chapter.5.

6.4.2. Synchronous Reference Frame Proportional Integral Controller (Sy-PI)

Experimental results of Sy-PI current control strategy employing C-HIL are presented in this section. A change in the reference currents i_{dg}^{e*} and i_{qg}^{e*} has been introduced. The feedback currents i_{dg}^{e} and i_{qg}^{e} are tracking the change in reference currents as shown in figure.6.8.

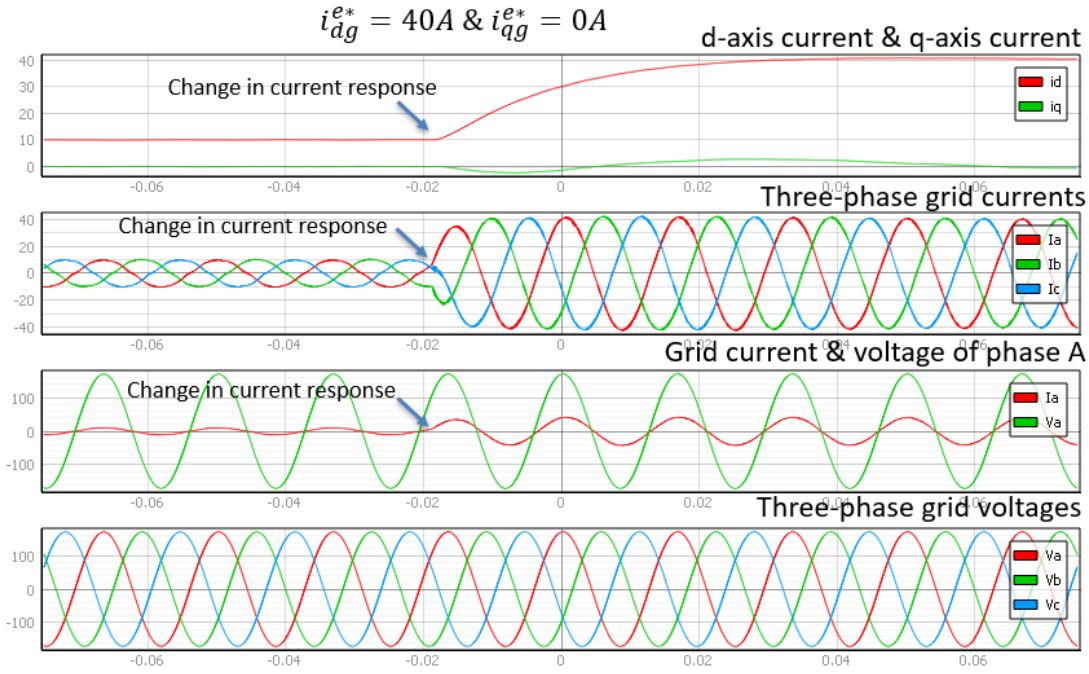

Figure.6.8. Experimental results of the grid currents & voltages of the Sy-PI current control strategy employing Typhoon CHIL system.

The change in the reference currents is also reflected in the three-phase grid current currents. These currents are in phase with the three-phase grid voltages because of the current references $i_{dg}^{e*} = 40$ and $i_{qg}^{e*} = 0$. These results are identical to the PSIM simulation results of the Sy-PI current control strategy presented in the Chapter.5.

6.4.3. Stationary Reference Frame Regulation of Synchronous Reference Frame Controller (St/Sy-PI)

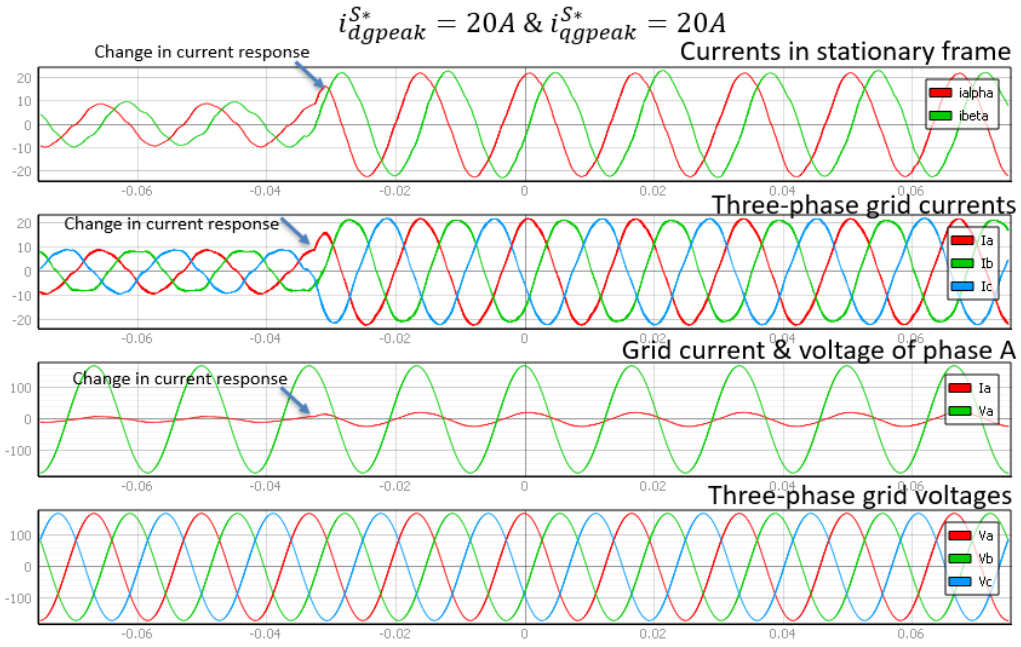

Figure.6.9. Experimental results of the grid currents & voltages of the St/Sy-PI current control strategy employing Typhoon CHIL system.

Experimental results of St/Sy-PI current control strategy employing C-HIL are discussed in this section. A change in the reference currents i_{dgpeak}^{S*} and i_{qgpeak}^{S*} has been introduced. The feedback currents i_{dg}^{S} and i_{qg}^{S} are tracking the change in reference currents as shown in figure.6.9. The change in the reference current also reflected in the three-phase grid current currents. These currents are in phase with the three-phase grid voltages because of an identical change in the peak of reference currents from 10 A to 20A. These results are identical to the PSIM simulation results of the St/Sy-PI current control strategy presented in the Chapter.5.

6.4.4. Stationary Reference Frame Proportional Resonant Controller (St-PR)

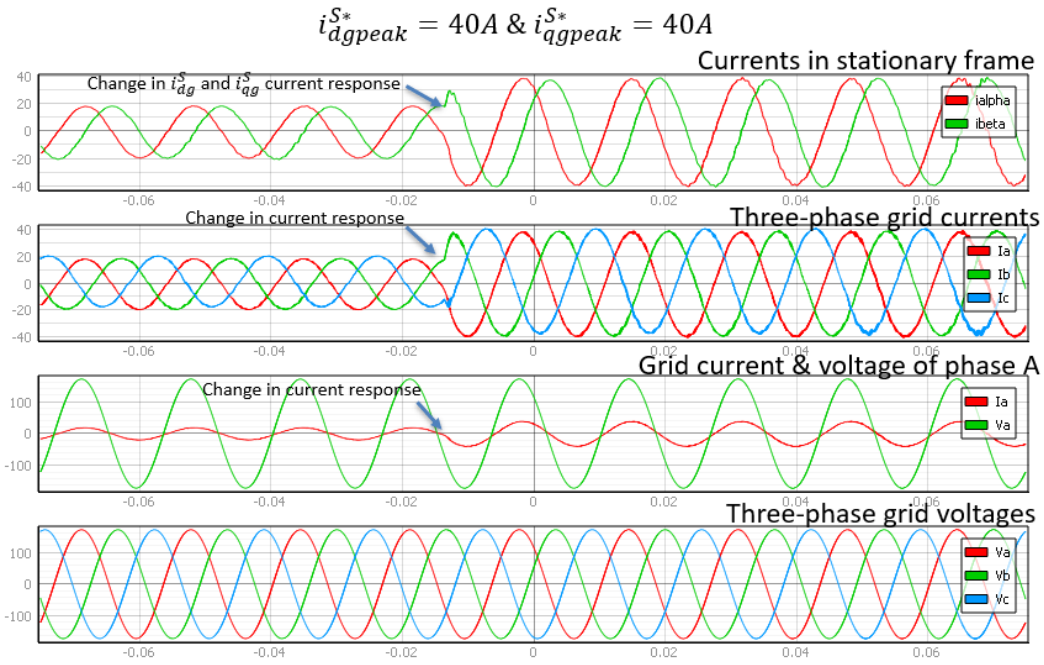

Figure.6.10. Experimental results of the grid currents & voltages of the St -PR current control strategy employing Typhoon CHIL system.

Experimental results of St -PR current control strategy employing C-HIL are discussed in this section. A change in the reference currents i_{dgpeak}^{S*} and i_{qgpeak}^{S*} has been introduced.

The feedback currents i_{dg}^{S} and i_{qg}^{S} are tracking the change in reference currents as shown in figure.6.10. The change in the reference currents is also reflected in the three-phase grid current currents. These currents are in phase with the three-phase grid voltages because of an identical change in the peak of reference currents from 20 A to 40A. These results are identical to the PSIM simulation results of the St- PR current control strategy presented in the Chapter.5.

6.5. Discussion

Analytical models of the St-PI, Sy-PI, St/Sy-PI, and St-PR current control strategies for a three-phase grid-tied inverter with an LCL filter are validated employing C-HIL experimental setup. The control algorithms of the respective current control strategy are perfectly tracking the reference signals in the respective reference frame. The experimental results employing C-HIL are identical to the PSIM simulation results presented in the Chapter 5.

CHAPTER 7: CONCLUSION

In addition to the classical synchronous reference frame PI current controller (Sy-PI), an analytical derivation of stationary reference frame equivalence of this Sy-PI current controller (St/Sy-PI) is established. These two controllers are closely related but not identical to stationary reference frame PR current controller (St-PR) because their analytical outcome results in same forward path transfer functions but differ in cross-coupling elements as proven in this paper. As an additional contribution of this thesis, the analysis presented in Section 3.3, Section 3.4, and Section 3.5 has also been used to realize a "generalized current control strategy" which encompasses all controllers, viz. Sy-PI, St/Sy-PI, and St-PR as "special cases". The stability of all of these current control strategies has been analyzed through Bode plot and root locus analysis by considering the same forward path transfer function. These three different current control strategies have been validated through PSIM and verified by Typhoon controller hardware in the loop experimental setup. The grid currents have been observed to track the reference signals in both, stationary reference frame and synchronous reference frame, for all three controllers.

BIBLIOGRAPHY

[1] Global Energy Observatory, Google, KTH Royal Institute of Technology in Stockholm, Enipedia, World Resources Institute. 2018. *Global Power Plant Database.* Published on Resource Watch and Google Earth Engine.

[2] IEA (2020), Electricity Market Report - December 2020, IEA, Paris. https://www.iea.org/reports/electricity-market-report-december-2020.

[3] E. P. Weichmann, P. D. Ziogas and V. R. Stefanovic, "Generalized Functional Model for Three-Phase PWM Inverter/Rectifier Converters," *IEEE Transactions on Industry Applications*, vol. IA-23, no. 2, pp. 236-246, March 1987.

[4] L. Salazar and G. Joos, "PSPICE simulation of three-phase inverters by means of switching functions," *IEEE Transactions on Power Electronics*, vol. 9, no. 1, pp. 35-42, Jan. 1994.

[5] N. Abdel-Rahim and J. E. Quaicoe, "Small-signal model and analysis of a multiple feedback control scheme for three-phase voltage-source UPS inverters," *PESC Record. 27th Annual IEEE Power Electronics Specialists Conference*, pp. 188-194 vol.1, 1996.

[6] Dushan Boroyevich, “Modeling and Control of Three-Phase PWM Converters,” *The 2nd IEEE International Power & Energy Conference,* Nov.2008.

[7] Byoung-Kuk Lee and M. Ehsami, "A simplified functional simulation model for three-phase voltage-source inverter using switching function concept," *IEEE Transactions on Industrial Electronics*, vol. 48, no. 2, pp. 309-321, April 2001.

[8] C.W. Brice et all, “Reference frames for simulation of electric motors and drives,” *International conference on electrical machines, Espoo, August 2000.*

[9] R.J. Lee, P. Pillay, and R.G. Harley, “D,Q Reference frames for the simulation of induction motors,” *Electric power systems research,* pp 15-26, April 1984.

[10] R.H. Park, “Two-reaction theory of synchronous machines,” *AIEE transactions*, vol 48, pp. 716-730, July 1929.

[11] Paul Krause; Oleg Wasynczuk; Scott D. Sudhoff; Steven Pekarek, "Reference-Frame Theory," *Analysis of Electric Machinery and Drive Systems,* IEEE, pp.86-120, 2013.

[12] Igor D.N. de Souza, Pedro M. de Almeida, Pedro G. Barbosa, Carlos A. Duque, Paulo F. Ribeiro, “Digital single voltage loop control of a VSI with LC output filter,” *Sustainable Energy, Grids and Networks,* Volume 16, Pages 145-155, June 2018.

[13] Jayalath and M. Hanif, "CL-filter design for grid-connected CSI," *2015 IEEE 13th Brazilian Power Electronics Conference and 1st Southern Power Electronics Conference* (COBEP/SPEC), 2015, pp. 1-6, Dec 2015.

[14] Jing Wang and A. Monti, "Current control of grid-connected inverter with LCL filter utilizing two-degree-of-freedom control," *2013 International Conference on Renewable Energy Research and Applications* (ICRERA), Oct 2013.

[15] Poh Chiang Loh and D. G. Holmes, "Analysis of multiloop control strategies for LC/CL/LCL-filtered voltage-source and current-source inverters," *IEEE Transactions on Industry Applications,* vol. 41, no. 2, pp. 644-654, March-April 2005.

[16] Y. Tang, P. C. Loh, P. Wang, F. H. Choo and F. Gao, "Exploring Inherent Damping Characteristic of LCL-Filters for Three-Phase Grid-Connected Voltage Source Inverters,” *IEEE Transactions on Power Electronics,* vol. 27, no. 3, pp. 1433-1443, March 2012.

[17] Y. Tang, P. C. Loh, P. Wang, F. H. Choo and F. Gao, "Exploring Inherent Damping Characteristic of LCL-Filters for Three-Phase Grid-Connected Voltage Source Inverters," *IEEE Transactions on Power Electronics,* vol. 27, no. 3, pp. 1433-1443, March 2012.

[18] P. Mattavelli and S. Fasolo, "Implementation of synchronous frame harmonic control for high-performance AC power supplies," *2000 IEEE Industry Applications Conference. Thirty-Fifth IAS Annual Meeting and World Conference on Industrial Applications of Electrical Energy*, pp. 1988-1995 vol.3, 2000.

[19] N. R. Zargari and G. Joos, "Performance investigation of a current-controlled voltage-regulated PWM rectifier in rotating and stationary frames," *IEEE Transactions on Industrial Electronics,* vol. 42, no. 4, pp. 396-401, Aug. 1995.

[20] M. P. Kazmierkowski and L. Malesani, "Current control techniques for three-phase voltage-source PWM converters: a survey," *IEEE Transactions on Industrial Electronics,* vol. 45, no. 5, pp. 691-703, Oct. 1998.

[21] Wooyoung Choi, C. Morris and B. Sarlioglu, "Modeling three-phase grid-connected inverter system using complex vector in synchronous dq reference frame and analysis on the influence of tuning parameters of synchronous frame PI controller," *2016 IEEE Power and Energy Conference at Illinois (PECI),* pp. 1-8, 2016.

[22] T. M. Rowan and R. J. Kerkman, "A New Synchronous Current Regulator and an Analysis of Current-Regulated PWM Inverters," *IEEE Transactions on Industry Applications,* vol. IA-22, no. 4, pp. 678-690, July 1986.

[23] D. G. Holmes, T. A. Lipo, B. P. McGrath, and W. Y. Kong, "Optimized Design of Stationary Frame Three Phase AC Current Regulators," *IEEE Transactions on Power Electronics,* vol. 24, no. 11, pp. 2417-2426, Nov. 2009.

[24] D. G. Holmes and B. P. McGrath, "Principles and practices of digital current regulation for AC systems," *2016 Applied Power Electronics Conference*, March 2016.

[25] D. N. Zmood, D. G. Holmes and G. H. Bode, "Frequency-domain analysis of three-phase linear current regulators," *IEEE Transactions on Industry Applications, vol. 37,* no. 2, pp. 601-610, March-April 2001.